



Cooperative Research Centre for
Landscape Environments
and Mineral Exploration



OPEN FILE
REPORT
SERIES



Australian Government
Geoscience Australia



Australian Government
Bureau of Meteorology



NEOTECTONICS, SALINITY, PALAEOCLIMATES AND VOLCANISM

Australian Earth Science Convention Pre-conference Field Trip
Adelaide – Melbourne 28 June to 2 July 2006

Compiled by:
David Gibson and Kate Boston

With contributions from:
Heike Apps, Steve Bourne, Kristen Cullen, Dan Clark, Jon Clarke,
Patrick de Deckker, David Gibson, Larysa Halas, Bernie Joyce,
Mike Sandiford, Liz Reid and John Wilford

CRC LEME OPEN FILE REPORT 235

June 2008

CRCLEME

for
THE ENVIRONMENT, ENGINEERING HYDROGEOLOGICAL
SPECIALIST GROUP

GEOLOGICAL SOCIETY OF AUSTRALIA

CRC LEME is an unincorporated joint venture between CSIRO-Exploration & Mining, and Land & Water, The Australian National University, Curtin University of Technology, University of Adelaide, Geoscience Australia, Primary Industries and Resources SA, NSW Department of Primary Industries and Minerals Council of Australia, established and supported under the Australian Government's Cooperative Research Centres Program.





Australian Government
Geoscience Australia



Australian Government
Bureau of Meteorology



NEOTECTONICS, SALINITY, PALAEOCLIMATES AND VOLCANISM

Australian Earth Science Convention Pre-conference Field Trip
Adelaide – Melbourne 28 June to 2 July 2006

Convened by the Environment, Engineering Hydrogeological Specialist
Group of the Geological Society of Australia and co-sponsored by
EEHSG, CRC LEME and Bureau of Meteorology

Compiled by:
David Gibson and Kate Boston

With contributions from:
Heike Apps, Steve Bourne, Kristen Cullen, Dan Clark, Jon Clarke,
Patrick de Deckker, David Gibson, Larysa Halas, Bernie Joyce,
Mike Sandiford, Liz Reid and John Wilford

CRC LEME OPEN FILE REPORT 235

June 2008

for
THE ENVIRONMENT, ENGINEERING HYDROGEOLOGICAL
SPECIALIST GROUP

GEOLOGICAL SOCIETY OF AUSTRALIA

© CRC LEME 2008

CRC LEME is an unincorporated joint venture between CSIRO-Exploration & Mining, and Land & Water, The Australian National University, Curtin University of Technology, University of Adelaide, Geoscience Australia, Primary Industries and Resources SA, NSW Department of Primary Industries and Minerals Council of Australia.

Headquarters: CRC LEME c/o CSIRO Exploration and Mining, PO Box 1130, Bentley WA 6102, Australia

Electronic copies of this publication in PDF format can be downloaded from the CRC LEME website: <http://crcleme.org.au/Pubs/OFRSindex.html>. Information on this and other LEME publications can be obtained from <http://crcleme.org.au>.

Hard copies will be retained in The Australian National Library, the Western Australian State Reference Library, and Libraries at The Australian National University and Geoscience Australia, Canberra, The University of Adelaide, and the CSIRO Library at the Australian Resources Research Centre, Kensington, Western Australia.

Reference:

Gibson D and Boston K (Compilers). 2008. Neotectonics, Salinity, Palaeoclimates and Volcanism. Australian Earth Sciences Convention Pre-Conference Field Trip, Adelaide-Melbourne, 28 June to 2 July 2006. 64pp. *CRC LEME Open File Report 235*.

Keywords:

1. Neotectonics. 2. Salinity. 3. Palaeoclimates. 4. Cainozoic Volcanism

ISSN 1329-4768

ISBN 1 921039 86 8

Addresses and affiliations of compilers

David Gibson

Cooperative Research Centre for Landscape
Environments and Mineral Exploration
c/- Geoscience Australia
PO Box 378
Canberra ACT 2601

Kate Boston

Cooperative Research Centre for Landscape
Environments and Mineral Exploration
c/- Geoscience Australia
PO Box 378
Canberra ACT 2601

Published by:

CRC LEME, c/o CSIRO Exploration and Mining
PO Box 1130
Bentley, Western Australia 6102

Disclaimer

The user accepts all risks and responsibility for losses, damages, costs and other consequences resulting directly or indirectly from using any information or material contained in this report. To the maximum permitted by law, CRC LEME excludes all liability to any person arising directly or indirectly from using any information or material contained in this report.

© **This report is Copyright of the** Cooperative Research Centre for Landscape Environments and Mineral Exploration, from the date of the original publication, which resides with its Core Participants: CSIRO Exploration and Mining and Land and Water, The Australian National University, Curtin University of Technology, The University of Adelaide, Geoscience Australia, Primary Industry and Resources SA, NSW Department of Primary Industries and Minerals Council of Australia.

Apart from any fair dealing for the purposes of private study, research, criticism or review, as permitted under Copyright Act, no part may be reproduced or reused by any process whatsoever, without prior written approval from the Core Participants mentioned above.

CONTENTS

1.	INTRODUCTION.....	1
2.	Day 1: Adelaide to Murray Bridge.....	2
2.1	Day 1 Stop 1: Sellicks Beach, Fleurieu Peninsula.....	2
2.2	Day 1 Stop 2: Rose Hill.....	5
2.2.1	Background.....	5
2.2.2	Identifying areas of deep weathering and its relationship to salinity.....	5
2.2.3	Mapping regolith using gamma-ray spectrometry.....	6
2.2.4	Deep weathering and tectonics.....	7
2.2.5	Deep regolith and salinity.....	9
2.3	Day 1 Stop 3: Milendella Fault at Cambrai, eastern Mt Lofty Ranges.....	10
3.	Day 2: Murray Bridge to Naracoorte.....	12
3.1	Day 2: Late Tertiary to Quaternary faulting in the Strathalbyn area.....	12
3.1.1	Bremer Fault.....	12
3.1.2	Ferries McDonald Fault.....	15
3.1.3	Sandergrove Fault.....	15
3.2	Day 2 Stop 1: Sandergrove Fault.....	17
3.3	Day 2 Stop 2: Garwood Quarry and Rankine Zinc Deposit.....	18
3.4	Day 2: En route Strathalbyn to Wellington.....	21
3.5	Day 2 Stop 3: The Coorong and lakes near Salt Creek.....	22
3.6	Day 2 Stop 4: Murray canyons.....	28
3.7	Day 2 Stop 5: Quaternary and Pliocene strandplain successions.....	30
3.7.1	Quaternary strandplains.....	30
3.7.2	Pliocene strandplains.....	31
4.	Day 3: Naracoorte Caves and Mount Gambier.....	33
4.1	Day 3 Stop 1: Naracoorte Caves.....	33
4.1.1	Megafauna, climate and Naracoorte research.....	34
4.1.2	Impacts of karst of the south east of South Australia.....	35
4.2	Day 3 Stop 2: Blue Lake and Pump House tour, Mt Gambier.....	36
4.3	Day 3 Stop 3: Mount Schank.....	37
5.	Day 4: Mount Gambier to Camperdown.....	39
5.1	Day 4: Mount Gambier to Chetwynd.....	39
5.2	Day 4 Stop 1: Chetwynd road cut.....	39
5.3	Day 4 Stop 2: Hamilton area volcanics.....	40
5.4	Day 4 Stop 3: Staughtons Hill.....	41
5.5	Day 4 Stop 4: Lakes Gnotuk and Bullenmerri.....	42
6.	Day 5 Camperdown to Melbourne.....	44
6.1	Day 5 Stop 1: Mt Leura.....	44
6.2	Day 5 Stop 2: Mt Porndon stony rises.....	46
6.3	Day 5 Stop 3: Floating Islands.....	49
6.4	Day 5 Stop 4 :Red Rock lookout.....	51
6.5	Day 5 Stop 5: Lake Corangamite.....	53
6.6	Day 5 Stop 6 :Lake Beeac.....	53
6.7	Day 5 Stop 6: Barabool Hills monocline.....	56
7.	ACKNOWLEDGEMENTS.....	59
8.	REFERENCES.....	60

LIST OF FIGURES

Figure 1. Day one route map and stops.....	2
Figure 2. Shaded relief image of the Mt Lofty Ranges and Fleurieu Peninsula	3
Figure 3. Topographic profiles and stratigraphic relationships across the Willunga scarp.....	4
Figure 4. Willunga Fault locality at Sellicks Beach.....	4
Figure 5. Rose Hill study area.....	5
Figure 6. Radioelement responses of bedrock and regolith materials from the Rose Hill area.....	6
Figure 7. K-residual image, Rose Hill.....	7
Figure 8. Locality geology, Rose Hill.....	8
Figure 9. Topographic cross section, Mt Lofty Ranges.	8
Figure 10. K-residual image draped over a DEM, Rose Hill.	9
Figure 11. Topographic profiles and stratigraphic relationships across the Milendella scarp	10
Figure 12. Photograph (a) and outcrop interpretation (b) of the Milendella Fault.....	11
Figure 13. Day 2 route map, stops 1 and 2.....	12
Figure 14. Northward oblique view across a DEM of the Angas Bremer area.....	13
Figure 15. Horizontal AEM slice with, Bremer and Ferries McDonald Faults.....	13
Figure 16. AEM flight line sections across Bremer and Ferries McDonald Faults.....	14
Figure 17. DEM showing closed valleys immediately west of the Bremer Fault	14
Figure 18. A. DEM showing scarp of Sandergrove Fault B. AEM conductivity slice for +20 to +15 m elevation	15
Figure 19. NanoTEM traverse across the Sandergrove Fault.....	16
Figure 20. Radiometric image showing high response alluvium.	16
Figure 21. 15-20 m depth AEM slice showing a narrow conductive band of sediment northeast of the River Angas that may mark an extension of the Sandergrove Fault.	17
Figure 22. Eastern end of the Garwood Quarry showing Cainozoic stratigraphy.....	19
Figure 23. An irregular erosional contact separating the bioclastic Mannum limestone from underlying older Cainozoic clastic sediments, Garwood Quarry	19
Figure 24. Erosional contact between lagoonal and aeolian sands, Garwood Quarry	20
Figure 25. Detail of aeolian cross-bedded sands, Garwood Quarry.....	20
Figure 26. Day 2 route map, stops 3-5.....	21
Figure 27. Quaternary strandplains of south east South Australia	23
Figure 28. Coastal and inland carbonate precipitating lakes and swamps of the south-east.....	24
Figure 29. Generalised cross section illustrating present ground-water-sea-water interface at the Coorong.....	25
Figure 30. Schematic representation of high wave energy coastal facies of the Coorong region and Eyre Peninsula coastline.....	25
Figure 31. Extent of land subject to winter flooding.....	26
Figure 32. Maps showing the location of the 23 lakes studied by De Dekker & Geddes (1980)	27
Figure 33. An early map of the Murray Canyons	28
Figure 34. 3-D image of the Murray Canyons	29
Figure 35. Detailed bathymetry contours of the Lacapede Shelf and adjacent Murray Canyons	29
Figure 36. 3-D view of Sprigg and De Couedic Canyons.....	30
Figure 37. Cross section exposed by the Woakwine Cutting through the Woakwine Range	31
Figure 38. Plot of shoreline elevation versus inferred age for coastal barriers of the Mount Gambier coastal plain.....	31
Figure 39. Pliocene palaeogeography and strandline morphology interpreted from geophysical data in the Murray, Otway and Port Phillip Basins.....	32
Figure 40. Chronostratigraphic chart for the late Neogene strandplain successions of the southeastern Australian basins.	32
Figure 41. Day 3 route map.....	33
Figure 42. Map of Naracoorte Caves	34
Figure 43. Pit A in Victoria Fossil Cave	35
Figure 44. Lower jaw of <i>Procoptodon goliah</i>	35

Figure 45. Marsupial lion (<i>thylacoleo carnifex</i>) skeleton	35
Figure 46. 5 Corners Cave.....	36
Figure 47. Aerial view of Blue Lake.....	36
Figure 48. Volcanic cones at Mount Schank.....	38
Figure 49. Small cone and dipping ash layers north-northwest of Mt Schank.....	38
Figure 50. Day 4 route map.....	39
Figure 51. Section at Chetwynd road cut.....	40
Figure 52. Five main regolith landform units of the basalt plains of the Newer Volcanic Province	41
Figure 53. The volcanic complex of Staughtons Hill.....	42
Figure 54. Lakes Bullenmerri and Gnotuk, plan and cross section.....	43
Figure 55. Lake Bullenmerri looking to the southwest.....	43
Figure 56. Day 5 route map.....	44
Figure 57. Features that can be viewed from Mt Leura lookout	44
Figure 58. Sketch map, Mt Leura.....	45
Figure 59. Mt Porndon flow units of Ellis (1971).....	46
Figure 60. Oblique view from west of LiDAR DEM over Mt Porndon	48
Figure 61. Vertical view of the LiDar DEM over the entire Mt Porndon lava field	49
Figure 62. Stony basalt slopes at Floating Islands Reserve	50
Figure 63. Dry floor of Lake Piron Yallock.....	50
Figure 64. LiDar DEM of the Red Rock volcanic complex area	51
Figure 65. Detail of the LiDar DEM showing dry maar lakes around Red Rocks lookout	52
Figure 66. View from Red Rocks lookout over dry Lake Werowrap to Lake Corangamite.....	52
Figure 67. Eastern shoreline of Lake Corangamite, with evaporate-encrusted basalt boulders.....	53
Figure 68. Oblique aerial photograph looking south over Lake Beac.....	54
Figure 69. LiDar DEM of Lake Beeac and surrounding areas	55
Figure 70. Groundwater map around Warrion Hill.....	55
Figure 71. Shaded digital elevation map of the Otway Ranges and topographic profile along Pliocene strandlines	56
Figure 72. Shaded digital elevation map of the Barabool Hills monocline and faulted contact between Tertiary fluvial sediments and a ca. 2-3 Ma lava flow.....	58

1. INTRODUCTION

This report describes stops for a pre-conference field excursion from Adelaide to Melbourne, associated with the 2006 Australian Earth Sciences Convention, with emphasis on neotectonics, salinity, palaeoclimates and Cainozoic volcanism. The excursion was run by the Environment, Engineering and Hydrogeological Specialist Group of the Geological Society of Australia. Various scientists were invited to join the tour and demonstrate important aspects of their research in the region. Many of the following site descriptions are direct copies of, or based on previously published articles in excursion guides, scientific journals, and websites. In all cases the sources of previously published text and illustrations are acknowledged.

2. DAY 1: ADELAIDE TO MURRAY BRIDGE

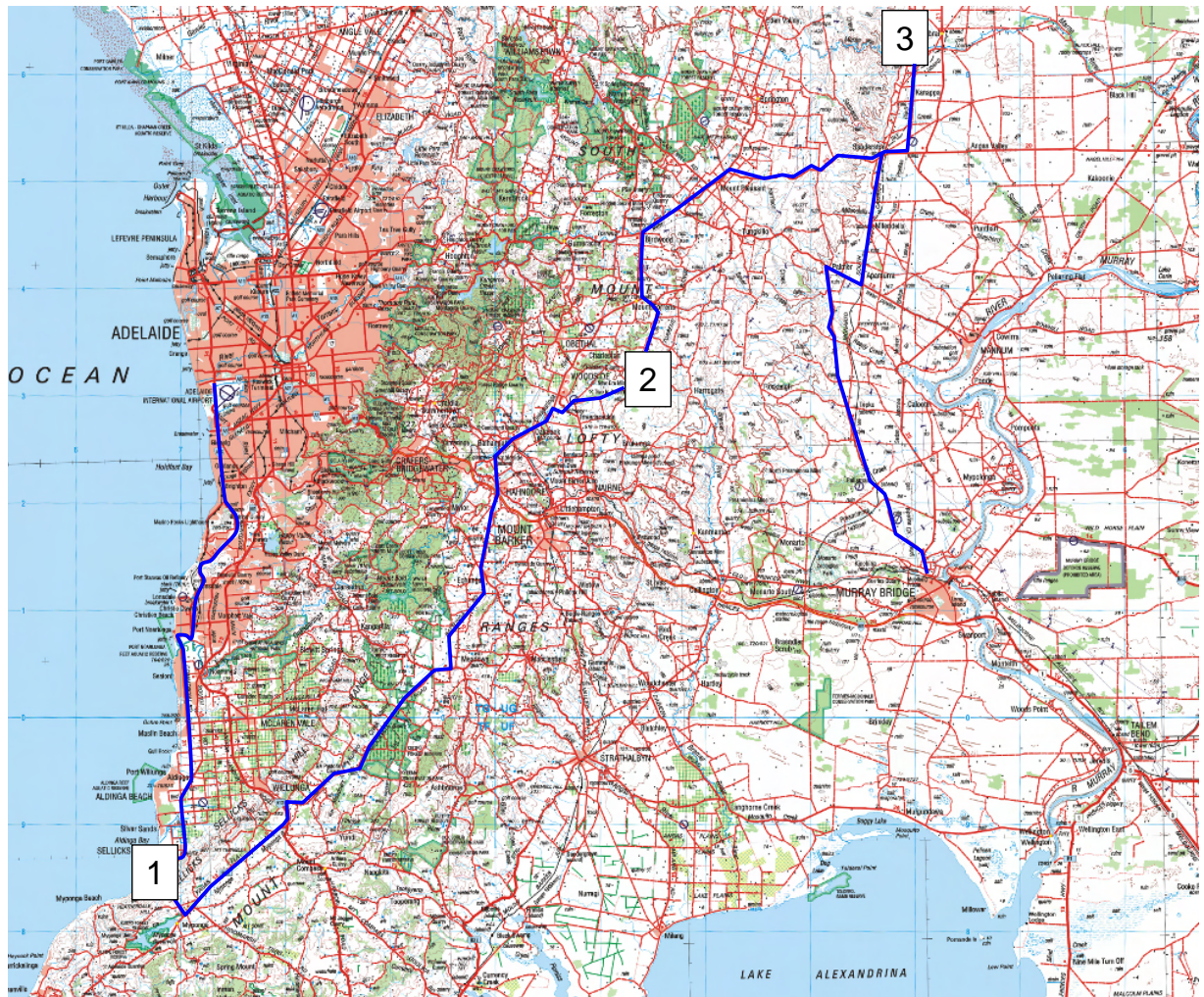


Figure 1. Day one route map and stops

2.1 Day 1 Stop 1: Sellicks Beach, Fleurieu Peninsula

Mike Sandiford

(text reproduced from Sandiford 2003a)

The Willunga scarp is exposed in spectacular profile at Sellicks Beach (Figures 2, 3), where marine processes have eroded sea cliffs up to 50 m into the alluvial fan, with a number of deep canyons penetrating through the footwall across the fault trace (May & Bourman 1984, Lemon & McGowran 1989). The canyon exposures include a near complete ~60 m-thick section through the alluvial fan which comprises conglomerate and ferruginous clay equivalent in age to those at Cambrai. These sequences unconformably overly the Oligocene – Lower Miocene Port Willunga Formation (equivalent of the Mannum Limestone), locally with very high-angle discordance (Figure 4a). A near-vertical fault contact between weakly metamorphosed Cambrian sedimentary rocks and the Quaternary has an exposed relief of ~50 m. Reverse-fault motion is indicated by steep east-dipping fault traces in the hangingwall sequence within metres of the main fault trace (Figure 4b). A prominent wave-cut bench in the footwall limestone sequence ~4–5 m asl (Figure 4a) is attributed to the ca 120 ka BP last interglacial high sea stand (May & Bourman 1984). Further south, correlative interglacial benches in the hangingwall of the Willunga Fault are up to 12 m asl (Bourman *et al.* 1998), implying a time averaged vertical displacement ~50–70 m/10⁶y. This estimate is independently corroborated reported

elevation differences of ~130 m in the Lower Pleistocene (ca 1.7 Ma) Burnham Limestone along the eastern margin of the St Vincents Basin (Belperio 1995, Bourman *et al.* 1998). The differential elevation of the Port Willunga Formation between the Myponga Basin (on the hangingwall block: Figure 2) and the St Vincents Basin (the footwall block) suggests a post- Early Miocene displacement of ~240 m (Tokarev *et al.* 1999). The presence of locally abundant basement clasts in the Port Willunga Formation fringing the Willunga scarp suggests some relief must have existed during the Oligocene and/or Early Miocene. Consequently, the present day ~360–400 m scarp relief (Figure 3) most probably exceeds the total post-Early Miocene displacement.

The record of Quaternary faulting in southeastern Australia on north–south- to northeast–southwest-trending faults is consistent with the contemporary in situ stress determinations showing east–west to southeast–northwest σ_{Hmax} (Denham *et al.* 1979; Denham & Windsor 1991; Hillis *et al.* 1999; Hillis & Reynolds 2000). Consequently, constraints on the time of initiation of this faulting record are relevant to the hypotheses concerning the origin of the in situ stress field. This faulting record can be traced back to at least until the earliest Pliocene. For example, in the Murray Basin the faults associated with the Iona and Neckarboo ridges have been active since the earliest Pliocene (Roy *et al.* 2000). In the interval 8–6 Ma, the various basins around southeastern Australia experienced significant inversion (Dickinson *et al.* 2001, 2002) with a corresponding transition in the nature of basin-fill from mainly carbonate to siliciclastics, most dramatically evidenced by the unconformity at Sellicks Beach (Figure 4a). In part, the ‘visibility’ of this inversion event, which is evident in many seismic profiles from the Gippsland and Otway Basins (Dickinson *et al.* 2001, 2002), has been greatly augmented by erosion associated with a global, terminal Miocene, regression (Haq *et al.* 1988). However, the local removal of up to 1 km of section on structurally controlled highs (Dickinson *et al.* 2001) is evidence of significant tectonism at this time, with the implied deformation rates significantly greater than those implied by the subsequent Pliocene–Quaternary faulting record. In the Otway and Gippsland Basins, the axis of the terminal Miocene inversion structures parallels the younger onshore Pliocene–Holocene structures, implying formation under a stress regime that was comparable with the in situ stress field, in the interval 8–6 Ma.

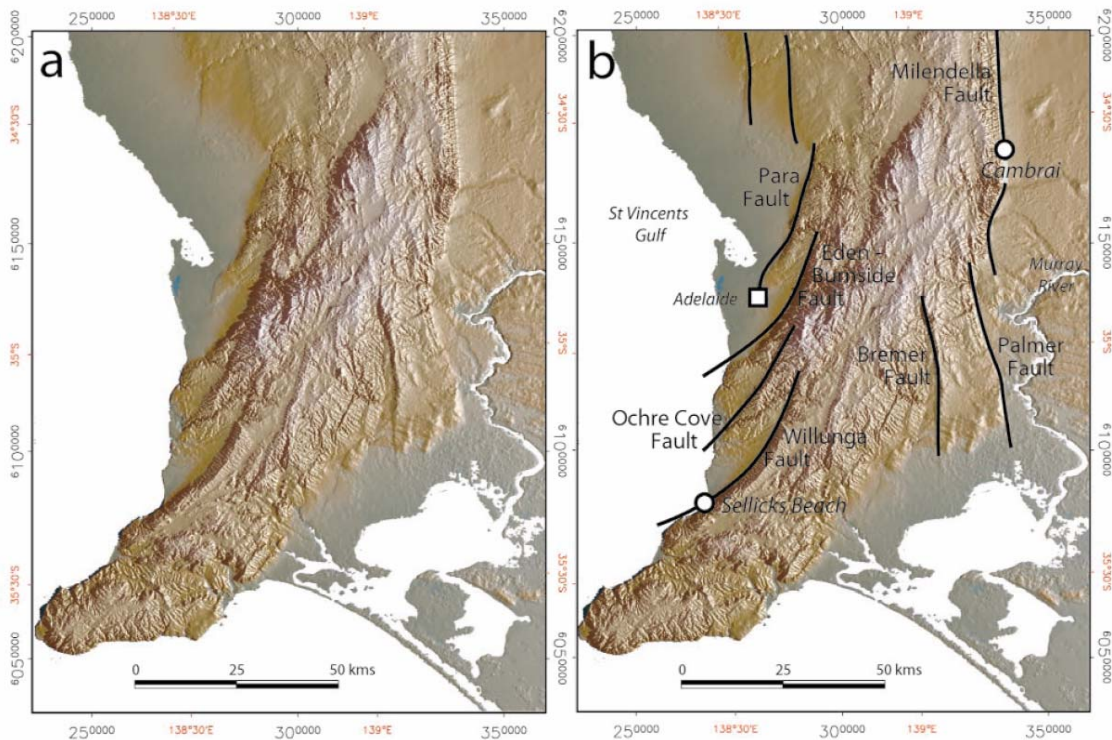


Figure 2. Shaded relief image of the Mt Lofty Ranges and Fleurieu Peninsula, South Australia, showing the main Quaternary faults referred to in the text. Image derived from a 100 m resolution digital elevation data provided by Department of Environment and Natural Resources, South Australia (reproduced from Sandiford 2003a. Copyright © Geological Society of Australia 2003).

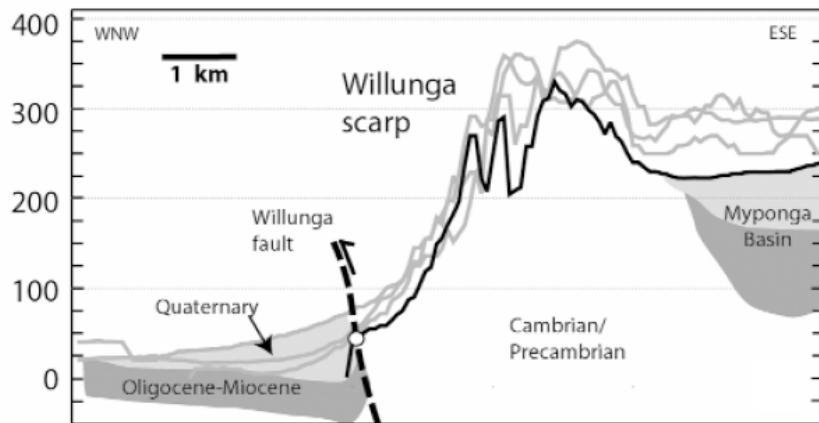


Figure 3. Topographic profiles and stratigraphic relationships across the Willunga scarp. Original data from DENR 100 m DEM shown in Figure 2. Stratigraphic thicknesses and extent are only approximate (reproduced from Sandiford 2003a. Copyright © Geological Society of Australia 2003).

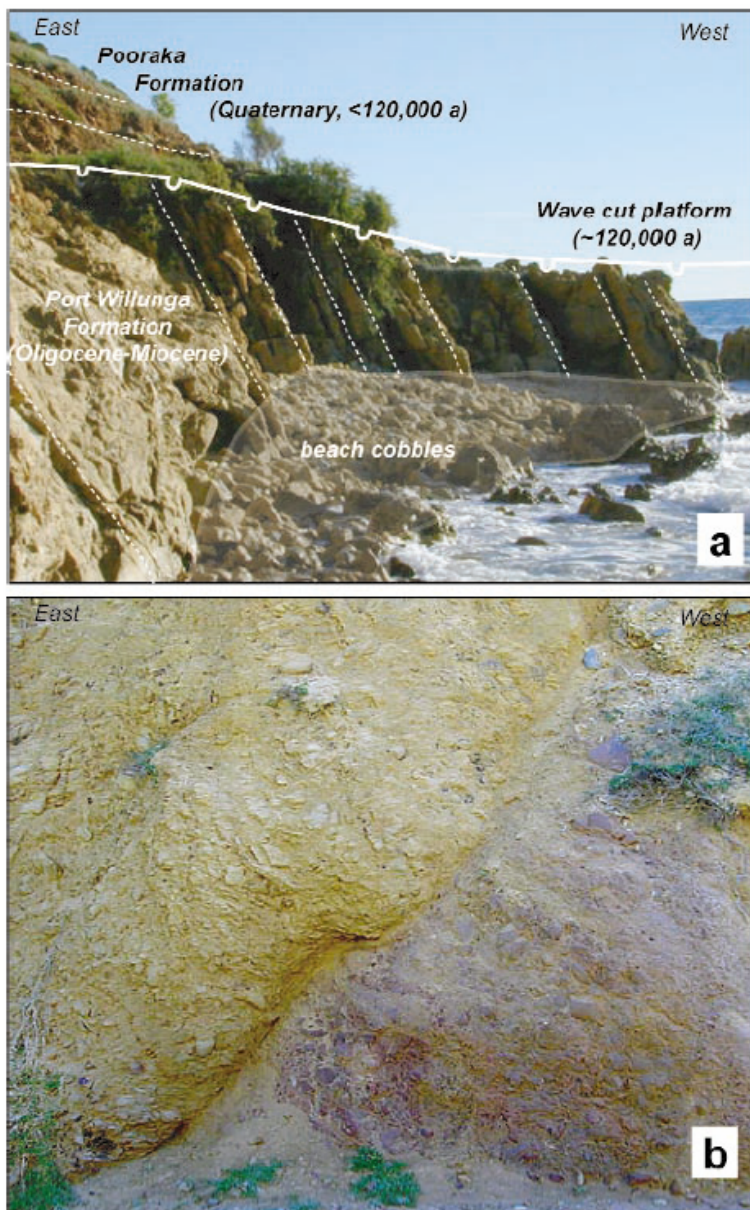


Figure 4. Willunga Fault locality at Sellicks Beach, Fleurieu Peninsula (AMG 262400E 6082900N Zone 54). (a) ca 120 ka BP wave-cut platform some 4–5 m asl in steeply dipping Oligocene – Early Miocene limestones of the Port Willunga Formation overlain by boulder conglomerates of the Pooraka Formation in the footwall of the Willunga Fault. Field of view is ~18 m across. (b) Inferred splay of the Willunga Fault showing reverse fault motion within brecciated Cambrian basement. Field of view is ~3 m across. In both cases the view is to the south-southwest (reproduced from Sandiford 2003a. Copyright © Geological Society of Australia 2003).

2.2 Day 1 Stop 2: Rose Hill

John Wilford

2.2.1 Background

Recent work in the Adelaide Hills has led to a greatly improved understanding of the inter-relationships between regolith, rainfall, salt stores and salinity processes in the central Lofty ranges. The research specifically led to the identification of major salt stores and regions within catchments where salt are being mobilised. This had not been done before.

This work has had a direct influence in developing remedial plans for salinity management in the region. For example Rural Solution SA has incorporated key components of CRC LEME's work into a new salinity/revegetation plan for the Bremer-Barker catchments in the Mt Lofty Ranges.

The research has also led to additional state funding to extend the initial project to incorporate the whole of the Lofty Ranges. This study has involved mapping deep weathering zones across the eastern Mt Lofty Ranges (from Fleurieu Peninsula to Nuriootpa). Products from this work are now being assessed.

2.2.2 Identifying areas of deep weathering and its relationship to salinity.

At this stop (Figure 5) we will visit a landscape that contains both very highly weathered to slightly weathered bedrock. Deep weathering over the Lofty Ranges is mainly associated with a partly-preserved, low relief, palaeosurface that developed prior to and during regional uplift forming these uplands. More recent tectonic activity resulting in faulting, uplift and associated erosion of the palaeosurface has formed a complex landscape mosaic where highly weathered landforms are juxtaposed against youthful ones exhibiting little regolith development. Stop x represents one of these complex landscape mosaics. Regolith on the palaeosurface typically includes mottled, kaolinised bedrock that is often ferruginous in the upper part of the profile and may be locally covered by colluvial and alluvial sediments.

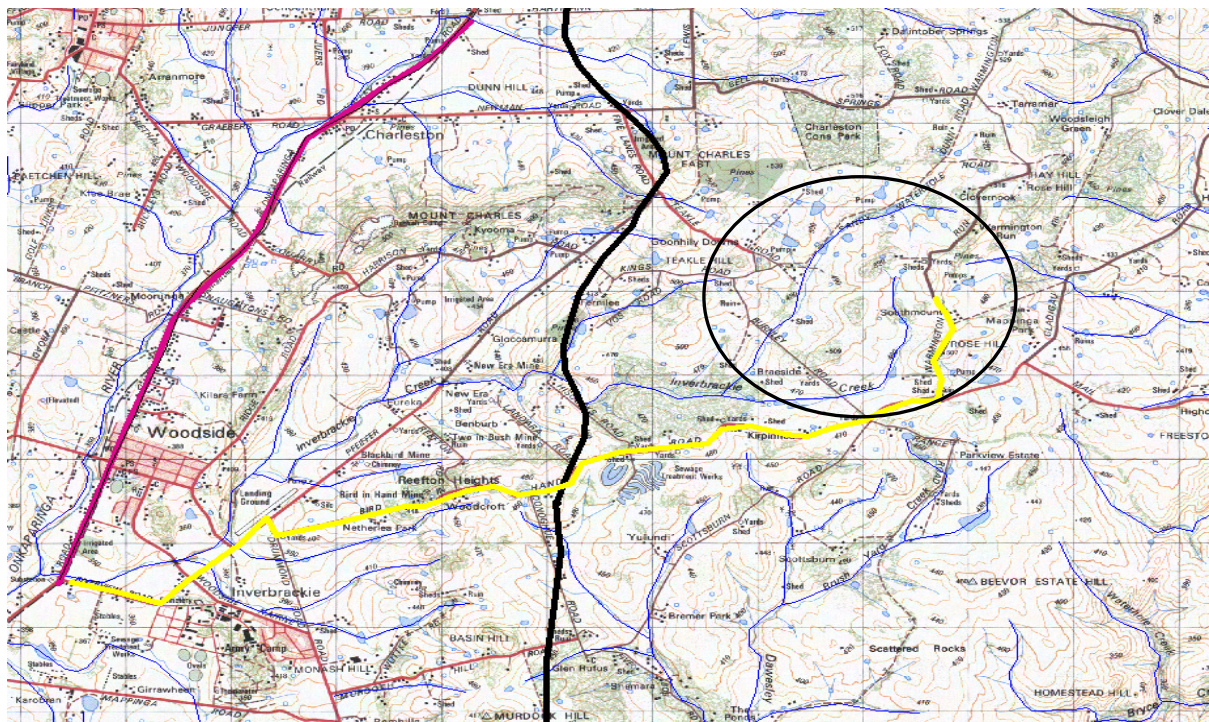


Figure 5. Rose Hill study area, from Adelaide 1:100 000 topographic sheet (6628)

The characteristics, age and distribution of these deeply weathered palaeo-landforms are intrinsically linked with the complex geomorphic, tectonic and weathering evolution of the region. As a result, the region has generated considerably scientific interest with numerous publications describing the landform evolution. Many papers describe differing views on the origin and age of the palaeosurface (e.g. Fenner 1930, Sprigg 1945, Campana 1958, Ward 1966, Alley 1977, Daily *et al.* 1974, 1979, Twidale & Bourne 1975, King 1976, Twidale 1976, 1994, Milnes *et al.*, 1985, Tokarev *et al.* 1999; Bourman & Lindsay 1989, Bourman *et al.* 1987, Bourman 1993, 1995).

2.2.3 Mapping regolith using gamma-ray spectrometry

These highly weathered areas have been identified using recently flown airborne gamma-ray imagery. A residual modelling approach has been used to separate regolith and bedrock radioelement responses. This approach uses a DEM-generated slope grid, geological polygons and individual radioelement grids (K, eTh and eU). The slope grid is used to partition areas in the landscape with relatively high slope angles and inferred shallow regolith. All pixels in the image corresponding to a $\geq 6^\circ$ slope threshold (based on field transect observations) for each geological unit were averaged to give an inferred bedrock mean. These values were then subtracted from each pixel in the original image to generate residual grids for K, eTh and eU. Radioelement values centred on the mean are inferred to reflect a bedrock response or thin soils over bedrock whereas deviations from this value are used to highlight regolith materials.

The residual grid for K was most effective at delineating areas of deep weathering. This is because K is a common component of rock-forming minerals in the area and is usually readily leached during weathering from the upper part of the regolith profile. In contrast Th and U generally increase in concentration during weathering due to their association with iron oxides and clays (Figure 6).

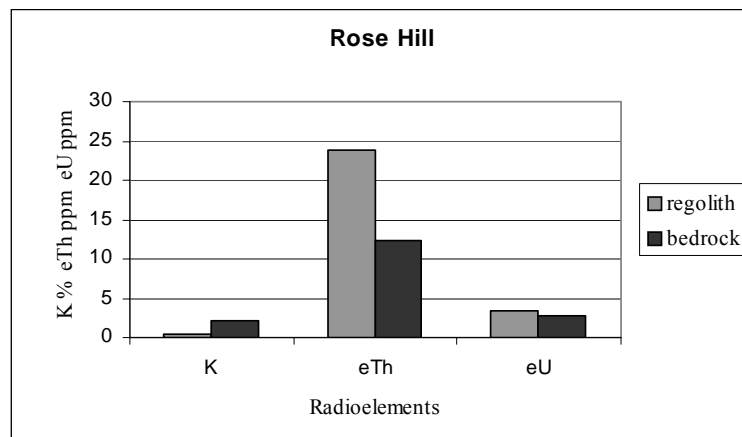


Figure 6. Radioelement responses of bedrock and regolith materials from the Rose Hill area

However, this approach will not work in K-deficient bedrock or where K is retained in the weathered zone (e.g. bonded within illite clays). These limitations need to be considered when interpreting the results or when applying such a methodology to other regions. Ground validation of the residual imagery is therefore an essential prerequisite governing the effective application of this approach.

The residual approach has been applied over the central part of the Mt Lofty Ranges and has identified weathering profiles up to 45 m deep, even though gamma-rays are only emitted from soil and bedrock to maximum depths of ~30 cm (Wilford 2004). It therefore follows that zones of ferruginous/leached soils and highly weathered bedrock detected by the K-residual approach are diagnostic in many places of much deeper weathering. This suggests that there is a relationship between the intensity or degree of surface weathering and weathering depth.

Part of the K-residual image and corresponding geological map over the Rose Hill area are shown in Figures 7 and 8. Potassium concentrations in the area are highly variable and largely reflect different degrees of bedrock weathering. Red hues correlate to slightly weathered and partly-exposed bedrock with surrounding thin soils (K values \approx inferred bedrock mean). Blue hues correlate with zones of deep weathering and ferruginised soils (K values $<$ inferred bedrock mean). These ferruginous soils are typically highly leached and acid and nutrient poor.

Landforms associated with these deeper weathering profiles tend to have low amplitudes, low stream gradients and broad valley profiles. These landform characteristics are thought to be the remnants of a palaeoplain that was subsequently disrupted by faulting/uplift associated with the formation of the Mt Lofty Ranges. As indicated by the K-residual image (Figure 7) regolith depths over the palaeosurface are quite variable. This may reflect partial erosion of the palaeosurface and/or the inherent variability of the weathering front created by localised differences in landscape position, bedrock type and structure.

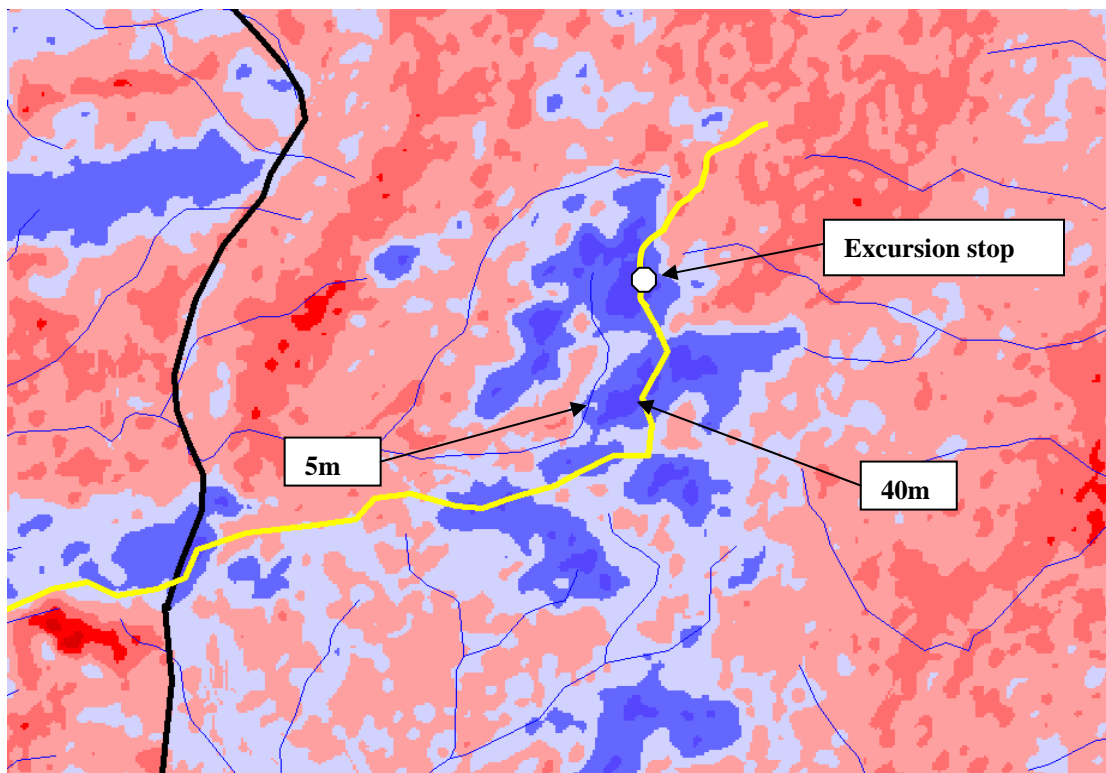


Figure 7. K-residual image, Rose Hill area, 4 km across, with depth to saprock in drillholes Red = slightly weathered bedrock. Blue = highly weathered bedrock. Black line is a major change in geology (see Figure 8)

2.2.4 Deep weathering and tectonics

Uplift of the ranges was expressed as a series of tilted blocks bounded by prominent scarps (Fenner 1930, Sprigg 1945, Tokarev *et al.* 1999). Quaternary faulting associated with these features has been documented by Bourman & Lindsay (1989) and Sandiford (2003a). The development of these structural zones, coupled with rapid drainage incision appears to have significantly influenced distribution or preservation of the palaeosurface. Deep weathering associated with the palaeosurface is preserved on both the upper (often coincident with drainage divides) and lower parts of the tilt blocks (Figure 9). Deep weathering on the palaeosurface is now being removed by headward erosion associated with a series of erosional scarps. In many places these scarps correspond to stream knickpoints.

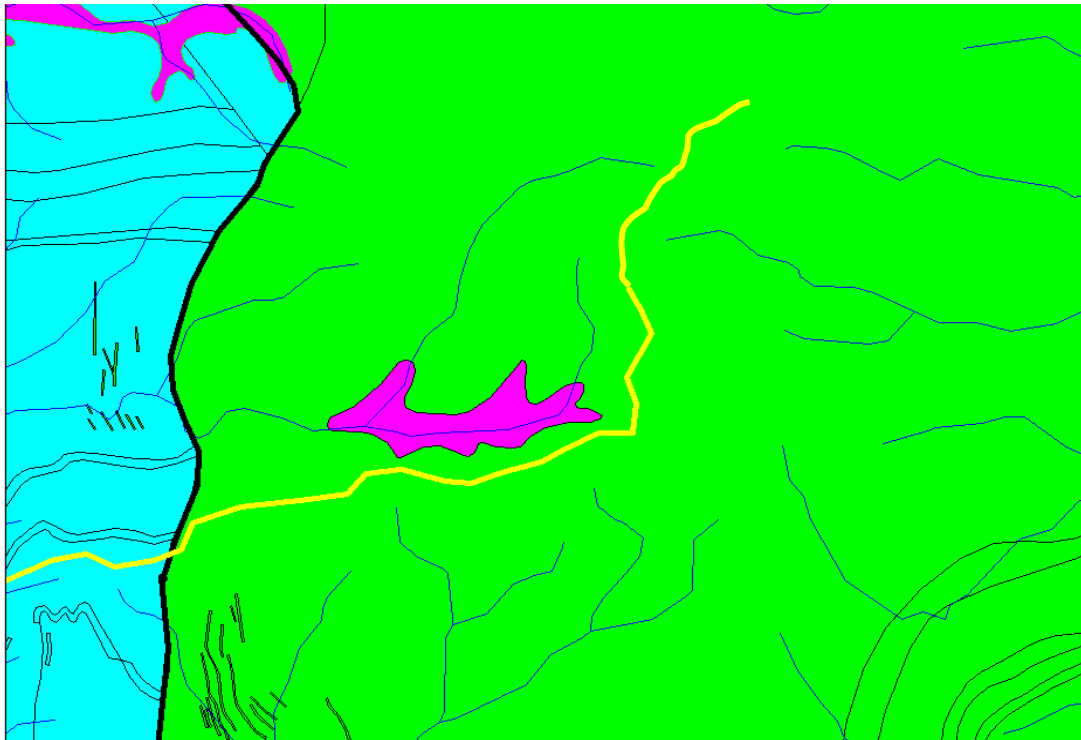


Figure 8. Locality geology, Rose Hill area. The Backstairs Passage Fm (green) consists mostly of meta-sandstones and meta-siltstones; Tarcowie siltstone (blue) and Quaternary alluvial and colluvial sediments (purple). Thick black line separates Neoproterozoic sediments (left) from Cambrian sediments (right).

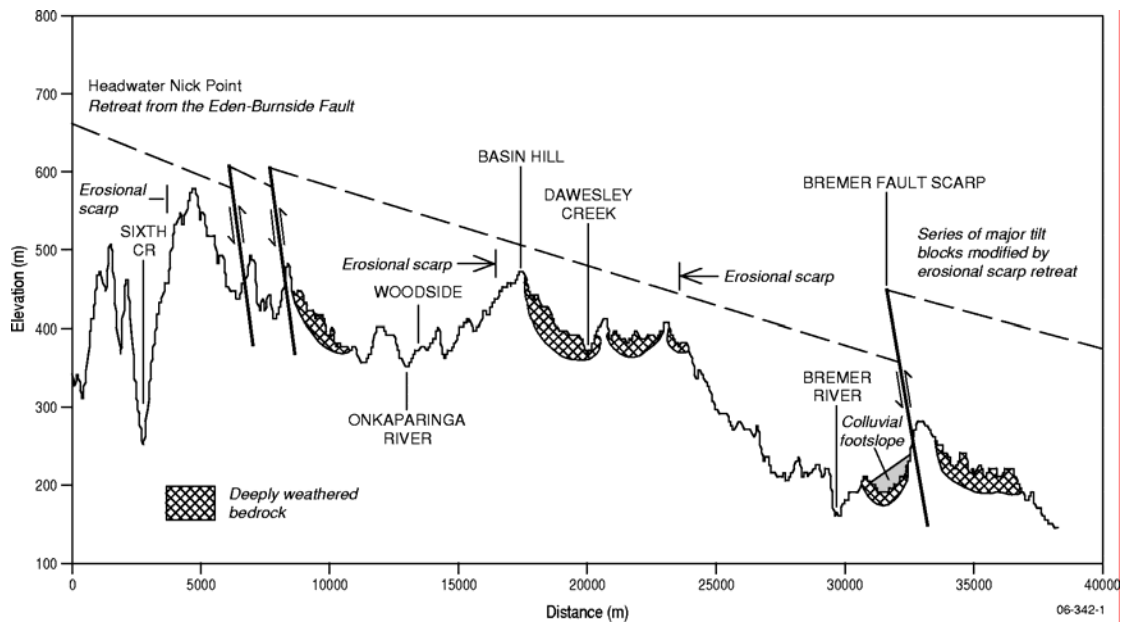


Figure 9. Topographic cross section highlighting zones of deep weathering, faults and associated tilt blocks, Mt Loft Ranges. Local erosional scarp retreat is progressively removing the deep weathering associated with the palaeosurface. The portrayed thickness of weathered materials is schematic and not to scale.

2.2.5 Deep regolith and salinity

These zones of deep weathering act as sluggish hydrological ‘sponges’ and through evapotranspiration form favourable sites for accumulation of both cyclic and bedrock weathering-derived salts. Weathering increases the capacity of the landscape to store salts because clays generated by the breakdown of primary rock minerals generally have much higher porosities and lower permeabilities than the original bedrock. Highly weathered regolith provides a deep substrate that allows evapotranspiration processes to concentrate salts within the profile. Relatively low hydraulic conductivities associated with clay-rich substrates also reduce the rate at which salts can be flushed from the profile. In addition, relatively low stream gradients and the subdued landform expression typical of these highly weathered palaeo-landscapes have lower groundwater transmissivities compared with less weathered landscapes which normally exhibit steeper valley profiles and hydraulic gradients. The latter characteristically have thin soils over fractured bedrock and consequently, are likely to have relatively high recharge rates with less time available for salts to be concentrated by evapotranspiration processes.

While regolith thickness and composition may determine the capacity of the landscape to store salts, rainfall largely determines the rates of recharge and groundwater fluxes. This in turn governs the concentration of salts in the profile. The influence of rainfall on the salt storage is particularly evident in the Mt Lofty Ranges due to the sharp orographic rainfall gradient that extends across the Ranges. The largest salt stores are in thick regolith on the drier (<400mm average annual) eastern side of the Mt Lofty ranges, whereas the highest salt exports are associated with thick regolith and high rainfall on the western side (>1000mm average annual). Rainfall at Rose Hill is somewhere between these ranges at approximately 700mm.

For a local area with uniform rainfall the highest stream salinities (based on stream EC) are associated with sub-catchments that are deeply weathered. The stream salinities tend to decrease on passing through areas with a shallow regolith cover (Figure 10). The most abrupt change in stream salinities are associated with valley knickpoints as these often separate weathered from less weathered parts of the catchment.

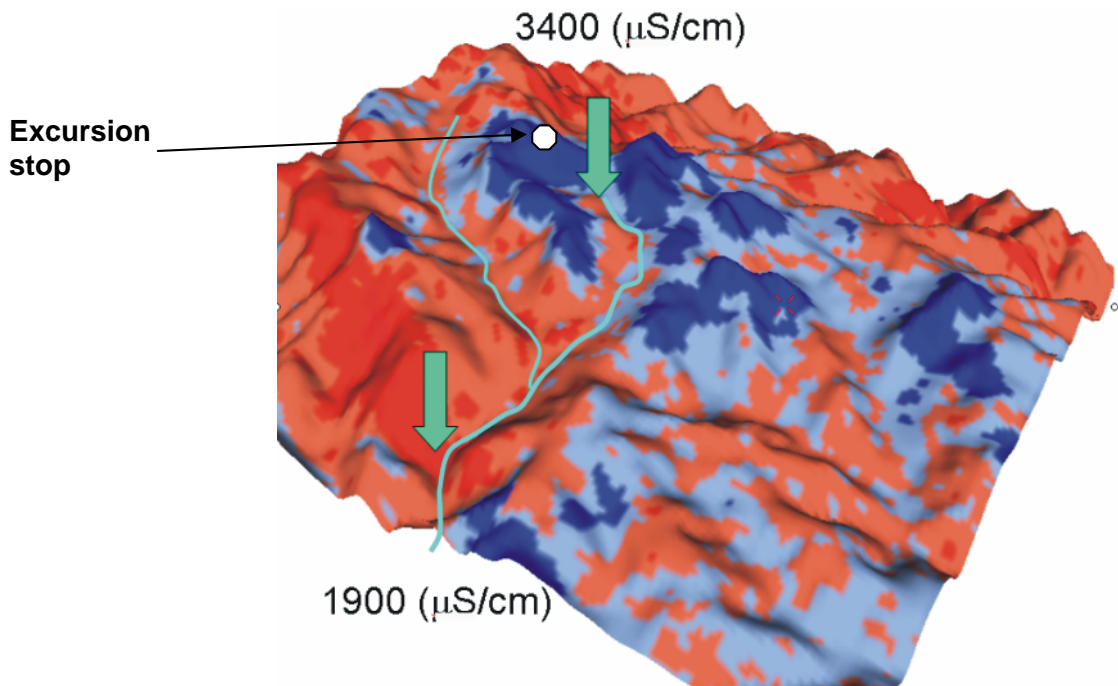


Figure 10. K-residual image draped over a DEM, Rose Hill area. Higher stream salinities correspond to sub-catchments dominated by thick regolith (Blue image response).

Information on regolith thickness, salt storage and relationships between rainfall and accumulation/leaching of salts in the regolith can now be used to target revegetation activities to reduce recharge in sub-catchments with high salt storages and salinity exports (Wilford, 2004).

2.3 Day 1 Stop 3: Milendella Fault at Cambrai, eastern Mt Lofty Ranges

Mike Sandiford

(text reproduced from Sandiford 2003a)

The Milendella Fault (Figures 2, 11) is exposed in two ~8 m-high, undercut creek-bank sections near Cambrai (Bourman & Lindsay 1989) (Figure 12a, b). The fault is defined by a west dipping thrust at the foot of the Milendella scarp, which has a total topographic relief of ~250–300 m from ~380–400 m asl at its crest to 160 m asl at the exposed fault trace to ~80–100 m at the base of the footwall pediments (Figure 12b). The fault juxtaposes metamorphosed Cambrian rocks of the Kanmantoo Group in the hangingwall above a footwall comprising a Lower Miocene limestone (the Mannum Limestone) and a Quaternary sequence comprising mottled ferruginous clay interbedded with coarse conglomerate. The Mannum Limestone, which outcrops as disrupted, rotated and locally overturned lenses, consists largely of bryozoal fragments with a minor (~5 vol%) clastic component. The Quaternary sequence includes a distinctive mottled clay resembling the Ochre Cove Formation (Ward 1966) that elsewhere has been shown to contain the Brunhes–Matuyama palaeomagnetic reversal at ca 780 ka BP, interbedded with angular conglomerates. The total post- Early Miocene throw on the Milendella Fault is at least ~60–90 m, based on the differential displacement of Mannum Limestone in the footwall sequence between the scarp and exposures of stratigraphic equivalents along the Murray River. A slightly greater minimum displacement is indicated further south, in the Bremer valley, where Middle Miocene (ca 16 Ma) *Lepidocyclina*-bearing Mannum Limestone is reported at ~170 m asl, about 160 m above the elevation of the nearest equivalent exposures some 23 km to the northeast in the Murray Basin (Lindsay 1986). Siliciclastic debris in the Mannum Limestone adjacent to the scarp suggests that deposition occurred close to the Miocene shoreline, and thus some of ~300 m present-day relief across the scarp is likely to have pre-dated the Early Miocene. At Cambrai, the Quaternary sequence is reported to have a thickness ~30 m (Mills 1965). The exposure shows that the fault places basement above the entire Quaternary sequence, implying a minimum displacement over the last ~1 million years of at least 30 m.

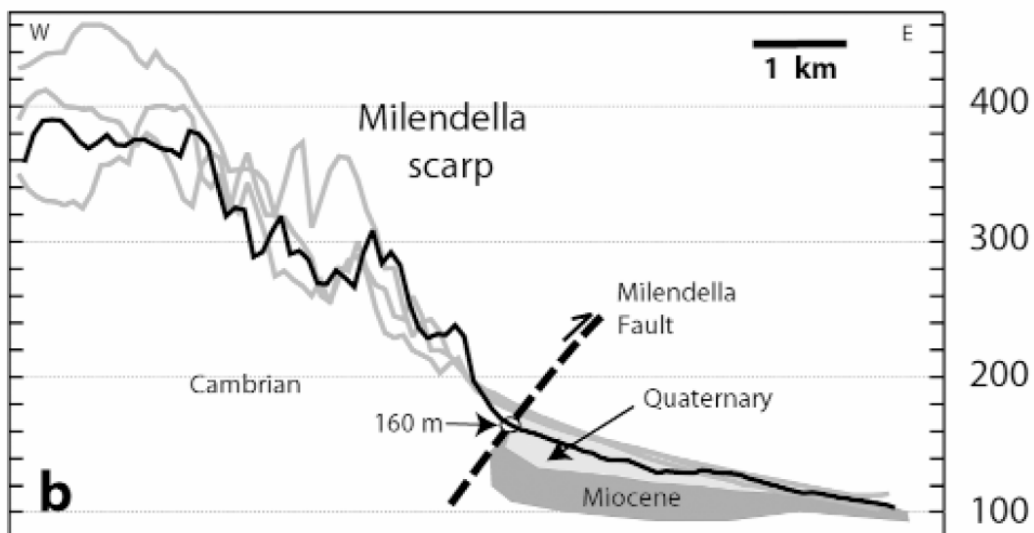


Figure 11. Topographic profiles and stratigraphic relationships across the Milendella scarp. Original data from DENR 100 m DEM shown in Figure 2. Stratigraphic thicknesses and extent are only approximate (reproduced from Sandiford 2003a. Copyright © Geological Society of Australia 2003).

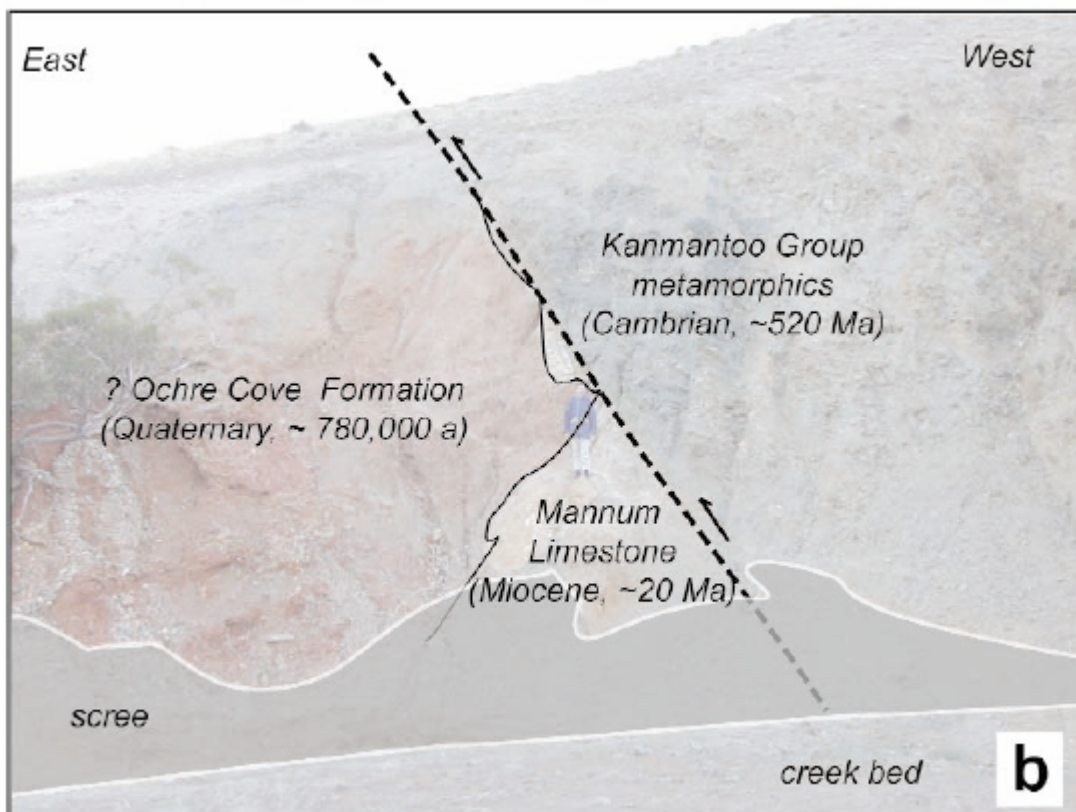


Figure 12. Photograph (a) and outcrop interpretation (b) of the Milendella Fault exposure near Cambrai, in the eastern Mt Lofty Ranges (AMG 338800E 6165900N Zone 54), first described by Bourman & Lindsay (1989). The view is looking south along the north–south-trending fault (reproduced from Sandiford 2003a. Copyright © Geological Society of Australia 2003).

3. DAY 2: MURRAY BRIDGE TO NARACOORTE



Figure 13. Day 2 route map, stops 1 and 2

3.1 Day 2: Late Tertiary to Quaternary faulting in the Strathalbyn area

David Gibson

3.1.1 Bremer Fault

This is well known north of the Strathalbyn area as a major north-trending structure. Its eroded scarp forms the steep eastern side of the asymmetric Bremer River catchment (Figure 2). The Angas Bremer Plains DEM (Figure 14) shows that a degraded west-facing scarp continues about 15 km into the Murray Basin area, disappearing about 12 km from the northern shore of Lake Alexandrina. In the north of the geophysics area, the fault displaces Pliocene barrier dunes, with offset of ~25 m vertically on the tops of the dunes. Further south, a low relief landscape mantled with Quaternary longitudinal dunes is offset by about 10 m (east side up), with the displacement fading to the south.

A combination of drill hole data and AEM imagery (Figures 15 and 16) show that in the subsurface, the basal unconformity of the Murray Basin (overlain by Eocene sediments) is offset by up to 100 m, but any sign of the offset fades out a few km south of the limit of the surface expression of the fault.

The varying offset of different age units shows that the fault has had a history of geologically recent movement spanning possibly back to the Early Tertiary, and continuing into the Quaternary, with approximate vertical movements of up to 75 m between Eocene and Pliocene, 15 m between Pliocene and the formation of the depositional surface (probably alluvial) on which modern longitudinal dunes have formed, and 10 m since formation of that surface.

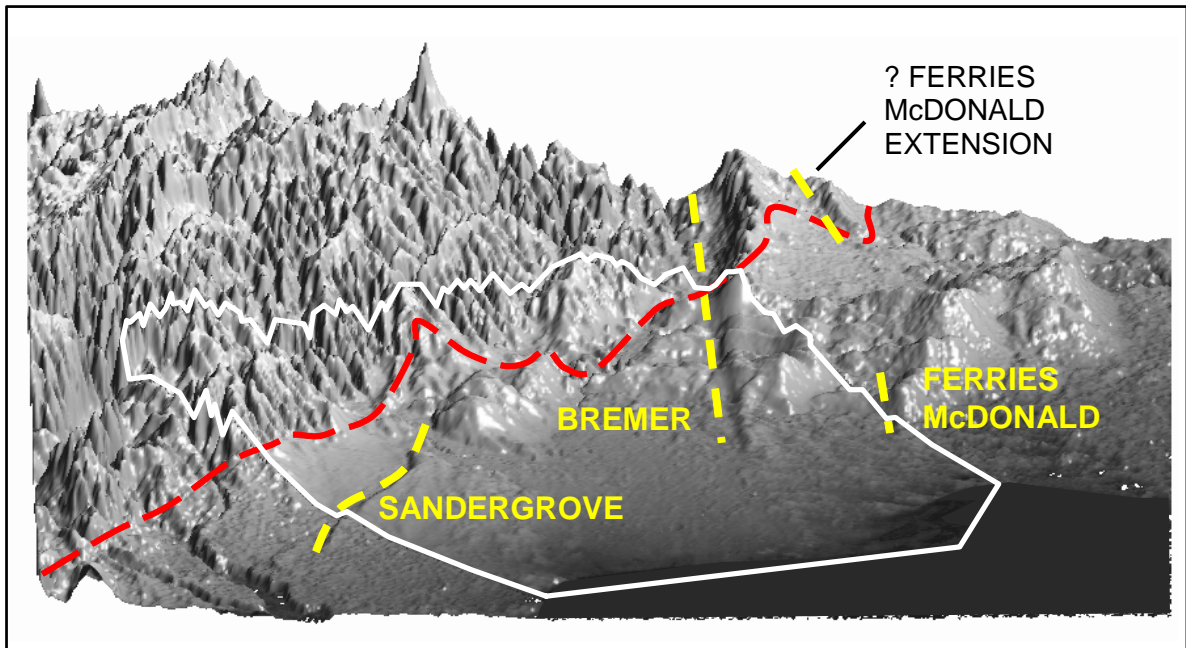


Figure 14. Northward oblique view across the Angas Bremer geophysics area (from airborne radar sensor, inside white boundary, maximum elevation 334 m) and SRTM 90 m DEM, with edge of Murray Basin in red and fault scarps in yellow. White box is ~37 km E-W and 33 km N-S. Geophysics flight lines oriented NE-SW inside white box.

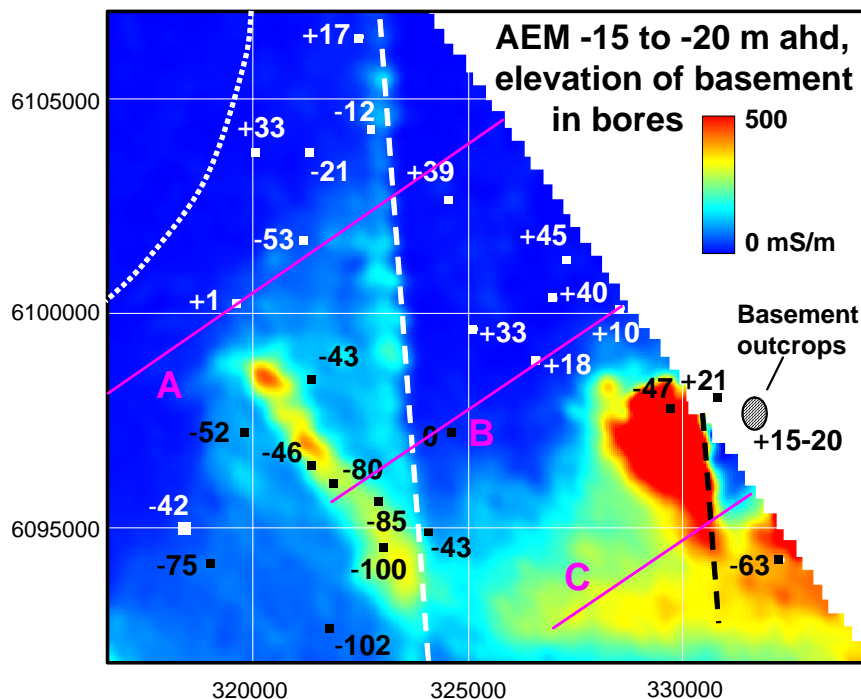


Figure 15. Horizontal AEM slice (-15 to -20 m elevation AHD) annotated to show elevation of basement in bores, Bremer and Ferries McDonald Faults (white and black), and flight line sections in Figure 16 (purple). The basement surface dips to the SE, and has been offset by the north-trending faults.

The Bremer River flows close to the fault angle depression north of the area. However, it leaves the close proximity of the fault near the northern edge of the study area, to flow along the surface trace of the basement/Murray Basin unconformity for around 12 km before debouching onto a broad alluvial plain. Movement of the fault does not appear to have influenced the position of the River within the study area. However, there are some closed depressions (~12 m of closure relief) immediately west of

the fault scarp in the area of Pliocene dunes (Figure 17). These may be depressions formed during the dune forming process, but it is considered more likely that they are sunklands formed due to downwarp of west-trending valleys close to the fault.

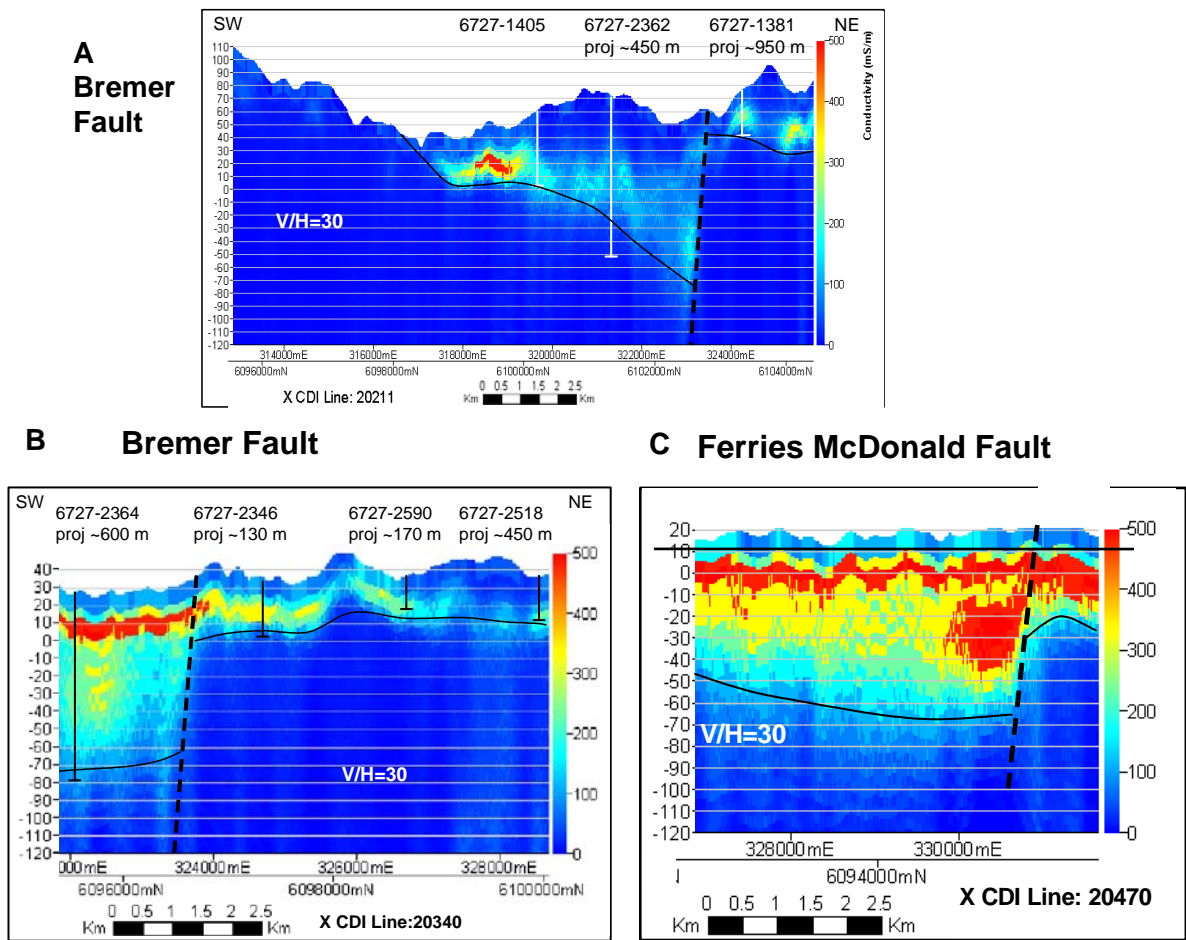


Figure 16. AEM flight line sections across Bremer and Ferries McDonald Faults annotated with drillholes with depth to basement and interpreted approximate location of faults and basement/Murray Basin unconformity.

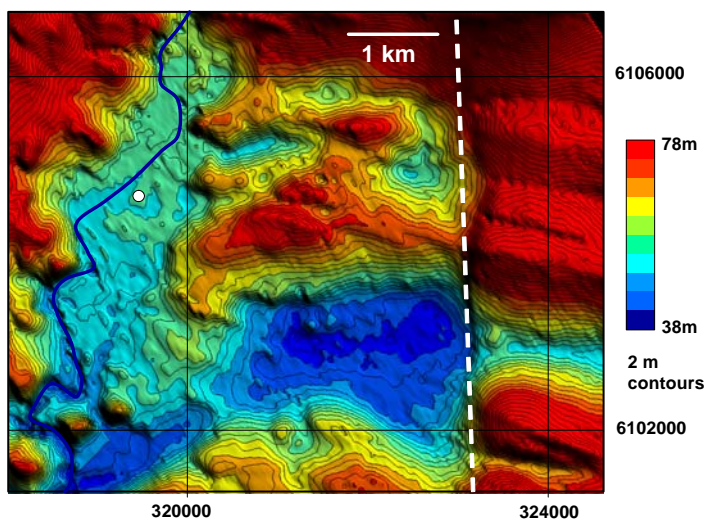


Figure 17. DEM with 2 m contours showing closed valleys immediately west of the Bremer Fault (white dashed line). Bremer River shown by solid blue line.

3.1.2 *Ferries McDonald Fault*

This fault was first described by Gibson (2004). A short low scarp on the DEM suggests a possible north-trending fault about 7 km east of the Bremer Fault at the margin of the Angas Bremer Plains Geophysics area (Figure 14). A pair of drillholes on either side of the possible structure and the AEM data show that the base of the Murray Basin sequence is offset by up to 70 m, west side down (Figure 15). There is also outcrop of basement on the upthrown block, just outside the geophysics area. The section in Figure 16 suggests that the offset reduces to the south. The fault scarp cannot be traced further north on the SRTM DEM as it has been obliterated by a major alluvial valley eroded through the Pliocene dunes. However, the SRTM DEM (Figure 14) shows a possible west facing fault scarp east of the Bremer Fault about 15 km to the north, and this could be an extension of the Ferries McDonald Fault.

3.1.3 *Sandergrove Fault*

The 10-15 m high northwest facing scarp of this fault (Figures 14, 18) was previously considered to be the rear of a Pleistocene shoreface dune (Maud 1972), or a purely erosional feature (S. Barnett, Dept of Water, Land and Biodiversity, pers comm. 2003). The AEM shows a resistor immediately southeast of the scarp, and a conductor to several tens of metres depth to the northwest (Figure 18B). Drillholes show that the conductor comprises Tertiary and Quaternary sediments with brackish water, and the resistor is basement. A line of drillholes (including 3 drilled by CRC LEME to help with validation of the AEM) along a NanoTEM line (Figure 19) show the broad geometry of the rock units around the fault. The basement unconformity appears to have been offset by about 60m northwest side down. However, the geometry of the sediment units indicates that this displacement occurred over a period of time, with the early Pleistocene clastic unit overlying Miocene limestone offset by a lesser amount. The geometry also requires complete erosion of the limestone from the area close to the upthrown side of the fault, prior to the onset of clastic deposition.

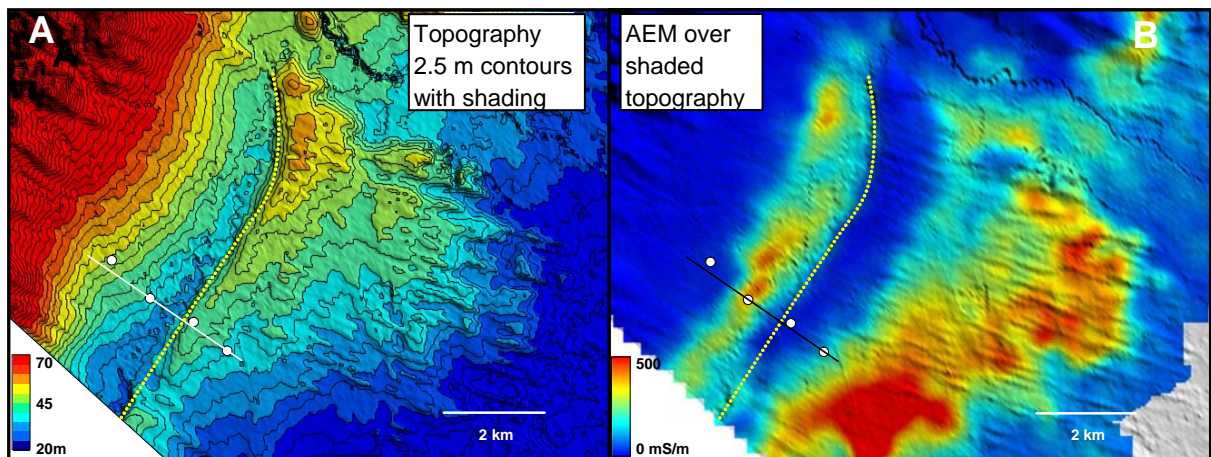


Figure 18. A. Shaded DEM with 2.5 m contours showing scarp of Sandergrove Fault (yellow dotted line). The channel of the River Angas appears as a series of sharp depressions in the NE of the scene. Drillholes and NanoTEM section in Figure 19 shown as white dots and line. B. AEM conductivity slice for +20 to +15 m elevation AHD showing resistive basement southeast of the fault and conductive water-bearing sediment to the northwest.

The DEM suggests that the scarp has a maximum slope of about 4° , not steep when compared with many other neotectonic features. However, it is probable that aeolian sediments have aggraded to the scarp, or that the Tertiary sediment capping the scarp has been eroded by wind. The long shallow slope down to the River Angas alluvial plain hosts low longitudinal sand dunes which appear to have been sourced from Sandergrove Creek, which runs along the fault angle depression. The DEM and radiometrics also show that Sandergrove Creek may also act as a floodwater distributary of the River Angas (Figure 20).

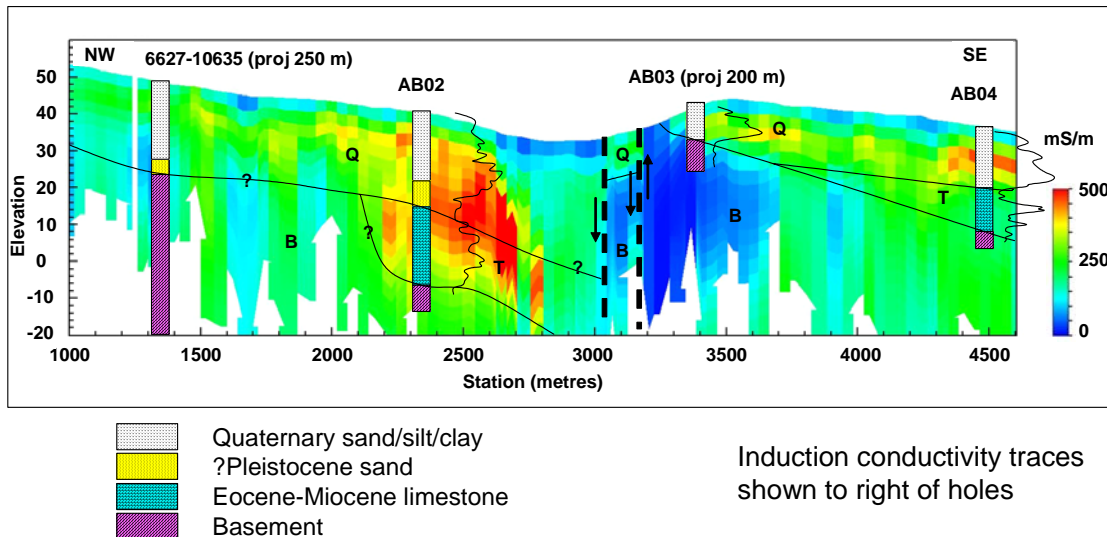


Figure 19. NanoTEM traverse across the Sandergrove Fault, with drillhole control.

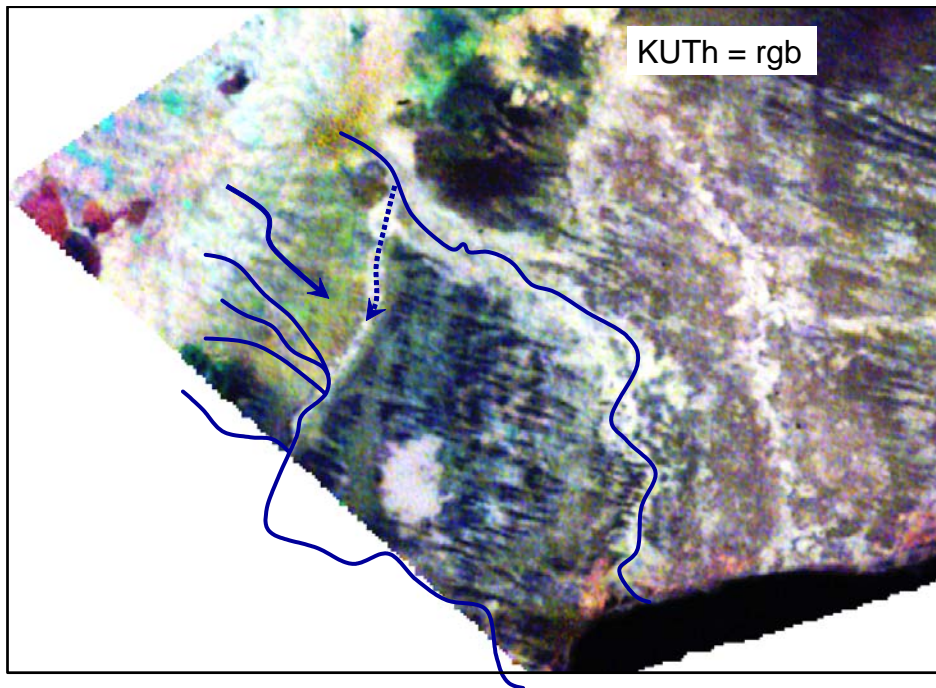


Figure 20. Radiometric image showing continuity of high response alluvium (white) from Angas River into the valley of Sandergrove Creek, suggesting it acted as a flood distributary for the Angas.

The Angas has eroded an antecedent valley across the rising fault scarp, but not smaller streams flowing from the hills to the northwest, which join Sandergrove Creek which flows along the fault angle depression. Since erosion of the antecedent valley, alluviation of the Angas valley has continued to a point where floodwaters can spill into the headwaters of Sandergrove Creek. It is probable that the Angas has increased its channel size since settlement, and that flooding does not now happen across the alluvial plain in this area..

The Sandergrove Fault probably continues to the northeast under the alluvial plain of the River Angas (Figure 21). A narrow conductive AEM band east of Strathalbyn may mark the northeast extension of the fault. A single drill hole in this band encountered 26.5 m of sand and gravel, in an area previously mapped as basement. Exposures in nearby ridge-top quarries suggest that the sediment is of Tertiary

age, underlying Miocene calcarenite (see Day 2 Stop 2). My interpretation is that this band of conductive sediment could either be downfaulted by the Sandergrove Fault, or may have been deposited in a Tertiary palaeovalley etched along weathered rock along the trace of the fault. The second explanation does not require Cenozoic movement along this part of the fault.

As the postulated extension of the fault passes within 2 km of Strathalbyn, and 1 km from the Rankine zinc deposit (930 000 tonnes @ 20% Zn) which is presently undergoing mining feasibility studies, there is some cause for concern for urban and mining infrastructure.

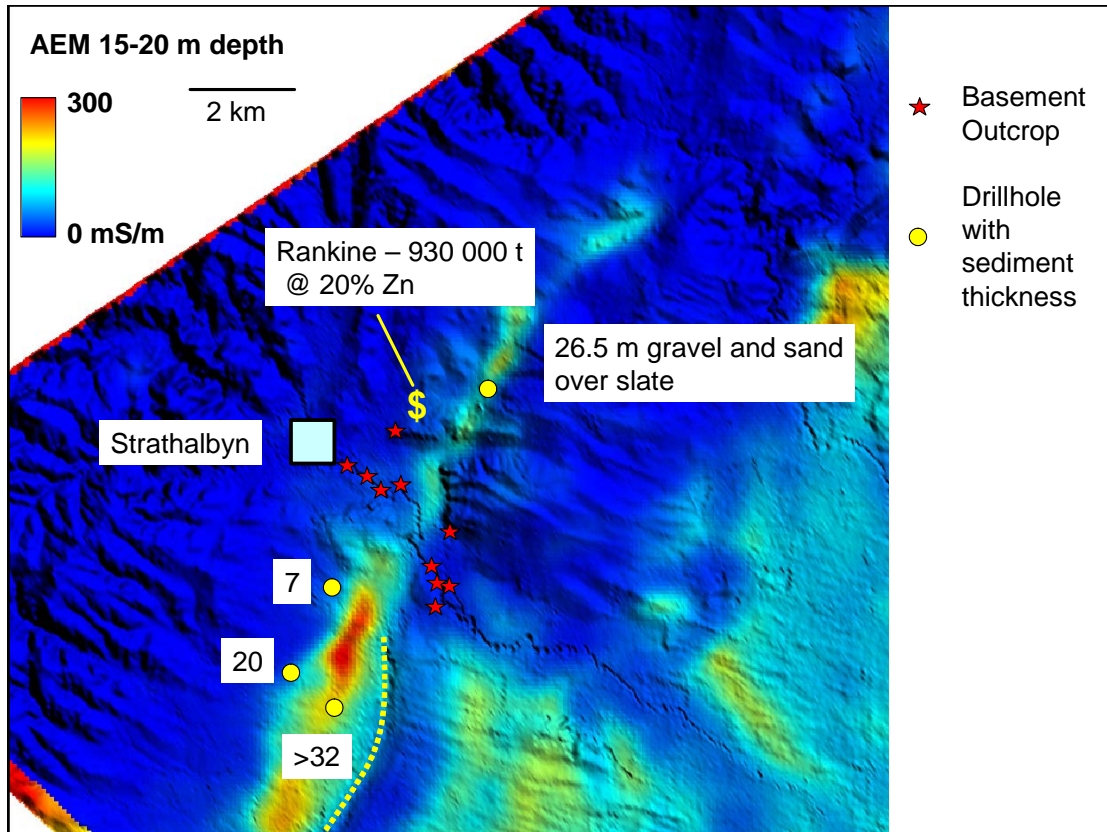


Figure 21. 15-20 m depth AEM slice over shaded DEM, with location of Sandergrove Fault scarp (yellow dotted line), drillholes and basement outcrops, showing a narrow conductive band of sediment northeast of the River Angas that may mark an extension of the fault.

3.2 Day 2 Stop 1: Sandergrove Fault

Strathalbyn to Sandergrove. Travel southwest from Strathalbyn on the Goolwa road, along the margin of the Murray Basin. In this area, the margin is onlap with sediments thickening to the SE, not faulted as at the Marne site visited on day 1. The 15 m high Sandergrove fault scarp is about 5 km to the SE of the road, parallel to the edge of the basin. However, it is difficult to see at this distance. About 7 km from Strathalbyn we turn left onto a dirt road which runs southeast towards the scarp. At the foot of the scarp we cross the small channel of Sandergrove Creek, and climb to our stop near the top of the scarp at the junction of Dry Plains and Tucker Roads.

Drill hole AB03 was drilled immediately east of this intersection, on the north side of a stock route easement. This hole penetrated 10 m of sediment over fine sandstone/greywacke basement. The sediment is muddy (mostly 50-80% silt and clay, with minor rounded pebbles to 30 mm in the bottom metre). This sediment must have been sourced from the west, and thus must have been deposited at a time when there was no scarp expression of the fault.

Drill hole AB02 was drilled immediately southwest of a group of farm buildings a little over 1 km to the NW of the site. The elevation of this hole is about 3 m below AB03, but it intersected clastic sediment to 25 m, over Tertiary limestone to 47 m, then basement. Thus there is a shallow half graben of Tertiary sediment to the NW of the fault.

Drive back to Strathalbyn along roads at the top of the scarp, observing where the River Angas alluvial plain spills over into the headwaters of Sandergrove Creek.

3.3 Day 2 Stop 2: Garwood Quarry and Rankine Zinc Deposit

Jon Clarke and David Gibson

The Rankine Zinc Deposit (<http://www.terramin.com.au/angas.php>) is situated beneath sewage ponds on the north side of the Strathalbyn Callington road 2 km E of Strathalbyn, and is undergoing final design for underground mining. Immediately after leaving Strathalbyn, an outcrop of the unconformity between basement and bioclastic limestone of the Miocene Mannum Formation is present on private property on the south side of the road, at about 80 m elevation. The Mannum Formation continues as a plateau capping to the east of this locality, but quarries on the plateau have exposed a variable thickness of Tertiary clastic sediments beneath the limestone, and AEM and water bore logs suggest there may be Tertiary palaeovalley filled with clastic sediment in this area (Figure 21). This palaeovalley appears to have been eroded along an extension of the Sandergrove Fault, but here there is no sign of Cainozoic movement.

The portal for the mine will be excavated in the Garwood Quarry on the south side of the road. Here, the Cainozoic sediments consist of the calcareous Mannum Formation and a basal clastic succession (Figure 22).

The Mannum Formation is a widespread Oligo-Miocene unit of the southern Murray Basin. Its stratigraphy, palaeontology, and sedimentology have been extensively described in the literature. It is a well-burrowed grainstone rich in fossil molluscs, echinoderms, and bryozoan, deposited in a high energy environment forming a barrier to the Miocene epic sea that deposited the marine sediments of the Murray Basin (Lukasik *et al.* 2000, Lukasik and James 1998). The Mannum Formation is dominated by upward-deepening cycles (Lukasik and James 2003). In the Garwood Quarry the Formation disconformably overlies clastic sediments of variable thickness.

At the western end of the quarry, the Mannum Formation unconformably overlies quartz gahnite rock, associated with the zinc mineralisation. This is within the blue (resistive) area of Figure 21 south of the \$ symbol for the Rankine deposit. At the eastern end of the quarry, the base of the clastic sediments is not exposed. The sediments comprise an upper unit of fine-grained, very well sorted quartz sand with very steep large scale foresets, suggestive of aeolian deposition (Figures 22, 23, 24). This unit is disconformably underlain by a lower unit of burrowed, coarse, rippled to cross-bedded sands with silty clay drapes (Figures 22 & 24). The interlaminated sands and silty clays resemble flaser bedding associated with strongly tidal depositional regimes. *Thalassonoides* burrows indicate normal marine salinities. This locality is within the conductive strip in Figure 21 east-southeast of the symbol for the Rankine deposit.

The basal sediments are interpreted as being a lower tidal lagoon facies with near-normal marine salinities overlain by an aeolian barrier facies. Together with the Mannum Formation the sediments in Garwood Quarry are interpreted as representing a single marine transgression. No datable fossils are known from the clastics (although shark's teeth have been reported by the quarry operators) but they are inferred to be Oligocene in age and slightly older than the Mannum Formation.

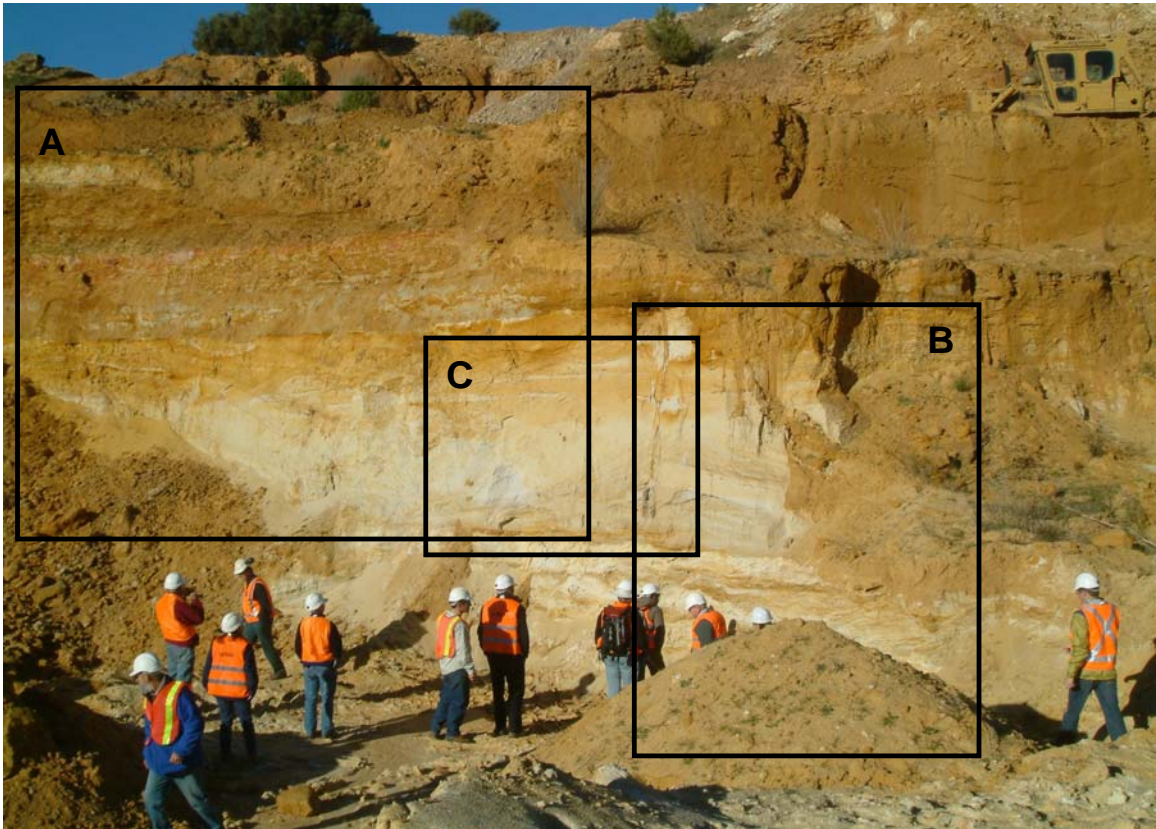


Figure 22. Eastern end of the Garwood Quarry showing Cainozoic stratigraphy. Box A is area described in Figure 23, Box B in Figure 24, Box C in Figure 25.

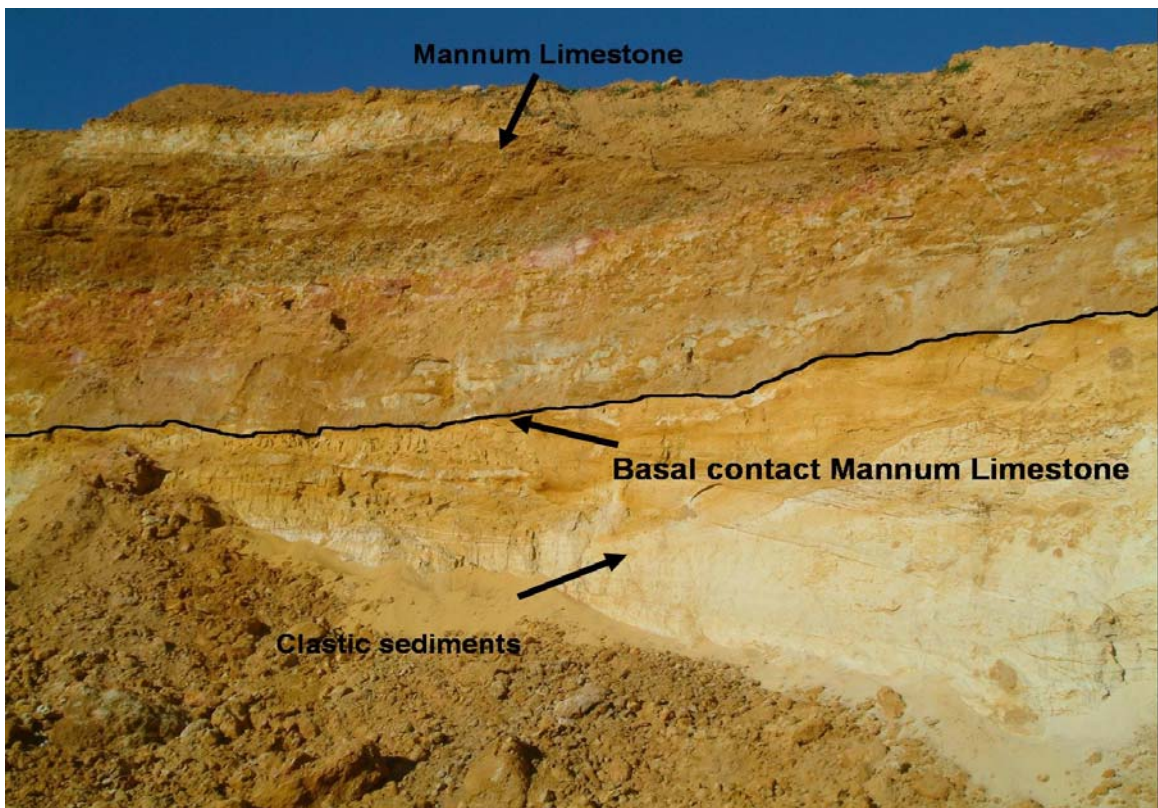


Figure 23. An irregular erosional contact separating the bioclastic Mannum limestone from underlying older Cainozoic clastic sediments.

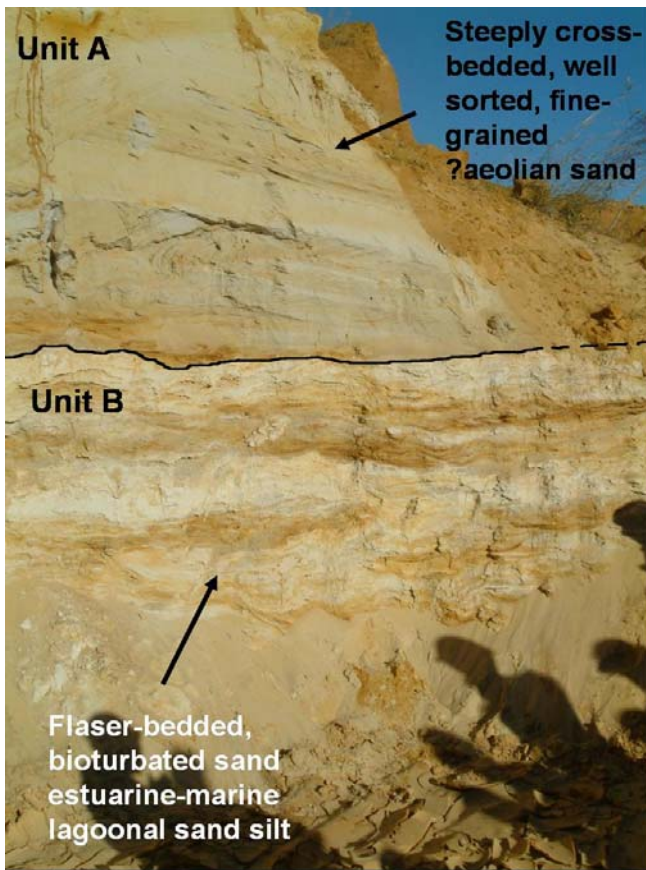


Figure 24. Erosional contact between interpreted lagoonal sands (unit B, lower) and aeolian sands (unit A, upper) in Garwood Quarry. Note large scale cross bedding in unit A.

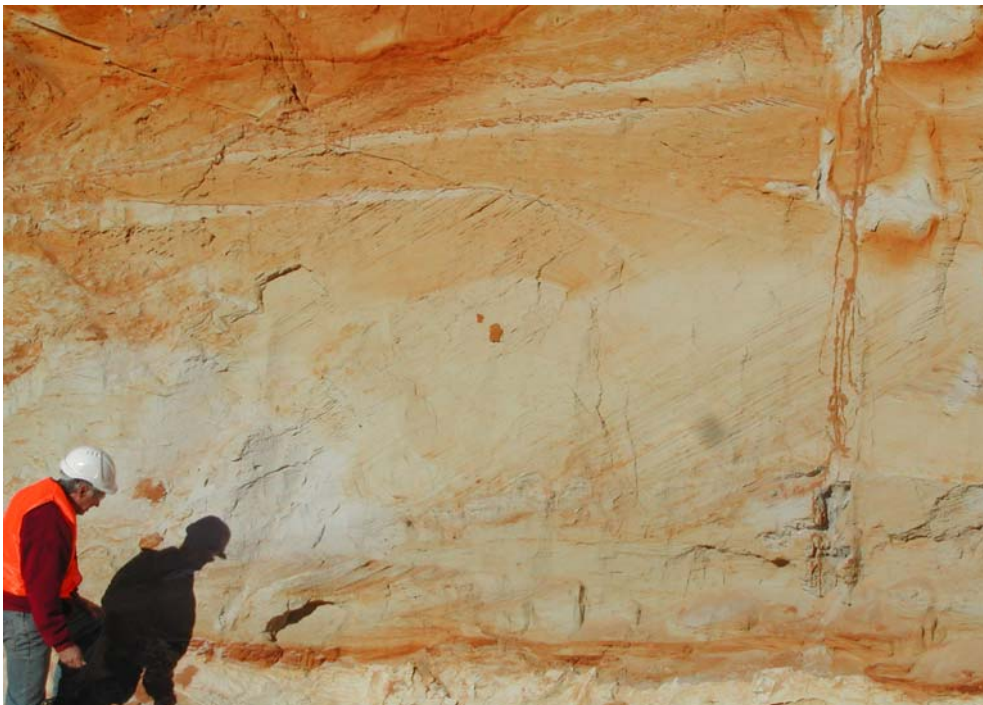


Figure 25. Detail of interpreted aeolian cross-bedded sands (unit B) in Garwood Quarry. The base of unit B is marked by the ferruginous band near the bottom of the photo.

3.4 Day 2: En route Strathalbyn to Wellington

The excursion route passes through vineyards of the Langhorne Creek area. Rainfall here is about 350 mm, and the original vineyards were flood irrigated using a series of levees and gates diverting natural flood waters of the Bremer River. There have been considerable new plantings, and good quality sub-artesian bore water from Tertiary limestone at 25-40 m depth was used for irrigation. However overproduction of water in the 60's-80s put strains on the aquifer, and raised a saline water table in the overlying alluvial sediment. Fresh water has been pumped from Lake Alexandrina, and great care was being taken by vineyard owners to not over-irrigate. However, drought and falling water levels in Lake Alexandrina have reduced the availability of lake water. The AEM survey and targeted water analyses show that the deep aquifer is being recharged by downward leakage from the Angas and Bremer Rivers through 20-30 m of Quaternary alluvium.

East of Langhorne Creek we pass into linear dunefields along the northern shore of Lake Alexandrina. Saline groundwater discharges in swales, forming small salinas. There is a commercial salt harvesting operation in a larger salina a few km to the north of the main road.

Wellington is the site of the first vehicle ferry on the Murray, established in 1846, and is site of a proposed weir to keep water levels in the lower reaches of the Murray at an elevation above the level of Lake Alexandrina.

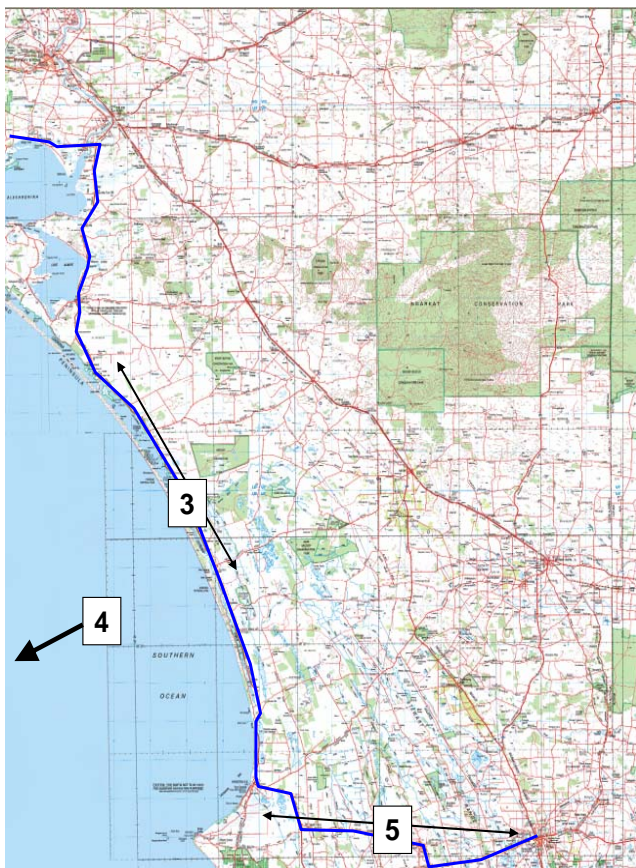


Figure 26. Day 2 route map, stops 3-5.

3.5 Day 2 Stop 3: The Coorong and lakes near Salt Creek

Patrick De Dekker

(Text reproduced from Belperio 1995)

The Coorong is a 130 km long, back barrier saline lagoon, created ~6000 years BP behind the evolving Younghusband Peninsula. It consists of a number of interconnected basins up to 4 km wide and 4 m deep that become increasingly restricted, hypersaline and ephemeral towards their southern end (Figures 27, 28, 29, 30, 31 & 32). Waters are derived from the ocean via the Murray Mouth, from the Murray River, and from seasonal rainwater and unconfined groundwater. Distinct seasonal fluctuations are superimposed on the marked salinity gradient. There is also a pronounced seasonal oscillation of water level of ~ 1 m that results in part from higher winter sea levels as well as the alternating dominance of winter rainfall and summer evaporation. Sediments of the Coorong lagoon consist of bioclastic magnesian calcite and aragonite sand and pelletal mud derived from the molluscs, ostracodes and foraminifera (Brown 1965). Cores indicate that the protected marine lagoon became increasingly restricted as sedimentation progressed, and hypersaline conditions subsequently developed in the southern half of the lagoon. Aragonitic mud characterises the seasonally exposed lagoon floor. Drainage channels constructed to the south of The Coorong have stopped the overflow from swamps reaching the lagoon in years of heavy winter rainfall and may have accentuated the trend towards hypersalinity.

Holocene coastal uplift has resulted in ~1 m of relative sea level fall, a factor that has compounded the effects of regressive sedimentation. As a result, at its southern end, the ephemeral Coorong lagoon has developed into a number of ephemeral lacustrine depocentres that are now largely removed from marine influence and are dominated by the groundwater regime. These ephemeral lakes have similar biota to the ephemeral lagoon facies, but also precipitate a variety of fine grained carbonate minerals during their annual evaporative phase as discussed by Alderman & Skinner (1957), von der Borch (1976), Warren (1988) and Rosen et al. (1989). These include partially ordered dolomite and poorly crystalline protodolomite, magnesite and hydromagnesite, magnesian calcite, aragonite and monohydrocalcite.

For further details the reader is also referred to Belperio (1995) p. 235, and studies by Allison & Harvey (1983), Burne et al. (1980), Burne & Ferguson 1983, Cann & De Dekker (1981), De Dekker & Geddes (1980), Holmes & Waterhouse (1983), Rosen et al. (1998), Schwebel (1983), von der Borch (1965), von der Borch & Lock (1979) and von der Borch et al. (1975).

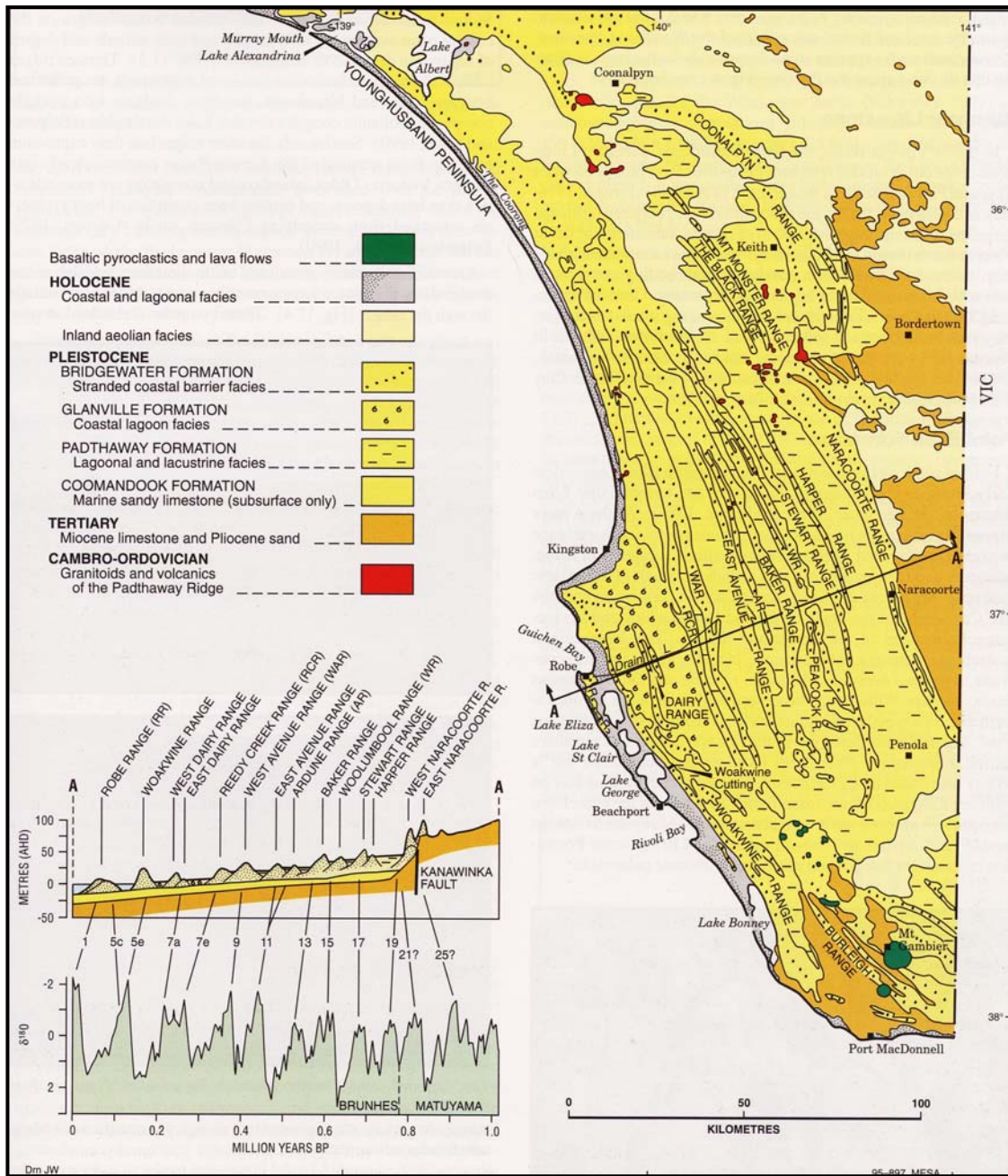


Figure 27. Quaternary strandplains of south east South Australia and correlation of shoreline sequences with oxygen isotope stages (reproduced with permission from Belperio 1995).

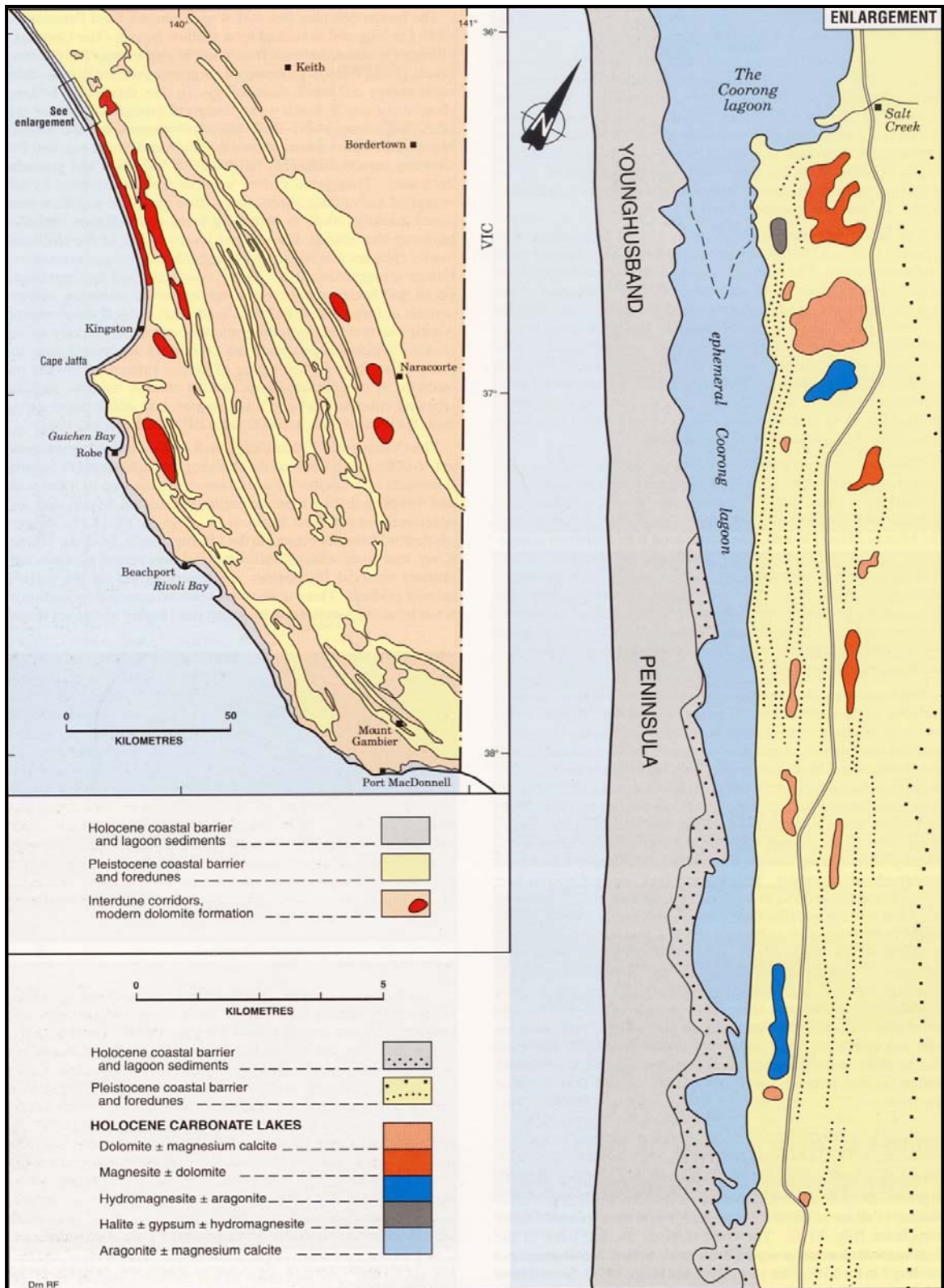


Figure 28. Coastal and inland carbonate precipitating lakes and swamps of the south-east (reproduced with permission from Belperio 1995, after von der Borch 1965 and von der Borch & Lock 1979)

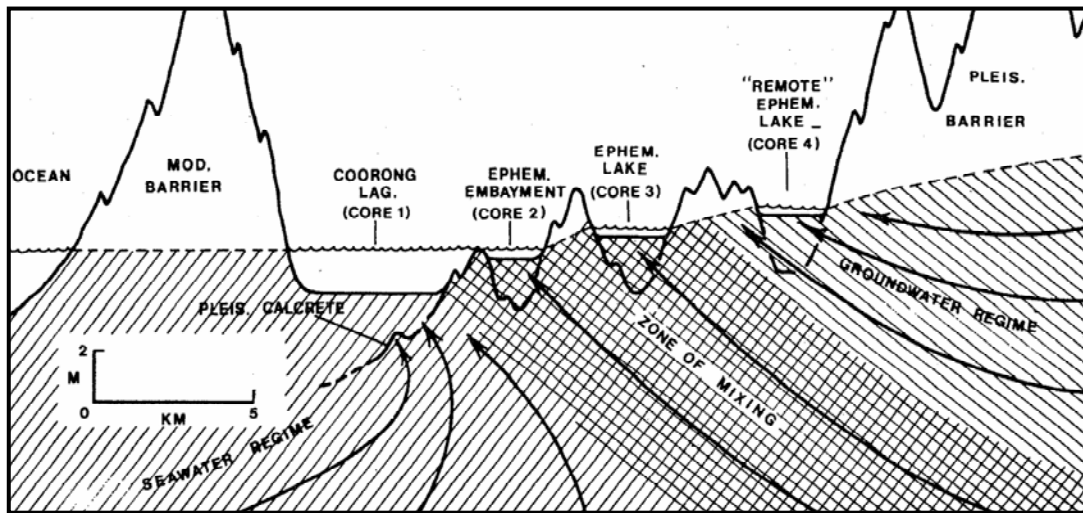


Figure 29. Generalised cross section illustrating present ground-water-sea-water interface at the Coorong. Possible ground-water flow lines are indicated (reproduced from von der Borch et al. 1975. Copyright © Geological Society of America Inc 1975).

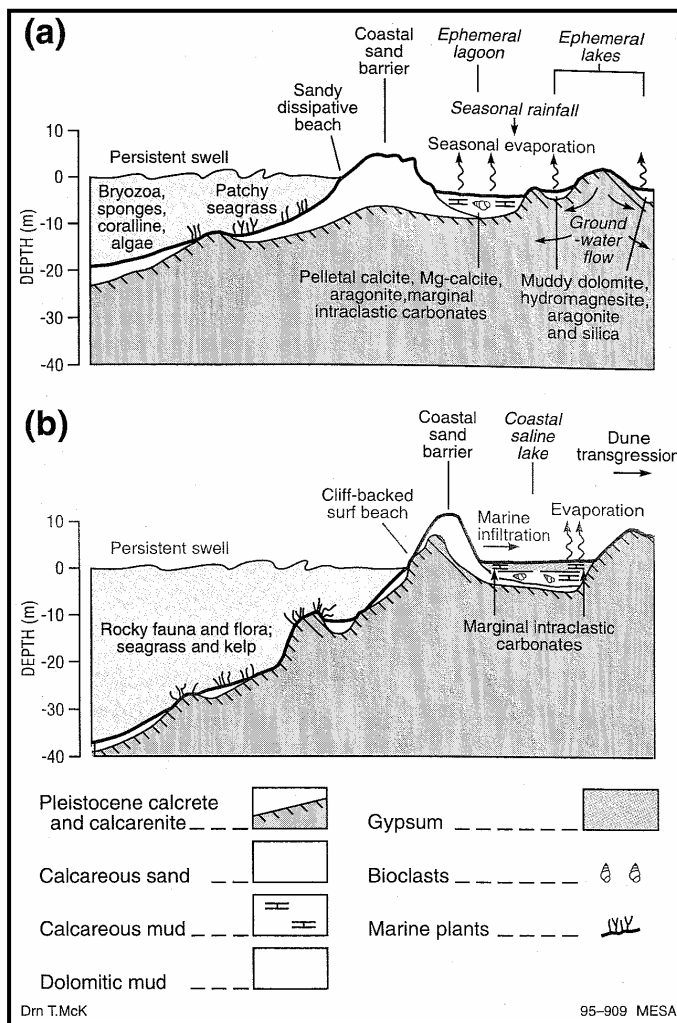


Figure 30. Schematic representation of high wave energy coastal facies of (a) the Coorong region (swell environment, cool temperate climate), and (b) Eyre Peninsula coastline (swell environment, semi-arid climate) (reproduced with permission from Belperio 1995).

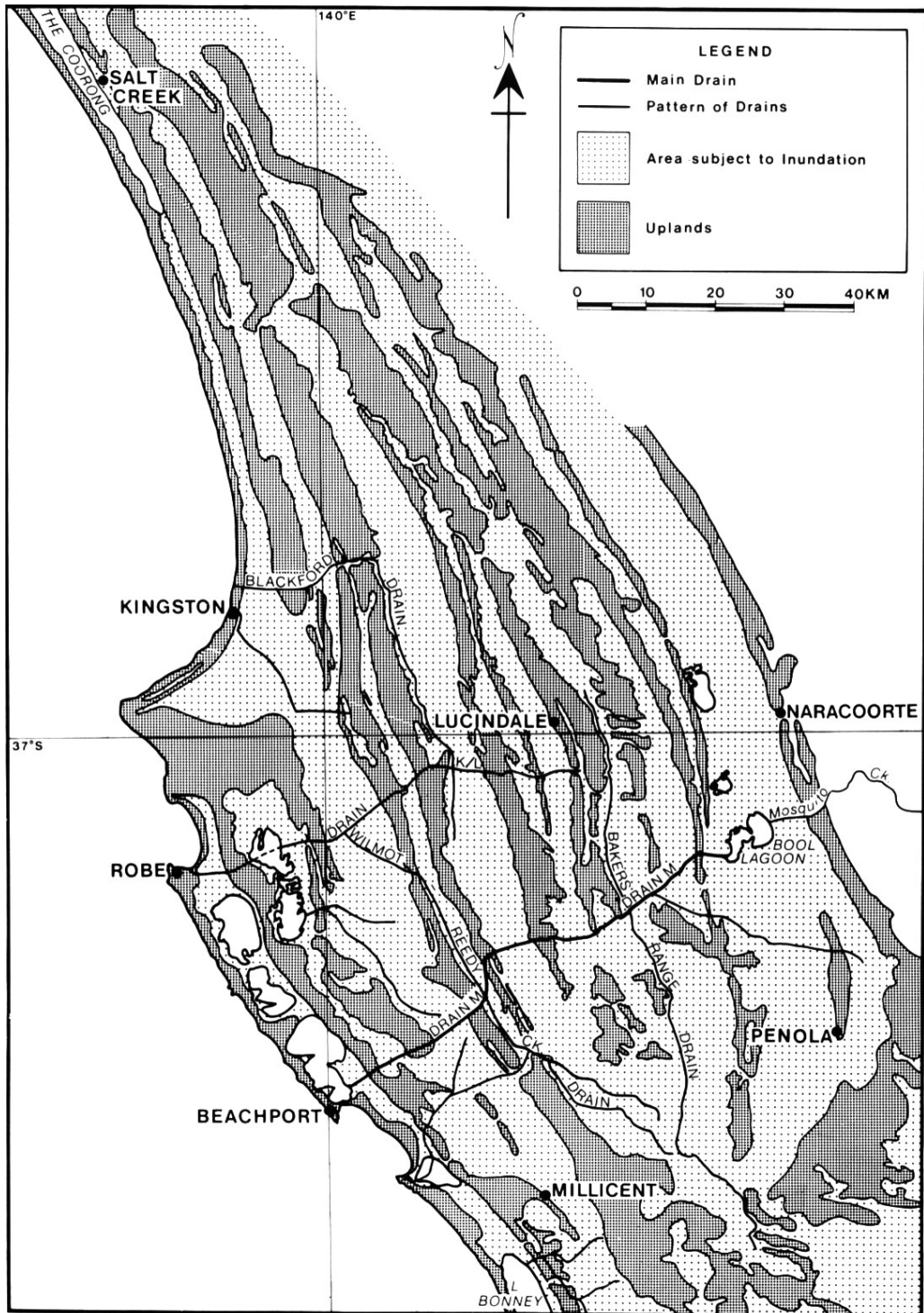


Figure 31. Extent of land subject to winter flooding (reproduced with permission from Holmes & Waterhouse 1983)

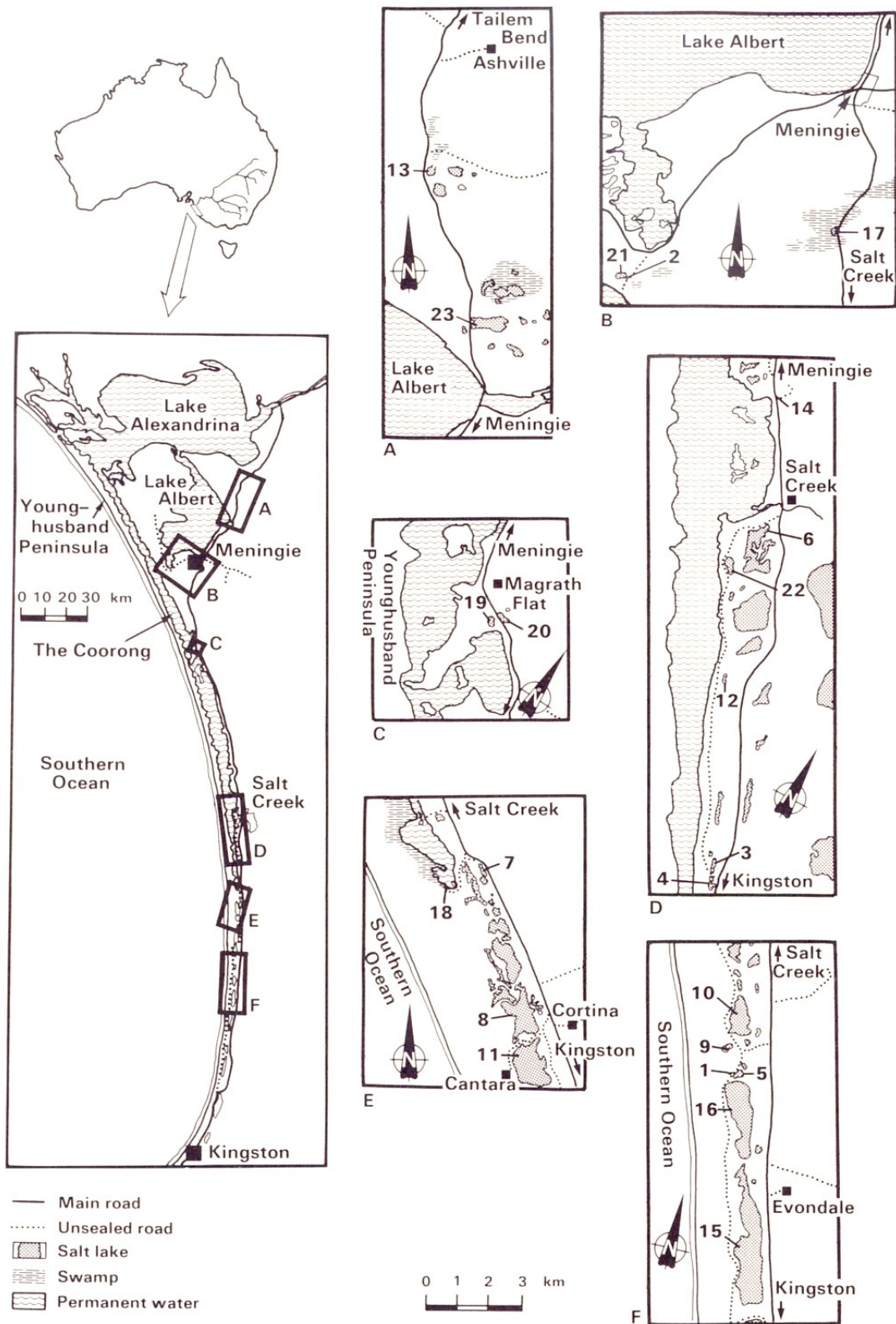


Figure 32. Maps showing the location of the 23 lakes studied by De Dekker & Geddes (1980) (reproduced from De Deckker & Geddes 1980)

3.6 Day 2 Stop 4: Murray canyons

Patrick De Dekker

(text reproduced from Hill et al. 2005)

The Murray canyons (Figures 33, 34, 35 & 36), are a group of deeply incised submarine canyons on a steep 400 km section of the continental slope off Kangaroo Island, South Australia. Some of the canyons are amongst the largest on Earth. The canyons, some 80 km long, descend from the shelf edge to the abyssal plain 5200 m deep. Sprigg Canyon, the deepest and one of the largest, has walls 2 km high. The thalwegs of the larger canyons are concave in profile, steepest on the upper continental slope (15 - 30°), with about 4° gradient on the mid slope, then level out on the lower slope to merge with the 1° continental rise. Between canyons, the continental slope is slightly convex to linear with a gradient of about 5 - 6°. Canyon walls commonly slope at 15 - 22°. The passive continental margin narrows to 65 km at the Murray canyons and links the Bight and Otway Basins. West-northwest-trending Jurassic - Cretaceous rift structures control the irregular shape of the central canyons.

At the western end, large box canyons, 1 km deep, are incised into thick sediments of the Ceduna Sub-basin. Formed by headscarp erosion, some of these canyons have coalesced by canyon capture. The upper parts of most canyons are cut into Cretaceous sediments and in some places are floored by basement rocks. Large deep-water holes, spaced about 5 km apart and up to several hundred metres deep, along the outlet channels of the larger and steeper canyons were probably gouged by turbidity currents resulting from major slope failures at the shelf edge, but may be sites of fluid discharges. Quaternary turbidites were deposited on the abyssal plain more than 100 km from the foot of slope. Canyon downcutting has been episodic since the latest Cretaceous, with peak activity since the Oligocene due to strong glacioeustatic fluctuations and cycles. Canyon development occurred during lowstands and early in transgressions when sediment input at the shelf edge was usually highest.

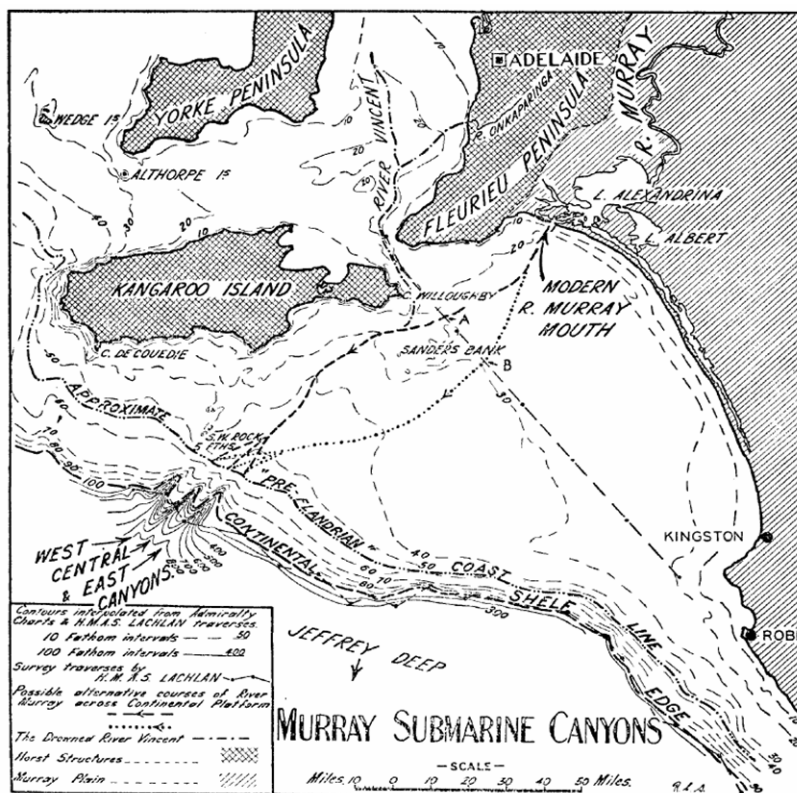


Figure 33. An early map of the Murray Canyons (reproduced with permission from Sprigg 1947)

The timing of canyon development is linked to major unconformities in adjacent basins, with downcutting events recorded or inferred during the Early Paleocene, Middle Eocene, Early Oligocene, Oligocene/Miocene transition (ca 24 Ma), Middle Miocene (ca 14 Ma) and latest Miocene -

Pleistocene. The early phases involved siliciclastic sediments only, while post-Early Eocene canyon cutting was dominated by biogenic carbonates generated on the shelf and upper continental slope. The Murray River dumped its sediment load directly into Sprigg Canyon during extreme lowstands of the Late Pleistocene when the Lapepede Shelf was mostly dry land.

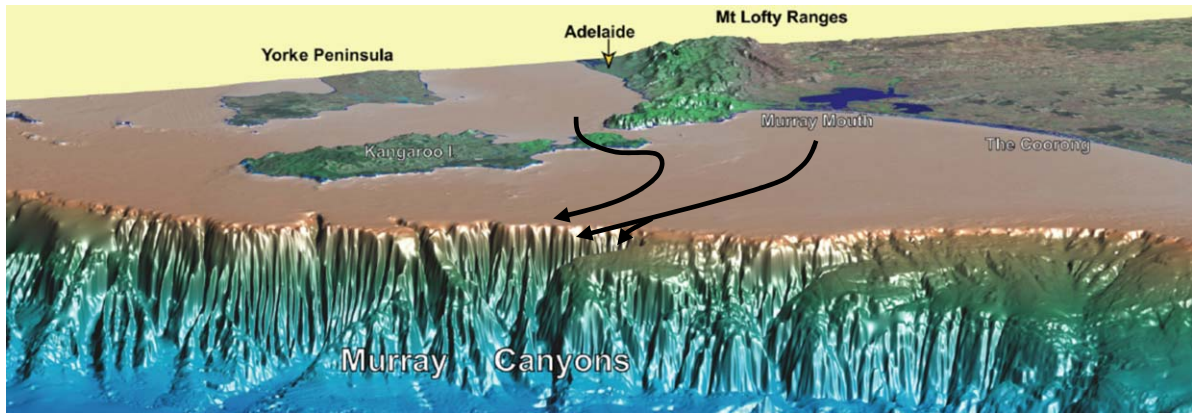


Figure 34. 3-D image of the Murray Canyons offshore South Australia to show the significantly incised topography of the canyons which continue down to approximately 5000 m. Note the vast expanse of the Lapepede shelf which extends down to approximately the 120 m contour which would have been close to the edge of the continent during the Last Glacial Maximum (LGM). Possible courses of the palaeo River Vincent and palaeo Murray on the dry shelf during the LGM are shown (adapted from Hill & De Deckker 2004. Original illustration Copyright © Commonwealth of Australia, Geoscience Australia 2004).

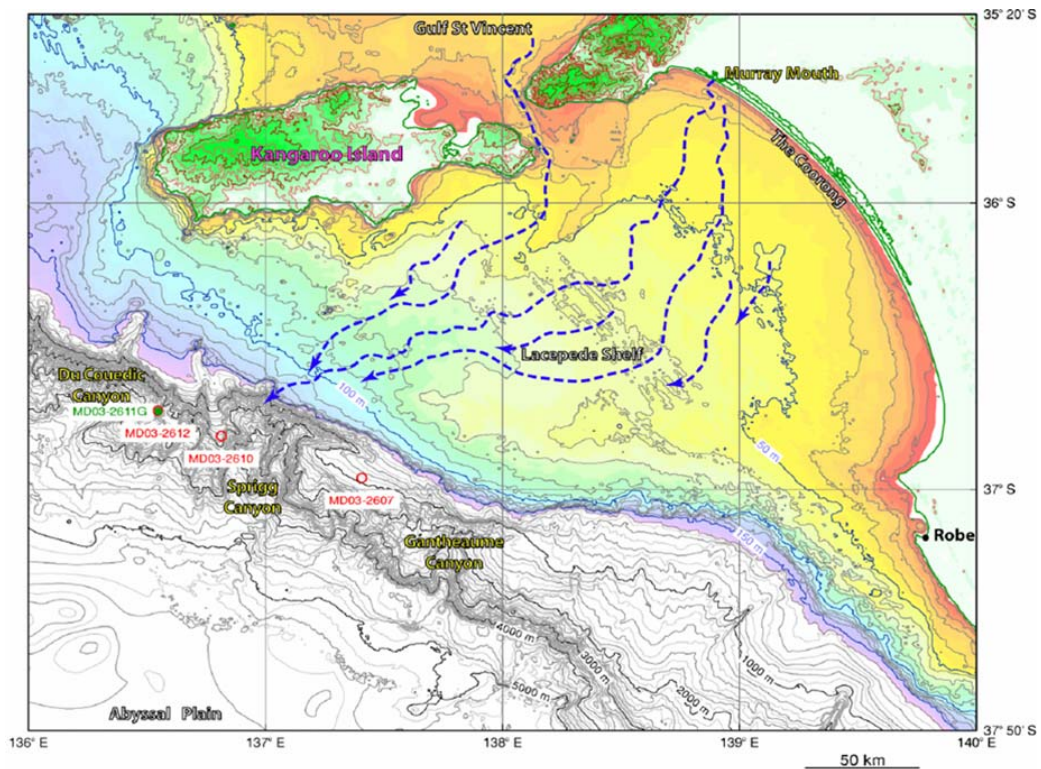


Figure 35. Detailed bathymetry contours of the Lapepede Shelf and adjacent Murray Canyons. The Murray River mouth moved back and forth across the Shelf numerous times during the Quaternary eustatic sea level cycles. Depths from the coast down to the 200 m isobath are coloured (red to purple), with the contour interval to the 150 m isobath being 10 m. The contour from the 200 m isobath and deeper is 100 m (reproduced from Hill & De Deckker 2004. Copyright © Commonwealth of Australia, Geoscience Australia 2004).

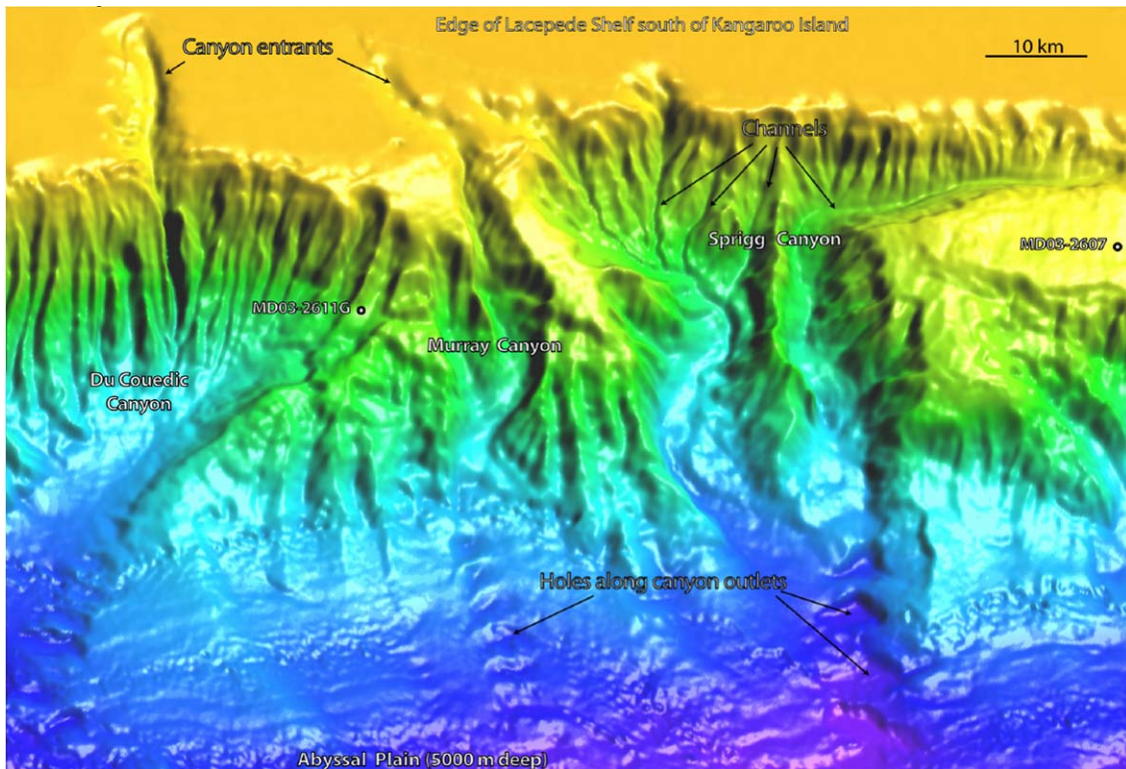


Figure 36. 3-D view of Sprigg and De Couedic Canyons (reproduced from Hill & De Dekker 2004. Copyright © Commonwealth of Australia, Geoscience Australia 2004).

3.7 Day 2 Stop 5: Quaternary and Pliocene strandplain successions

Dan Clark and Patrick De Deckker

3.7.1 Quaternary strandplains

(text reproduced with permission from Belperio 1995)

Bioclastic barrier shoreline deposits preserved as conspicuous subparallel topographic ridges across the coastal plain and on the continental shelf are collectively known as the Bridgewater Formation (e.g. Sprigg, 1952). The surface upon which the ridges rest rises to 60 m above sea level at the Kanawinka escarpment and around the Mt Gambier volcanic centre. The stranded coastal ridges on the coastal plain average 15 m in height, and their altitude and degree of separation decrease to the northwest (Figure 27). Thirteen ridges related to specific Pleistocene sea-level highstands are preserved between Robe and Naracoorte, but these coalesce into a single composite aeolianite complex towards Lake Alexandrina. Five sediment facies associated with shoreline deposits of the Bridgewater formation are exposed in various drains and cuttings through the ranges (Figure 37).

Since the earliest studies of Sprigg (1952), it has been recognised that there is good agreement between the uplifted coastal plain sequence and *de facto* global climatic and Milankovitch insolation signatures. In the absence of more complete chronological data, reasonable age estimates can be made by matching individual barriers to the oxygen isotope record and utilising the indicated palaeomagnetic and geochronological constraints (Figure 27). A relatively complete sequence of stranded high seal-level deposits from stage 1 to stage 19 is suggested, indicating coastal sedimentation in phase wit global climatic events. Former sea-level highstands may be estimated by correcting shoreline elevation for tectonic uplift. A rate of uplift of 0.07mm/yr for the past 800 000 years is indicated by the highly coherent plot of shoreline elevation versus inferred age for a Robe-Naracoorte line of section (Figure 38).

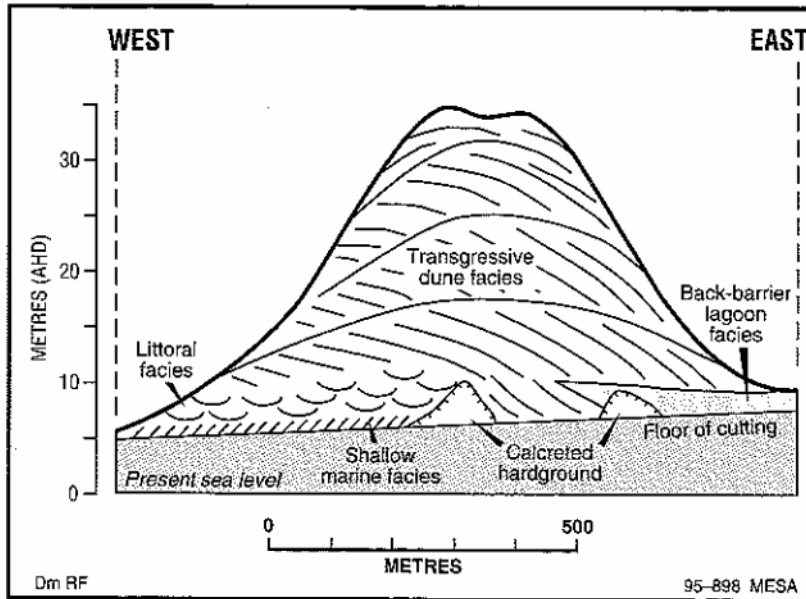


Figure 37. Cross section exposed by the Woakwine Cutting through the Woakwine Range (reproduced with permission from Belperio 1995)

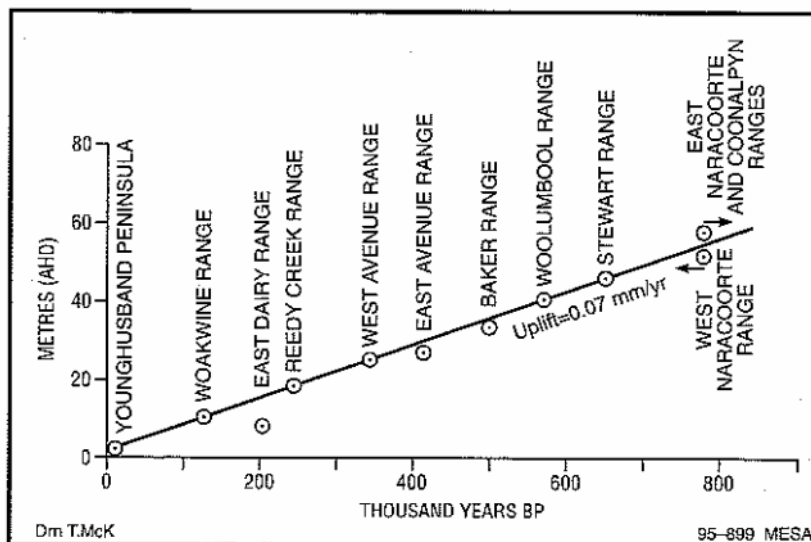


Figure 38. Plot of shoreline elevation versus inferred age for coastal barriers of the Mount Gambier coastal plain (reproduced with permission from Belperio 1995)

3.7.2 Pliocene strandplains

(text reproduced from Wallace et al. 2005)

Digital elevation and magnetic data from the southern Victorian basins (Otway, Port Phillip, Gippsland Basins) have enabled the recognition of a vast Late Miocene – Pliocene strandplain succession that is a correlative of the Murray Basin Loxton-Parilla strandplain (Figure 39). A combination of ferricrete formation and erosional dissection has made the strandline geometries visible on geophysical images and allowed the mapping of strandlines across most of the onshore Otway (often under continuous basalt cover), Port Phillip and Gippsland Basins. Strontium isotope ages from well-preserved molluscan assemblages of the exposed strandplain successions indicates the earliest sediments were deposited above the Upper Miocene unconformity at around 5.8±0.2 Ma (latest Miocene, Beaumaris, Figure 40). The youngest exposed strandplain sediments (from the Jemmys Point Formation, Gippsland) are Late Pliocene (ca 3.0 – 2.5 Ma), although younger strandlines occur offshore. Elevation differences across the strandplain of the Victorian basins give a quantitative measure of cumulative Plio-Pleistocene uplift. A broad east – west axis of regional uplift is present

along the Western Highlands – Dundas Tablelands, with maximum uplift in the range of 250 m being indicated. The western extension of this axis affects the Mt Gambier coastal plain (Gambier Axis). The Padthaway High forms another uplift trending northwest from the Dundas Tablelands into the Murray Basin. The unconformable relationship between the Pliocene and Quaternary strandline systems across Victoria may be caused by intensified latest Pliocene Quaternary uplift and/or eustatic changes associated with the development of the Quaternary glacial episode. The strandplain successions of southern Victoria have probably developed during the latest Miocene and Pliocene in response to a period of relatively stable base-level (little uplift or eustatic fluctuation). Recognition of the southern Victorian strandline successions may provide potential new targets for heavy-mineral exploration.

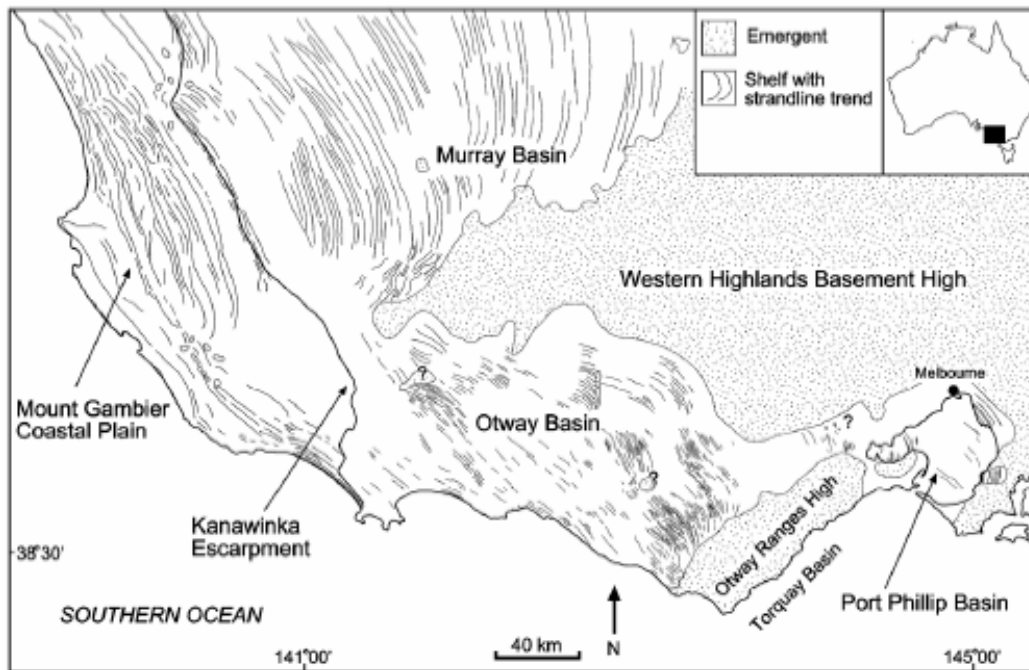


Figure 39. Pliocene palaeogeography and strandline morphology interpreted from geophysical data in the Murray, Otway and Port Phillip Basins. The Quaternary strandlines on the western side of the Kanawinka Escarpment are derived from Sprigg (1952) (reproduced from Wallace et al. 2005. Copyright © Geological Society of Australia 2005)

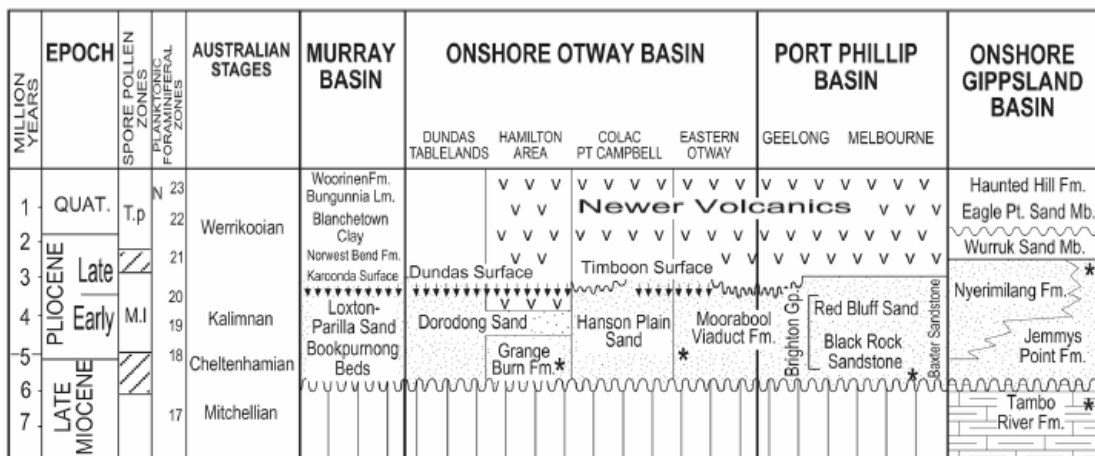


Figure 40. Chronostratigraphic chart for the late Neogene strandplain successions of the southeastern Australian basins. Strontium isotope ages are denoted with asterisks (reproduced from Wallace et al. 2005. Copyright © Geological Society of Australia 2005).

4. DAY 3: NARACOORTE CAVES AND MOUNT GAMBIER

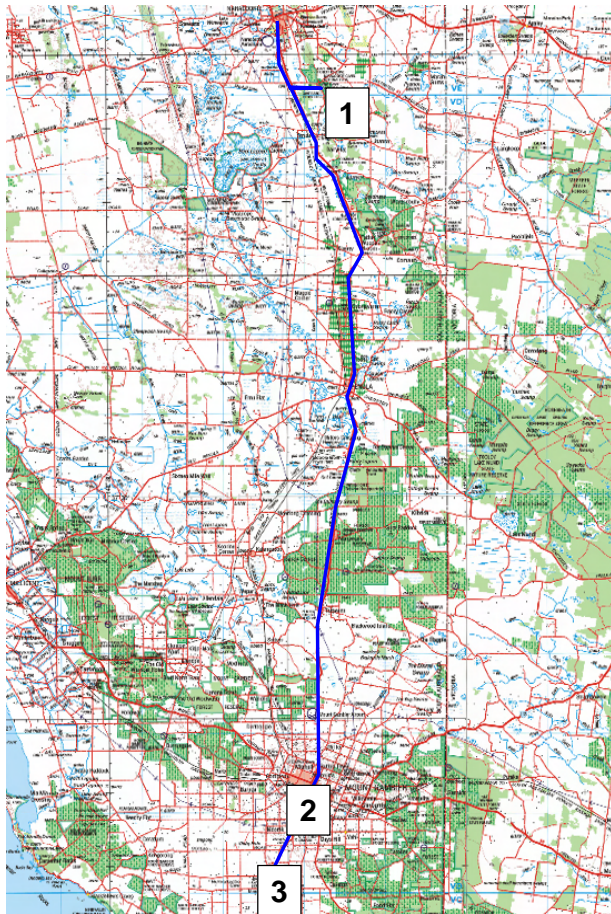


Figure 41. Day 3 route map

4.1 Day 3 Stop 1: Naracoorte Caves

Steve Bourne and Liz Reed

*(following 3 paragraphs and Figure 42 reproduced from Naracoorte Caves Website
<http://www.naracoortecaves.sa.gov.au/parks/naracoorte/caves/index.html>)*

Naracoorte Caves National Park, South Australia's only World Heritage Site (previously a Conservation Park), was proclaimed by the Governor of South Australia as a National Park (50Kb PDF) on 18 January 2001. It is located in the Limestone Coast tourism region in the southeast of South Australia. The importance of the fossil record at Naracoorte Caves was officially recognised in 1994, when the site was inscribed on the World Heritage List. The park preserves 600 ha of remnant vegetation, with 26 caves contained within the 305 ha World Heritage Area.

The Naracoorte Caves World Heritage inscription recognises the extensive fossil record of the park. The caves have acted as pitfall traps, collecting animals for at least 500,000 years, preserving the most complete fossil record we have for this period of time. The bones of Megafauna species such as *Thylacoleo carnifex* (Marsupial Lion), Thylacine, *Zygomaturus* and sthenurine kangaroos are found within the 20 fossil deposits found to date. Naracoorte Caves contain clues to help interpret the geological and evolutionary history of Australia.

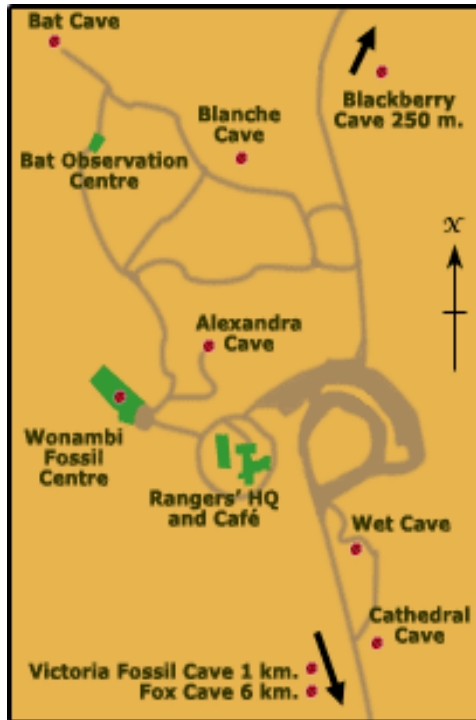


Figure 42. Map of Naracoorte Caves (reproduced from Naracoorte Caves website <http://www.naracoortecaves.sa.gov.au/parks/naracoorte/caves/index.html>)

4.1.1 *Megafauna, climate and Naracoorte research*

Liz Reid

There are 26 caves within the World Heritage listed Naracoorte Caves National Park in the South East of South Australia. These caves contain nearly 100 sites of Quaternary age ranging from greater than 500,000 years to those still accumulating fauna today. This allows the investigation of a virtually continuous record of Quaternary climate and faunal change over an extended time period. The caves have acted as pitfall traps and predator dens for millennia and preserve a diverse vertebrate fauna. In addition they contain a wealth of palaeoenvironmental information in deep sediment deposits and abundant speleothems. The locality is unrivalled globally among Quaternary fossil localities for the number of sites within one locality, excellence of preservation, species diversity and the extended time span of accumulation.

The Fossil Chamber within the Victoria Fossil Cave was discovered in 1969 and contains one of the largest deposits of Pleistocene age vertebrates in the world (Figures 43, 44 & 45). Over 100 species of mammals, reptiles, birds and amphibians have been discovered, including many extinct megafaunal species. Recent research has centred on understanding the taphonomy of the deposit in order to determine how representative this deposit is of the original palaeocommunity at Naracoorte.



Figure 43. Pit A in Victoria Fossil Cave



Figure 44. Lower jaw of *Procoptodon goliah* -much of the Naracoorte Caves fossil material is beautifully preserved.



Figure 45. Marsupial lion (*Thylacoleo carnifex*) skeleton reconstructed from bones found in Naracoorte Caves. This 100 kg beast would have had a stronger bite than any species, living or extinct, of similar size, such as hyenas and Tasmanian devils.

4.1.2 Impacts of karst of the south east of South Australia

Steve Bourne

Horizontally bedded Oligocene to Pleistocene limestones underlies the southeast of South Australia and a small portion of western Victoria. These limestones are highly permeable and possess a wide array of karst features (Figure 46). The region is extensively cleared, with less than 13% native vegetation cover remaining. It has also been extensively drained. Intensive primary and secondary industries are a feature of the region and are supported by vast quantities of water drawn from the unconfined and confined aquifers. The unconfined aquifer was once described as “one of the best in the world”. The Regional Economic Board boasts 30% of the state’s production from 2% of the state’s area. This has come at a cost to the landscape.



Figure 46. 5 Corners Cave: A small dairy was established on the edge of 5 Corners Cave, enabling owners to wash dairy waste directly into the cave. This was stopped when a link to the Blue Lake was established.

4.2 Day 3 Stop 2: Blue Lake and Pump House tour, Mt Gambier

Bernie Joyce and Patrick De Dekker.
(text adapted from Thurgate & Spate 2004)

The Blue Lake (Figure 47) is a signature feature of Mount Gambier. It is one of four craters that form the Mount Gambier Volcanic Complex. The Blue Lake is renowned for the remarkable colour change from grey in winter to a deep aqua blue in summer (Telfer 2000).



Figure 47. Aerial view of Blue Lake (reproduced from explanatory poster at Blue Lake tourist entrance).

The Blue Lake is a volcanic maar crater, and it formed from a series of violent explosions commencing around 28 000 years ago (Anon 2001, Sheard 1978, Leaney et. al. 1995). The crater sits on top of the Gambier Limestone, which can be seen exposed in sections of the walls. The lake is not karstic in origin, but it does intersect the regional aquifers, so the physio-chemical properties of the lake closely resemble those found in the cenotes of the region.

Although local legends claim that the lake is bottomless, bathymetric surveys found that it has a maximum depth 77m and a total volume $36.75 \times 10^6 \text{m}^3$ (Tamuly 1969). The surface area is 60 ha and the shoreline is over 5 km long. The Blue Lake provides the town water supply for the city of Mount Gambier and during our visit to this site you will be taken on a guided tour of the pump station facilities.

Stromatolites have been recorded in five locations around the Blue Lake. It is likely that they occur around much of the perimeter of the lake. Although some forms are present that resemble those found in the cenotes, most of the stromatolites of the Blue Lake are very different in terms of external morphology, internal structure and associated microbes.

Eight stromatolite forms or morphotypes were recorded during a brief survey of the site (Thurgate 1996). These include large reef structures, conical towers, tabular structures and several columnar forms including large club-shaped structures and small conical forms. Diatoms dominate the microbial community responsible for stromatolite development, and the composition of species is unique to this site. Several species of the macroalgae, *Chara* grow on the stromatolites at shallower depths, while below 20 m, an unidentified moss grows over the structures.

Stromatolites in the Blue Lake are largest at depths of 5-10 m below the lake surface, where a single structure may tower to 12 m above the lake bed. Generally the size, abundance and complexity of stromatolite structures decrease with depth. However the clarity of the water and seepage of carbonate-rich groundwater in deeper parts of the lake allow the development of structures up to 2 m tall in depths of up to 45 m below the surface.

As the town water supply, there have been numerous studies of the hydrology of the lake and as well there is a long-term ongoing monitoring program. Issues in lake management include (Telfer 1994):

- Urban, industrial and agricultural activities within the groundwater capture zone have created diffuse and point sources of pollution (eg Lamontagne 2002)
- Stormwater is being diverted into the groundwater capture zone and is causing a decrease in salinity over time
- Groundwater extraction (in lake and wider area) may have contributed to drop in regional water table

4.3 Day 3 Stop 3: Mount Schank

Bernie Joyce

(first paragraph reproduced from Anon 2001)

This volcano rises abruptly from the plain 14 km south of Mount Gambier, and shows evidence of two phases of volcanic activity. A small cone on the southern side of the mount was produced by the early phase, together with a basaltic lava flow to the west (the site of current quarrying operations). The later phase created the main cone, which now slightly overlaps the original smaller ones (Figure 48). These cones consist of bedded ash, consolidated to form tuff layers, which are visible on the inside walls of the crater and in the quarry on the eastern side of the mount. Work by the University of Adelaide Physics Department has revealed that Mount Schank erupted about 4500 years ago. Mount Schank differs from craters at Mount Gambier in that its floor is dry, being approximately at the level of the surrounding plain.

A line of small cones (Figures 48 & 49) marks a north-northwest-trending fissure north of the main cone.

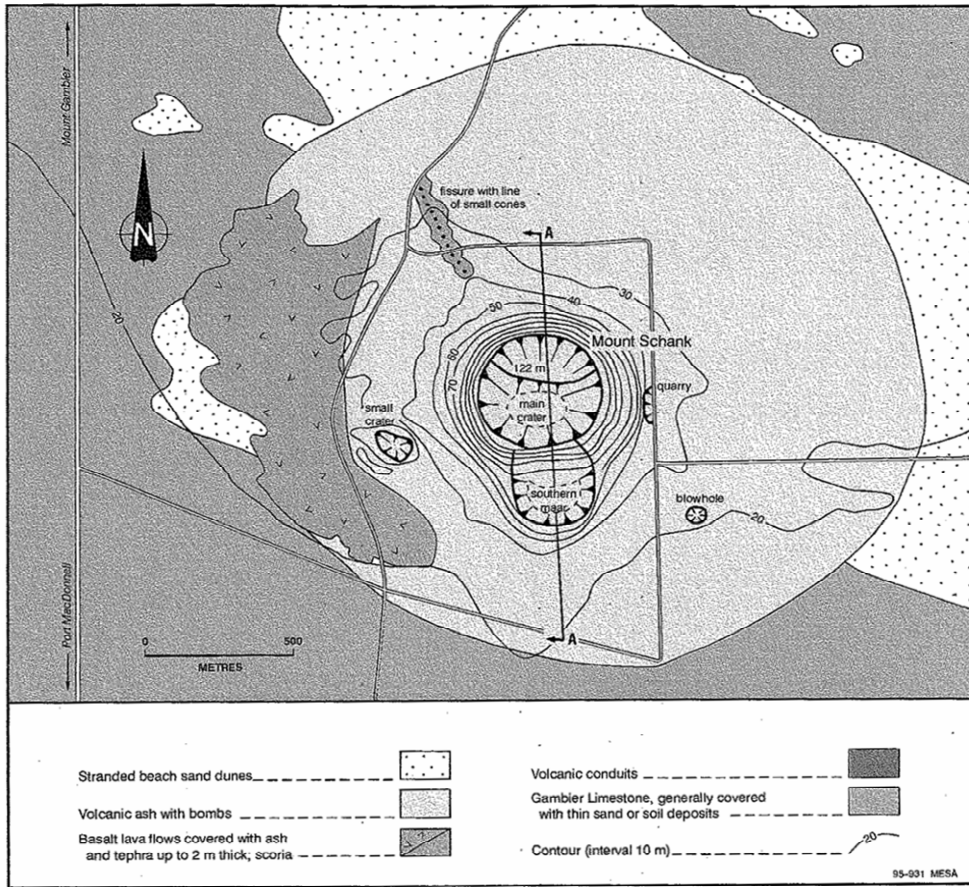


Figure 48. Volcanic cones at Mount Schank (reproduced from Anon 2001)



Figure 49. Small cone and dipping ash layers exposed in a road cut north-northwest of Mt Schank (in background).

5. DAY 4: MOUNT GAMBIER TO CAMPERDOWN

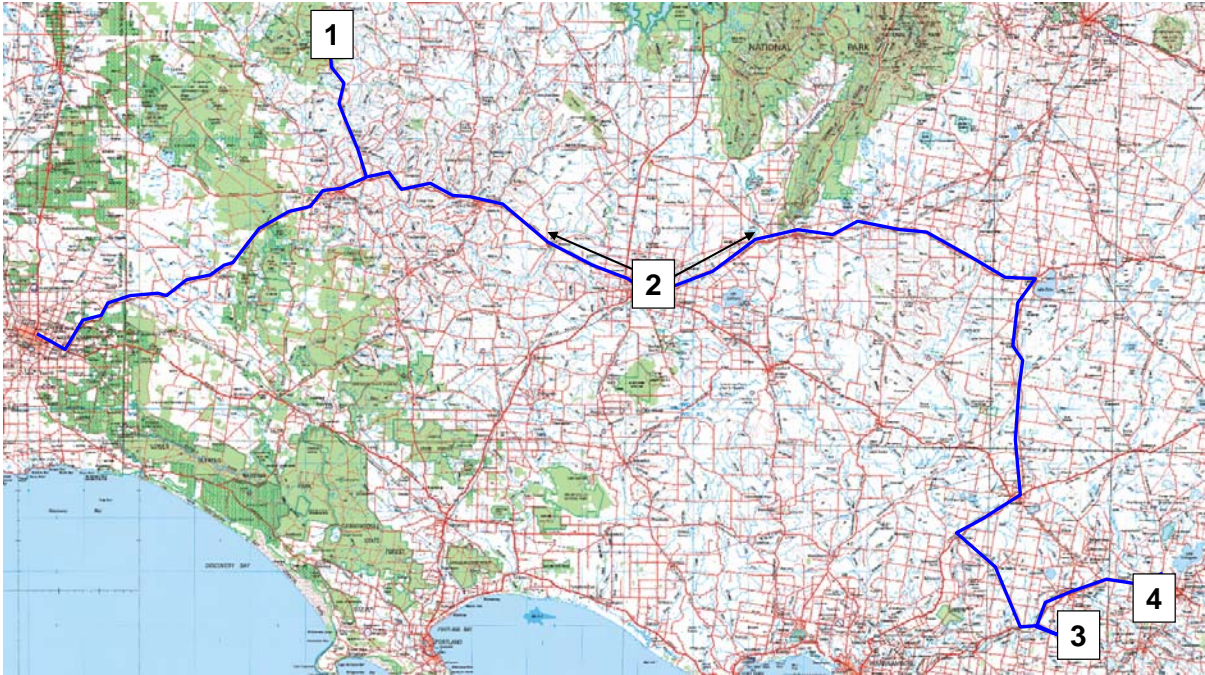


Figure 50. Day 4 route map.

5.1 Day 4: Mount Gambier to Chetwynd.

The excursion route takes us east-northeast across the low relief surface of the Quaternary strandplain. Around 50 km from Mt Gambier we cross the 30 m high west facing scarp of the Kanawinka Fault, which has displaced the strandplain sediments. After dropping into the valley of the Glenelg River at Casterton, we pass onto the domed landscape of the Dundas Tableland.

5.2 Day 4 Stop 1: Chetwynd road cut

Bernie Joyce

(text reproduced from Paine 2003. See also Paine et al. 2004))

The Chetwynd road cutting occurs approximately 3 km south of Chetwynd on the Casterton-Edenhope Road, slightly east from the extension of an approximately north-trending Th anomaly on the Merino Tableland to the south. Here, the cutting, with elevations ranging from 170 m ASL to 185 m ASL, provides exposures of Permian fluvio-glacial deposits that are unconformably overlain by ferruginised sediments (Figure 51). Ferruginisation of the Permian sediments is evident particularly in the upper portion of the unit where a boxwork fabric has formed as Fe-rich joint fills form positive relief features on the exposed face of the cutting. The remainder of the unit is characterised by diffuse fawn coloured mottles that increase in concentration towards the top of the unit. Overlying this unit is a thin, ferruginous oolite-rich clay that is grouped here with the Duddo Limestone. This poorly exposed unit is characterised by <1 mm oolites and various ferruginised bryozoan and echinoid fragments set in dark brown clay. In thin-section the oolites are characterised by a series of concentrically-banded cutans arranged around a variety of cores including goethitised bryozoan or echinoid fragments, quartz grains or earlier homogenous ferruginous oolites. Overlying the Duddo Limestone is a fine to medium quartz-rich sand that is grouped here with the Dorodong Sands. At the cutting this unit can be subdivided into a number of facies based largely on grain size. The basal unit comprises well-sorted, very fine clast-supported quartz sand with other minor detrital minerals including muscovite,

tourmaline and ilmenite. The overlying unit is *characterised* by clast-supported, bimodal, fine to medium quartz sands. Accessory detrital minerals, which form a greater percentage of the mineral suite than the enveloping units, include tourmaline, rutile, ilmenite and zircon. This unit is relatively Fe-rich in comparison with the surrounding sediments and in the exposure has an irregular hackly facade. The uppermost unit in the exposure comprises moderately sorted medium quartz sand. Detrital minerals throughout the unit are weakly cemented by goethite-stained clays that partly fill the available pore space.

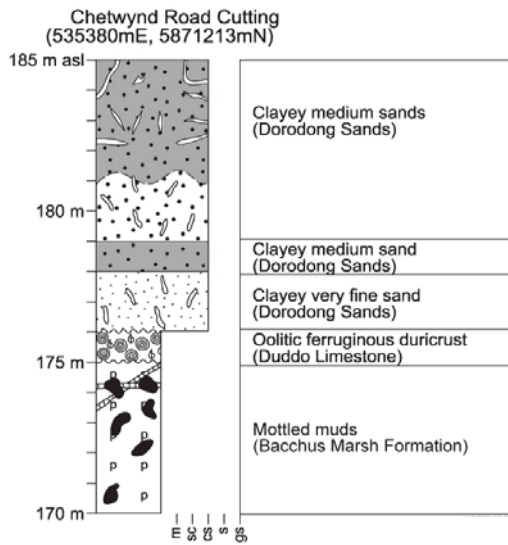


Figure 51. Section at Chetwynd road cut (adapted from Paine 2003)

5.3 Day 4 Stop 2: Hamilton area volcanics

Bernie Joyce

(text reproduced from Joyce 2005)

The Western Plains of Victoria lie to the south of the western uplands, extending to the coastline in the west, and approaching the Otway Ranges in the southeast. Towards the end of the Pliocene, the sea, which had been close to the southern edge of the Western Uplands, retreated southwards and exposed a new surface of marine sediments, and weathering and soil development began on the plains.

Streams extended from the uplands, and lakes and swamps formed. About 5 million years ago volcanoes began to erupt on the new plains and also in the adjacent uplands, and activity has continued almost to the present day, continually disrupting the drainage lines and forming further lakes and swamps.

The flat to undulating plains are mainly composed of thin lava flows overlying a Tertiary marine plain, which remains exposed in some areas. The youngest flows retain their original stony rise relief and rocky outcrop, whereas the older flows have weathered to undulating level plains and plateaus. Low lava shields and higher scoria cones probably mark the source of flows.

The oldest flows in the Newer Volcanic Province, dated by K/Ar at 3 to 5 Ma, show deep (>10 m) pallid kaolinitic profiles with mottles and occasional ferruginous nodules, suggestive of a late Tertiary climate that was conducive to deep weathering. Valleys are incised into and sometime below the base of the lava flows (Hamilton and Clay units in Figure 52).

By contrast, flows of intermediate age (1-3Ma) have only 1 to 2 metres of red black swelling clay soil and form undulating to level, relatively stone free plains, often with well developed gilgai (Dunkeld regolith landform unit). Valleys are narrow and shallowly incised, and small lakes and swamps are numerous.

Flows of less than 1 Ma, many of which are late Quaternary in age and some less than 20 000 ka (Rouse and Eccles regolith landform units), have well preserved flow features including a varying surface relief of 10 m or more (locally known as stony rises) and little or no soil cover. These young flows are associated with lakes and swamps, both at their margins, due to disrupted drainage, and also on their irregular surfaces.

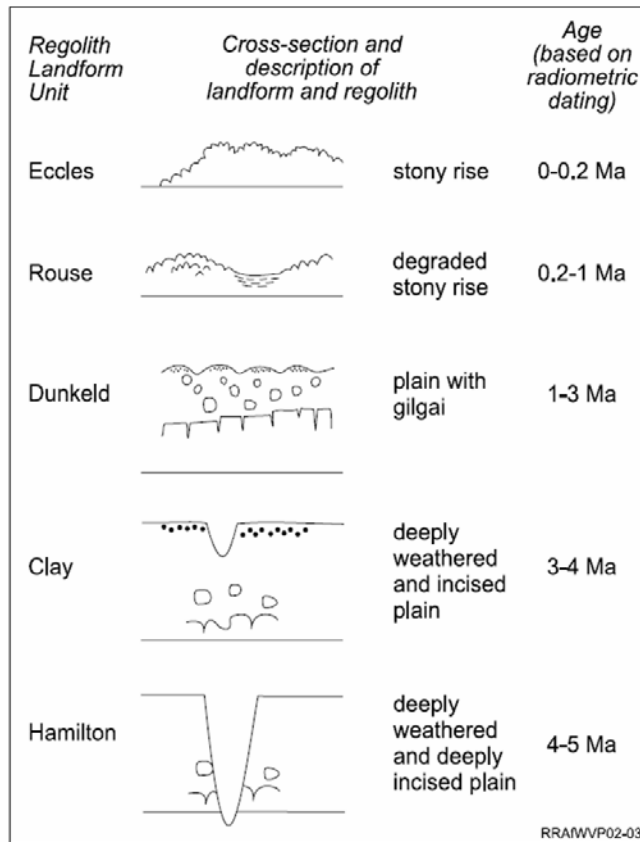


Figure 52. The five main regolith landform units of the basalt plains of the Newer Volcanic Province of western Victoria (reproduced from Joyce 2003).

5.4 Day 4 Stop 3: Staughtons Hill

Bernie Joyce

(Text reproduced from Joyce 1988a)

Staughtons Hill (Figure 53) is a good example of a complex volcano. It consists of a maar (Keayang Swamp), several broad scoria mounds (for example Mt Cunnies Hill) and a small spatter-rimmed crater (Lake Mumblin) which seems to have a larger diameter outer rim. This complex is unusual in that it sits on an uplifted block of Tertiary sediments. The uplift probably occurred at the same time as the volcanic activity.

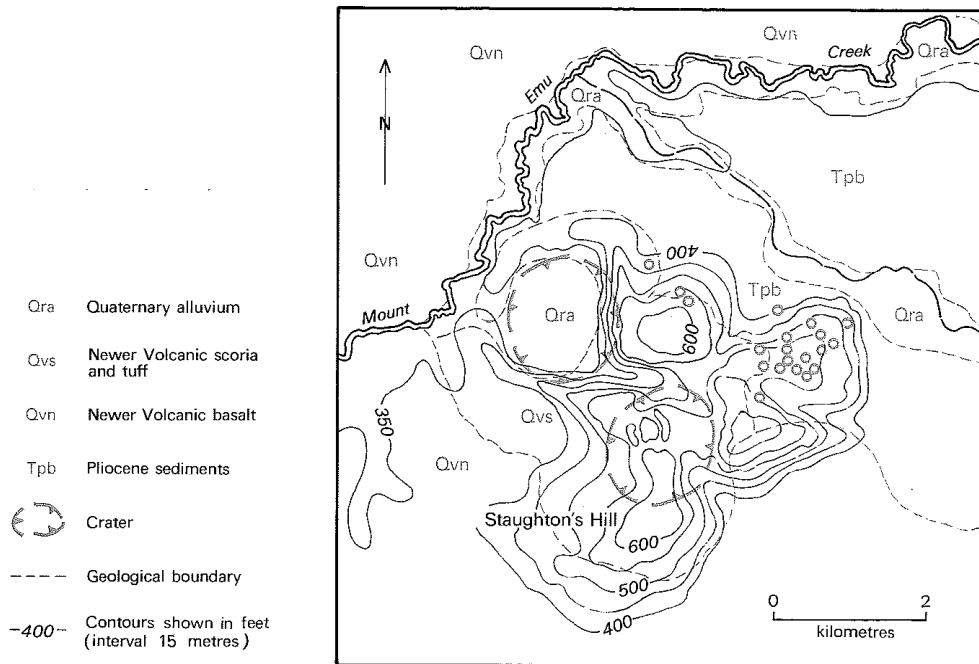


Figure 53. The volcanic complex of Staughton's Hill, 8 kilometres south of Terang. Solution sinkholes shown by small circles (reproduced from Joyce 1988a).

5.5 Day 4 Stop 4: Lakes Gnotuk and Bullenmerri.

Bernie Joyce

(text reproduced from Joyce 1988b)

These two lakes occupy maar craters (Figures 54 & 55). The Tertiary sediments underlying the maar deposits are present in road cuttings both to the east and west of this site a yellow clay, now largely obscured. The Tertiary strata are overlain by a basalt lava flow, which outcrops as a bluff around the edge of Gnotuk to the north. On the road to the west, new cuttings show this lava overlying the Tertiary clay, and being in turn overlain by two bedded tuffs (just before the house on the left) separated by a soil horizon. Thus at least two maar eruptions have occurred, probably representing the eruptions of Bullenmerri and Gnotuk.

It was noted in 1967 that the water level in Bullenmerri was at 147 metres and in Gnotuk at 105 metres, but both reached bottom at about 85 metres giving Bullenmerri a depth of 62 metres and Gnotuk 20 metres. The water in Bullenmerri is brackish, but Gnotuk is three times as saline as the sea. Thus the lakes represent separate bodies of water, although Bullenmerri overflowed into Gnotuk in the 1840s or 1850s and an overflow channel has been cut through the rim between the two lakes.

Since 1850 there has been a steady fall in lake levels at an average rate of 19 cm a year, due probably to climatic changes. Exposed benches marking former high shorelines can be seen on the northwest rim of Bullenmerri. Landslides have occurred in the tuff and underlying Tertiary sediment as the lake level has fallen.

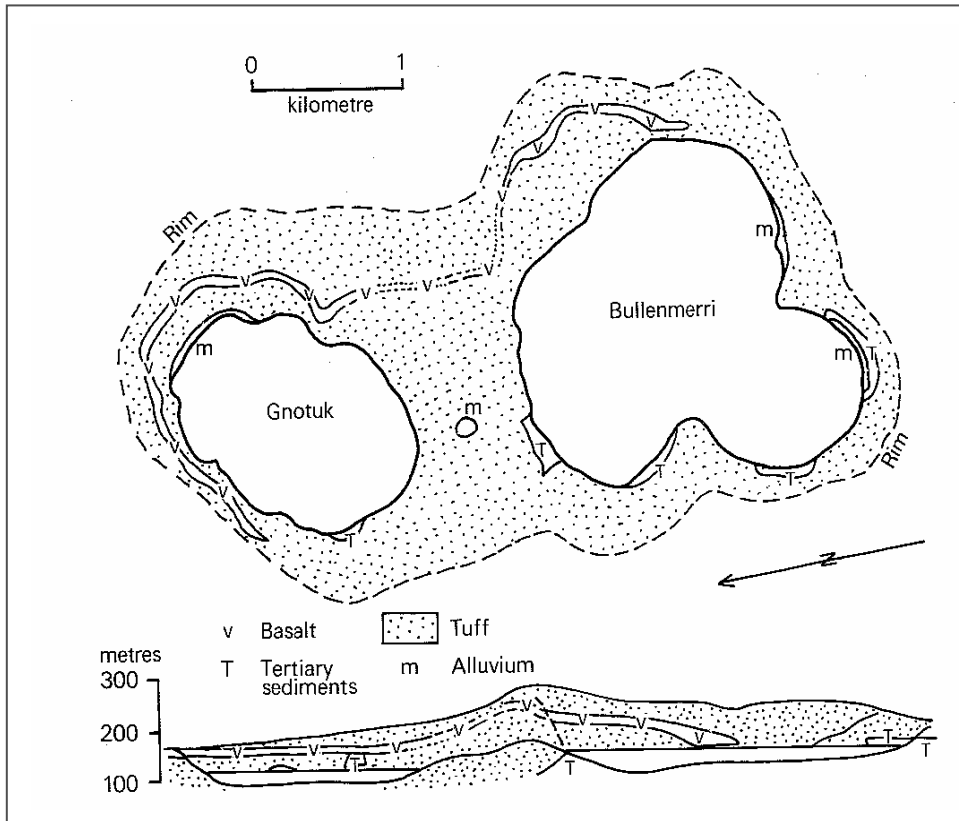


Figure 54. Lakes Bullenmerri and Gnotuk, plan and cross section (reproduced from Joyce 1988b).



Figure 55. Lake Bullenmerri looking to the southwest.

6. DAY 5 CAMPERDOWN TO MELBOURNE

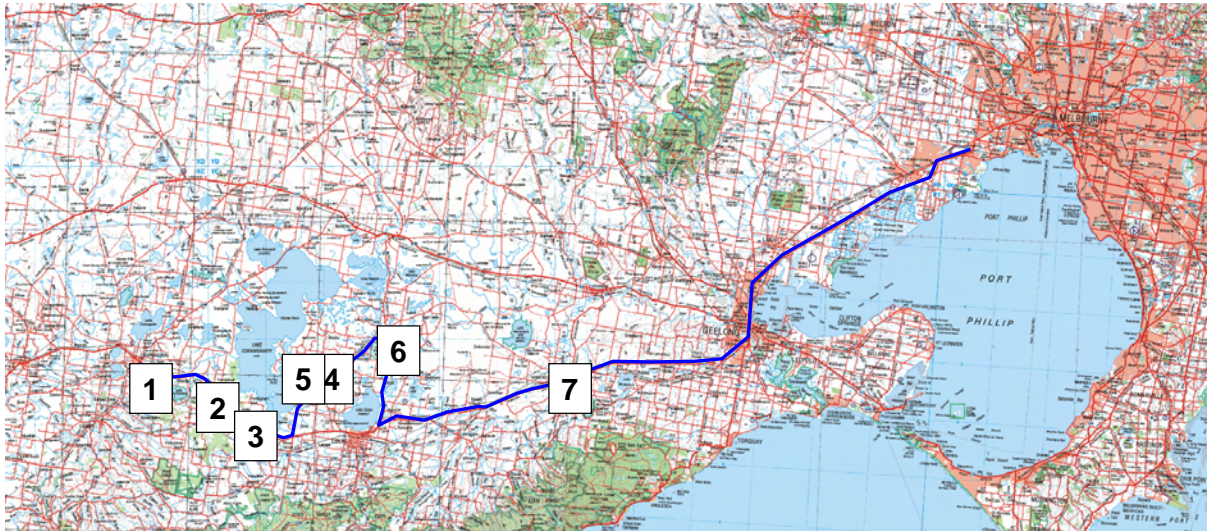


Figure 56. Day 5 route map.

6.1 Day 5 Stop 1: Mt Leura

Bernie Joyce

(text adapted from Joyce 1988b)

From the top of Mt Leura more than 20 volcanoes, mainly scoria cones and maars, can be seen, as well as some of the large shallow saline lakes of the area, with lunettes on their eastern sides (Figure 57). Over the horizon to the north are Palaeozoic rocks of the Central highlands, whilst to the southeast are Mesozoic sandstones of the Otway Ranges. The volcanic plain of Western Victoria extends more than 50 km north-south between these uplifted blocks of older rocks, and stretches out of sight to both east and west.

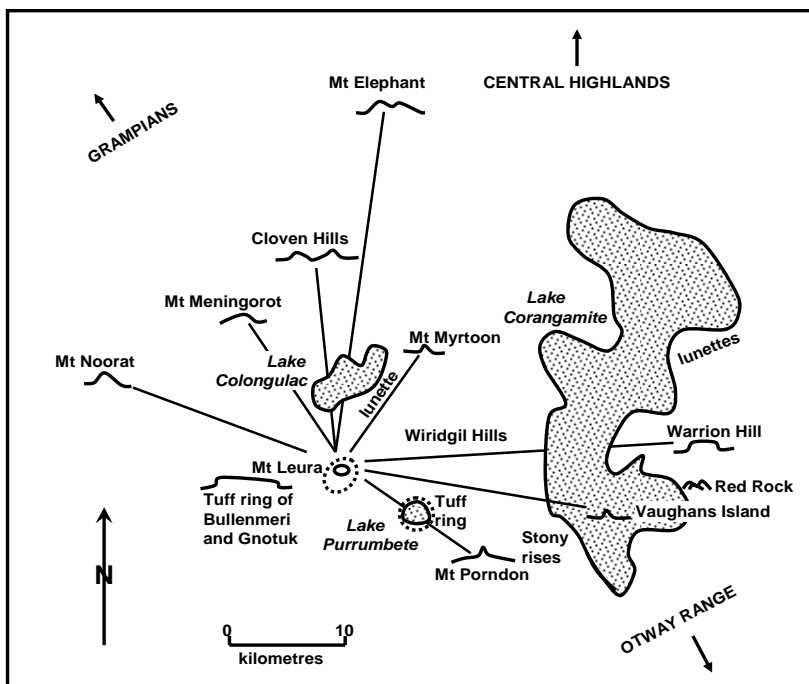


Figure 57. Features that can be viewed from Mt Leura lookout (redrawn from Joyce 1988b)

Mt Leura itself is a scoria cone; the road cuttings on the way to the lookout show good exposures of the scoria. Mt Leura and several other small scoria cones, including Mt Sugarloaf, are nested inside the crater of Leura maar (Figure 58). Camperdown lies on the northern rim of the maar; the ridge crossing the highway just to the east of town is the tuff ring. The quarries in the tuff ring to the north-east show excellent cross sections through the tuff; air-fall bedding and cross bedding can be clearly seen through binoculars.

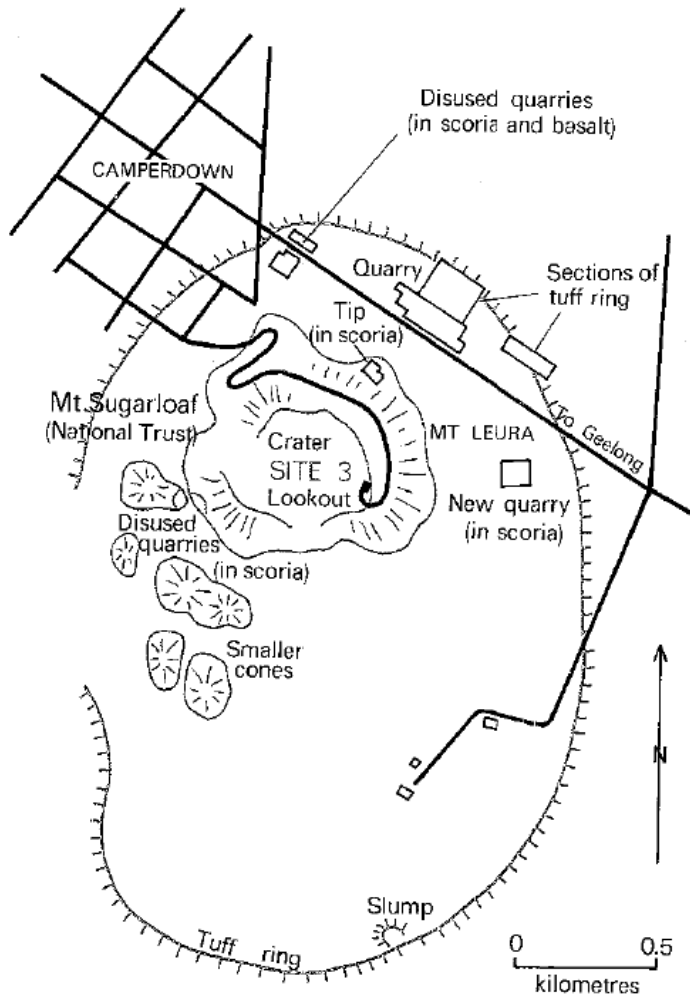


Figure 58. Sketch map, Mt Leura, showing tuff ring and scoria cones (reproduced from Joyce 1988b).

Scoria from the small cones in the maar overlies the tuff. The new quarry to the southeast of Mt Leura is in scoria, and shows many basalt bombs and some small lava flows. It is a good example of a modern quarry siting, being invisible from both the highway and the town.

Mt Sugarloaf, one of the other scoria cones, has been erroneously described as one of only three perfect scoria cones of its type in the world, and partly on this ground was purchased by the state Government and National Trust to prevent further quarrying. Mt Sugarloaf owes its origin to southwesterly directed fire-fountaining, which built up a cone on the rim of Mt Leura crater.

Mt Leura Maar may be 22 000 years old, based on the dating of the Lake Colongulac tuff which could have come from this eruption point.

6.2 Day 5 Stop 2: Mt Porndon stony rises

David Gibson

The stony rises around Mt Porndon have been studied for many years, probably because of their easy access along the Princes Highway, and the unusual nature of the Mt Porndon lava disc. Flow units and flow directions were postulated by Ellis (1971), published in Nicholls et al. (1993), based on airphotos and field mapping (Figure 59).

A new LiDAR DEM of the area has been made available by the Corangamite CMA, and we have been using this at 2 m pixel cell size, with vertical noise of about 10 cm. This shows a wealth of topographic information not previously available on DEMs, and has the advantage over airphotos that vegetation effects are minimalised (vegetation is filtered from the DEM) and changes of elevation of less than 1 metre can be clearly imaged (Figures 60 & 61). The DEM shows that Ellis' units need to be revised. In particular, several of his scarp boundaries are in fact reversed in direction of facing from what the DEM shows, and the order of extrusion may not correspond to the order of topographic steps, as shown by Ellis.

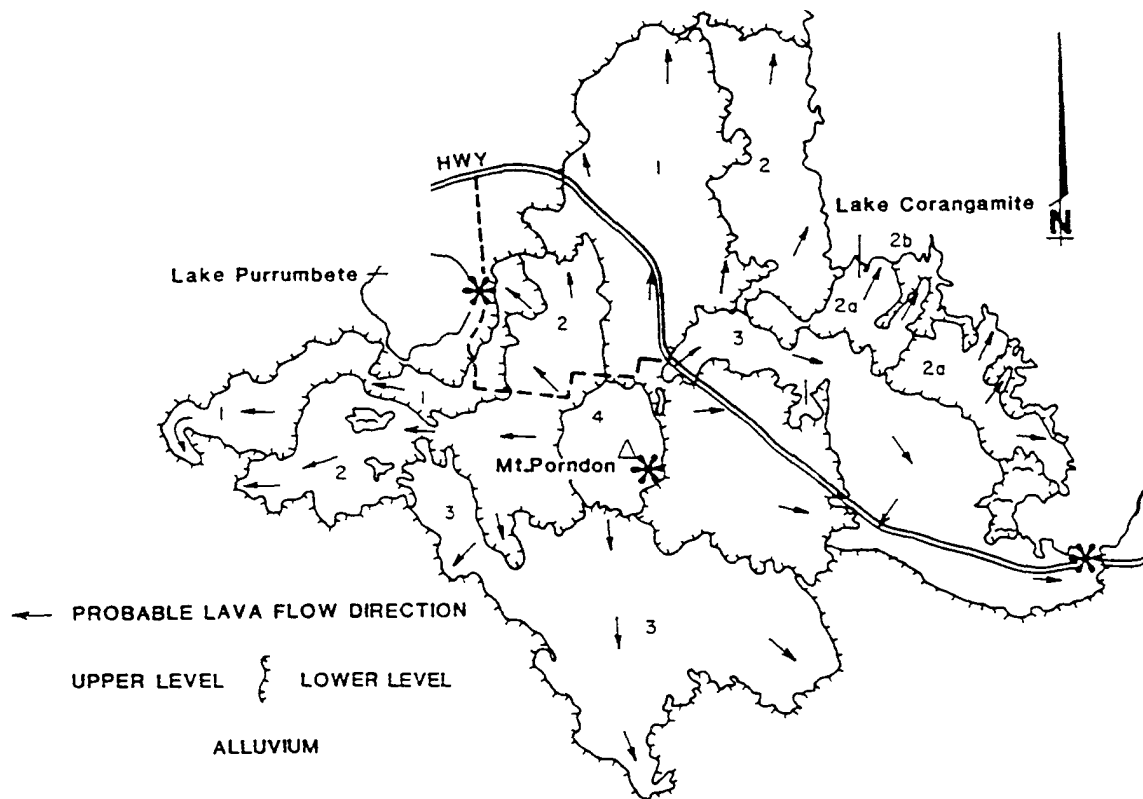


Figure 59. Flow units of Ellis (1971). Compare this with Figure 61 (reproduced from Nicholls et al. 1993. Copyright © Commonwealth of Australia, Geoscience Australia 1993).

The DEM shows that there are 7 main topographic components to the Mt Porndon volcanic area (Figures 60 & 61). Some of these have been recognised by previous workers (Ellis 1971, McKee and Thomas 1976):

1. Scoria peaks up to 100 m high, maximum elevation 290 m. There are 4 major peaks with curved elongated crests and no craters, surrounding a central cone with a crater breached to

- the west. The peaks without craters are all shown as scoria cones by McKee and Thomas (1976). The DEM suggests that rather than being individual cones, the four craterless peaks are remnants of the rim of a large cone that has blown out to the SW, and that the central cratered cone is a younger feature over the same vent that sourced the larger structure .
2. A 2 x 1.5 km area of undulating topography, with local relief mostly to 20 m. Elevation is mostly 185-210 m. This corresponds with an area of nepheline basanite lavas (the youngest of the lavas) resting on hawaiite lavas of unit 3, with some areas of scoria (as shown by McKee and Thomas, 1976). There are several small irregular shaped windows through the scoria and basanite into the hawaiite of unit 3. The geological map of the central area of the Mount Porndon complex published by McKee and Thomas (1976), from unpublished Honours reports from the University of Melbourne appears to correlate very well with the topography as shown by the DEM.
 3. A hawaiite “lava disc” surrounding unit 2, with elevation mostly 175-185 m. This has an abrupt outer margin mostly 15-20 m high (but locally >40 m in the south) with a stony slope of mostly 20° to 40°. Local relief and slope on this unit are mostly low. There are numerous small scale features, such as a 50 m wide and 4-8 m deep depression parallel to and about 30 m inboard from the crest of the marginal slope of the unit, smaller edge-parallel depressions further inboard, small cones up to 100 m across and 15 m high (some with craters) and small craters (not associated with cones) up to 100 m across and 20 m deep. McKee and Thomas (1976) conclude that as the slope of the southern part of the disc is from the rim towards the cones, the lava was extruded at ring fractures at the rim, and flowed inwards. Another interpretation is that the unit is made up of a single thick inflated lava flow that has been contained by cooled edges, and then partly subsided due to drainage of fluid lava (Skeats and James 1937, Ollier 1969). There are two locations (in the west and south) where surrounding pahoehoe flows appear to have been sourced from breakouts at the edge of the disk. McKee and Thomas (1976) measured gravity anomalies over the disc, and concluded that the basalt is 330 m thick, possibly filling a caldera. Their model requires that the basalt of the disk did not flow outward past the caldera wall. This appears unlikely, given the relief across the edge of the disc. However, the edge of the disc may represent a ring fault and the disc has been raised by faulting since extrusion within a caldera defined by the ring fault. The unusual shape of the disc especially in the south, suggests a flow rather than a caldera fill. A major promontory in the disc outline in the south coincides with a valley between older flows (here the rim of the disc reaches >40 m high), suggesting that the lava has preferentially flowed down the valley, and that the interpretation of an inflated flow is correct. The edge-parallel linear depressions also attest to a flow edge rather than faulted origin for the outer margin.
 4. Broad smooth surface (<1m local relief, pahoehoe?) flows with well defined arcuate, stony flow fronts typically 1-5 m high (this being the thickness of the individual flows) at up to 800 m spacing. The plan view of the flow fronts displays local angular features (breakouts and re-entrants) of up to 50 m. Locally there are small shallow blister-like depressions with raised rims and up to 2 m relief, and other more elongate lobate depressions. Slope of the flow surfaces are in the order of 5 m/km away from the central disc.
 5. Narrow, elongate flows with very low relief concordant crests (<1 m local relief) and lower gradient (<1-2 m/km away from the central disc) than unit 4, with depressions that range in shape from rounded depressions to linear, sinuous and branching valleys, many without outlet. The depressions range in size from a few tens to hundreds of metres across, and are up to 15 m deep. Thus these flows may be up to 15 m thick. Many of the depressions have concordant bases. The flows appear to have originated as long, narrow inflated lobes of very fluid lava, with areas where the top of the flow has locally become welded to the bottom of the flow prior to inflation, or with collapse structures due to the draining of lava after inflation, thus forming the depressions.
 6. Flows with rough surface flows, forming egg carton-like terrain with local relief mostly < 10 m, with a wavelength of 50-300 m.
 7. Rough surface flows as above, but with lava rises separated by valleys floored with lacustrine sediment adjacent to Lake Corangamite and along the southern margin of the area of flows. This geometry may result from either local disconnected lobes of flows covering a low relief

sediment surface, or sediment being deposited over the lower parts of the flows during high water stands of Lake Corangamite

The scoria cones and basanite flows are the youngest features, overlying the hawaiite of the lava disc. The order of extrusion of the surrounding lava shield is complex. The youngest flows, at highest elevation and closest to the disc are smooth-topped flows of unit 4. Some groups of flows have clearly originated at small vents adjacent to the lava disc, or possibly by rupture of the rim of the disc. Some of the unit 4 flows appear to be continuous with unit 5 flows, ie a single flow has changed morphology, possibly due to cooling or loss of volatiles. In other areas, the heads of unit 5 flows actually stand 5-10 m above the immediately adjoining unit 4 lavas. This suggests a point source with unit 4 for the inflated unit 5 flows, possibly a lava tunnel or a local vent.

In addition, some of the rugged high relief areas seem to have originated by flows of units 4 and 5 changing character. Thus there appears to be an extremely complex order of eruption. In most general terms, the most outlying and lowest elevation flows have a rugged surface, and the youngest, highest elevation flows have smooth surfaces.

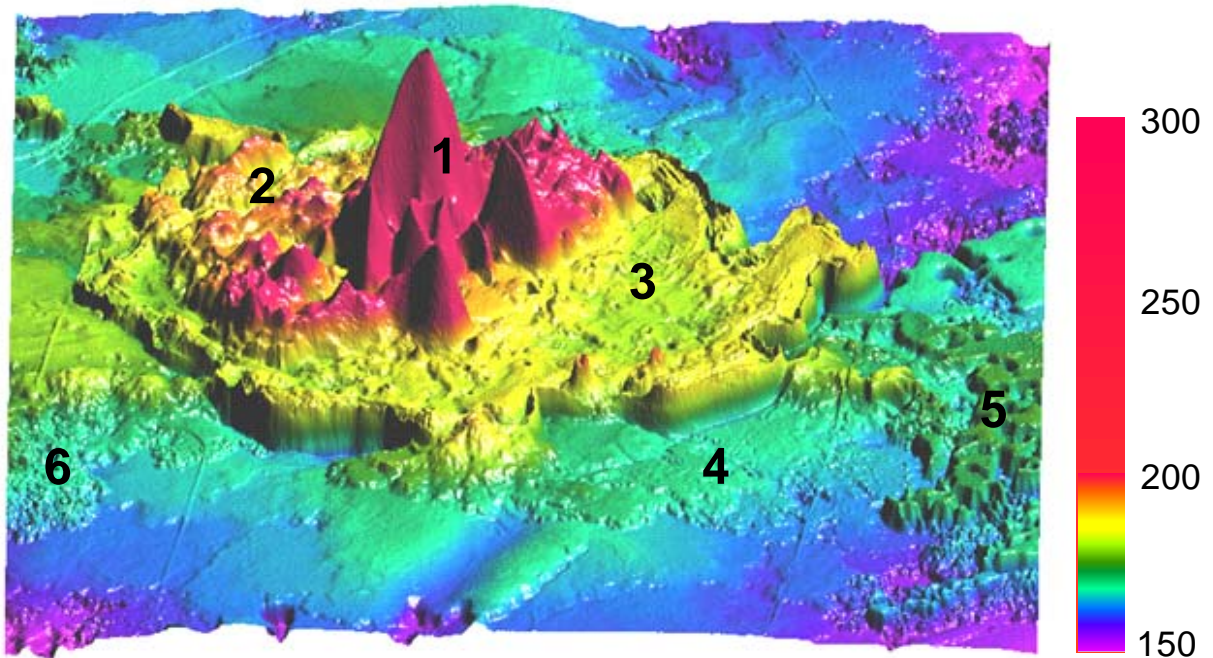


Figure 60. Oblique view from west of LiDAR DEM over Mt Porndon and the central part of the surrounding shield, showing 6 of the 7 volcanic morphologies described in the text. The maximum elevation of Mt Porndon from the LiDAR DEM is 289 m.

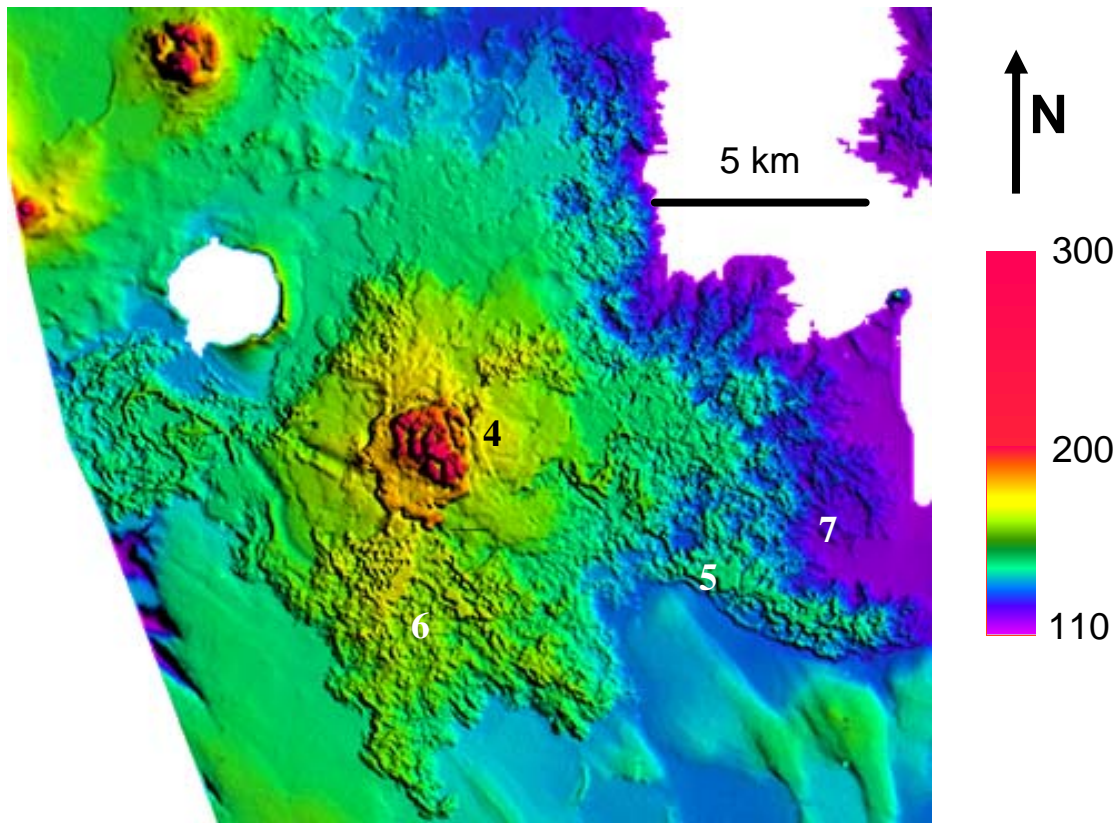


Figure 61. Vertical view of the LiDar DEM over the entire Mt Porndon lava field with examples of some of the different flow morphologies. Lake Corangamite (white) is in northeast, Lake Purrumbete in the northwest. North-northwest oriented Pliocene shoreline dune sands in the south continue north beneath the lava flows.

6.3 Day 5 Stop 3: Floating Islands

Patrick De Dekker and David Gibson

(text adapted from <http://www.walkabout.com.au/locations/VICColac.shtml>)

The floating Island Flora and Fauna Reserve (5 ha) is located in Lake Pirron Yallock which abuts the north side of the Princes Highway east of Mt Porndon (Figures 62 & 63). The lake (when it contains water) contains a number of small islands that support scrub, reeds, tussock grasses and eucalyptus saplings. However, their notoriety rests mostly in their capacity to change position quite rapidly (there are some estimates of shifts of up to 20 metres in a few minutes).

One theory about the development of the lagoon is that it was originally a peat swamp which developed in a depression in a lava flow from Mt Porndon. It flooded each winter and dried up in the summer. In the centre was an island of peat on which potatoes were grown. In 1938 the peat caught fire and smouldered for several months, lowering the level of the swamp and the island. Then, in 1952, especially heavy rains caused the swamp to fill to a particularly high level. The peat broke away from the basalt floor, complete with its vegetation, and began to float. The seasonal swamp was then turned into a permanent lagoon as the result of nearby roadworks and the clump of peat broke into a series of islets. Wind is thought to be the cause of their motion although another theory suggests that currents are caused by the influx of ground water which, being a different temperature, creates a differential that causes some impetus to occur.



Figure 62. Stony basalt slopes at Floating Islands Reserve



Figure 63. Dry floor of Lake Piron Yallock.

6.4 Day 5 Stop 4 :Red Rock lookout

David Gibson

(first paragraph of text adapted from Cas et al. 1993)

The lookout is at the top of the scoria cone complex of the Red Rock Volcanic Complex (Figures 64 & 65). The complex was initiated by the eruption of stony rise lavas which are partly preserved between Lake Corangamite and Lake Colac (Leach 1977). The next eruption phase was a maar-forming phase, represented by lakes such as Lakes Coragulac, Purdigulac, and Gnalinegurk (Figure 66). The final phase was the scoria cone building phase, represented by the hills and several small craters and lakes surrounding Red Rock Lookout. Leach (1977) has suggested there are 14 eruption points contained within the scalloped margins of the maars, and 28 points within the scoria cone complex.

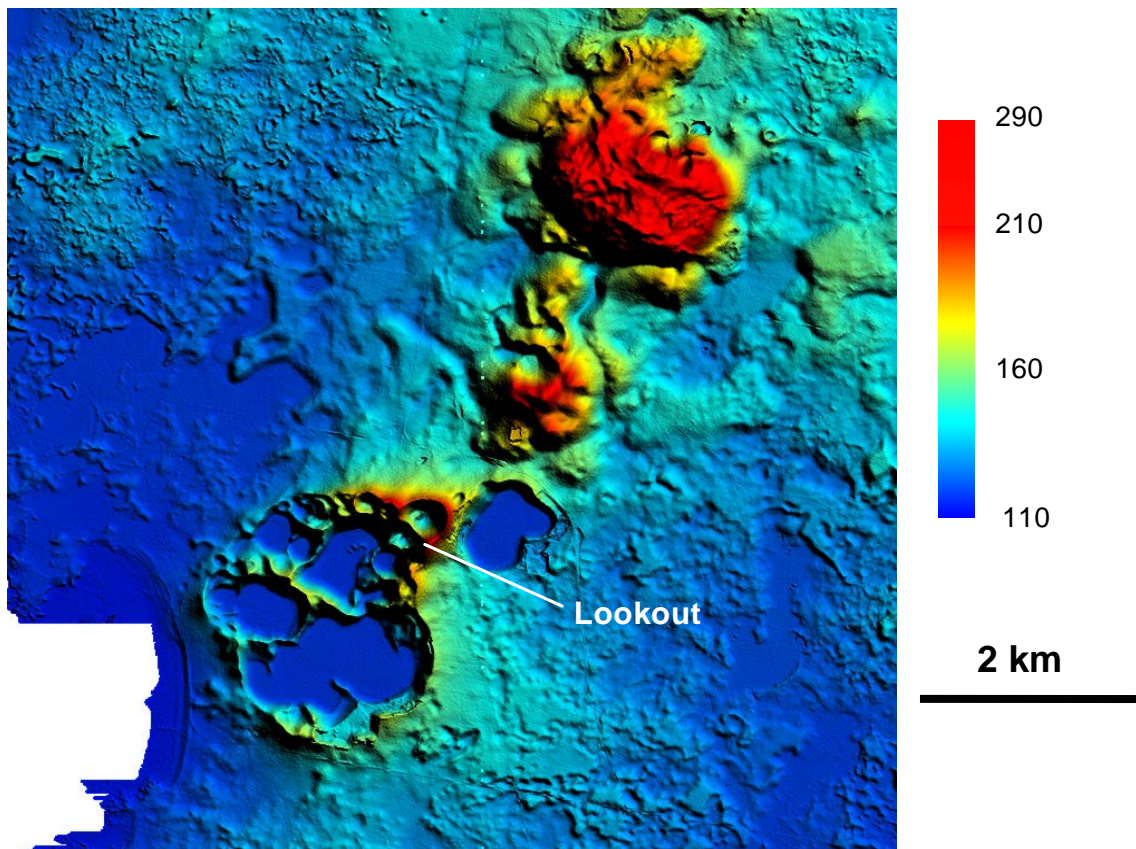


Figure 64. LiDar DEM of the Red Rock volcanic complex (small dry lakes and peaks in the southwest) , Mt Alvie (centre) and Warrion Hill (northeast). Southeastern shoreline of Lake Corangamite is present in the far southwest.

The LiDar DEM survey of the area (Figure 64) was flown when the maar lakes were dry, and thus the surface of sediment in the lakes has been imaged. The elevation of each individual lake floor shows only minimal variation. However, almost all lake floors, including all the major lakes, occur at 118 to 120 m elevation, and the floors of the 4 major lakes occur over a 1 m elevation range (Figure 65, Table 1). Given the various sizes of the lakes and their surrounding catchments, and thus varying potential for sediment supply, there does not appear to be a reasonable explanation for the small spread in elevations.

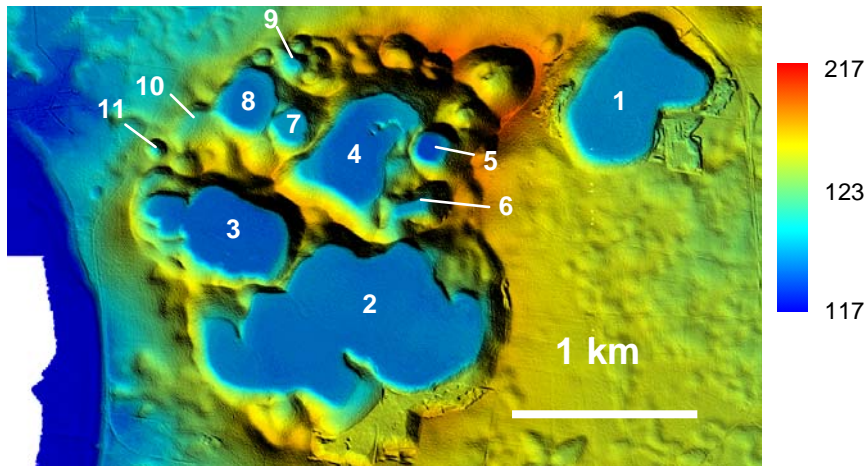


Figure 65. Detail of the LiDar DEM showing dry maar lakes around Red Rocks lookout. 1. Lake Coragulac. 2. Lake Purdigulac. 3. Lake Gnalinegurk. 4. Lake Werowrap. 5-11. un-named small lakes. Note logarithmic colour lookup table for elevation.

Lake	Elevation of bed (metres)
1 (L. Coragulac)	119.1
2 (L. Purdigulac)	118.6
3 (L. Gnalinegurk)	118.1
4 (L. Werowrap)	118.3
5	117.8
6	119.7
7	119.7
8	118.5
9	120.4
10	124.2
11	121.6

Table 1. Elevation of dry maar lake floors around Red Rocks lookout, lake numbers shown in Figure 65.



Figure 66. View to the southwest from Red Rocks lookout over dry Lake Werowrap to Lake Corangamite.

6.5 Day 5 Stop 5: Lake Corangamite

David Gibson

Lake Corangamite (Figure 67) is Victoria's largest inland lake. It has a surface area of 234 square kilometres, and no natural outlet. The salinity of the water is three times saltier than sea water, which restricts aquatic life, including no fish. The high salinity arises due to inflow of saline groundwater (the lake is a groundwater discharge site) from the surrounding volcanic areas (see day5 stop 6, Lake Beeac). However, there is a salinity gradient within the lake, as some groundwater recharge areas (for example stony lava rises between Mt Porndon and the lake) supply relatively fresh water to the lake. The lake is very shallow, and the shoreline location varies markedly with water level. The highest recent level was in 1960. The lake results from disruption of drainage by Quaternary lava flows, and formerly occupied a much larger area than today (Currey 1964).



Figure 67. Eastern shoreline of Lake Corangamite, with evaporate-encrusted basalt boulders and lake floor mud exposed due to low water levels.

6.6 Day 5 Stop 6 :Lake Beeac

Patrick De Dekker

(text reproduced from De Dekker 2003)

There are a number of saline playas east of Lake Corangamite in the Newer Volcanics Province of western Victoria that are characteristically rich in bicarbonate and which also are the sites of authigenic dolomite (CaMgCO_3) and magnesite (MgCO_3) precipitation. These lakes (Figure 68) are also undersaturated with respect to both calcite and aragonite. Yet, there are many other lakes adjacent to those lakes that do not contain dolomite nor magnesite. The best known playa with dolomite and magnesite is Lake Beeac, which has been studied for its water chemistry, sediment composition and sedimentological history (Williams & Buckney 1976, De Deckker & Last 1988, 1989, Last & De Deckker 1990, 1992).

The area is characterized by Quaternary basalts that flowed, in places on several occasions, over a low-lying topography. The outstanding topographic features are Warrion Hill, Mt Hesse and Mt Gellibrand (Figure 69).

Thompson (1971) identified a progressive increase of salinity of shallow groundwaters away from Warrion Hill, which showed that the dolomitic lakes occurred above a very specific range of groundwater salinities (Figure 70). Thus, Thompson identified a possible link between groundwater chemistry and processes, especially knowing that the playa lakes are in fact ‘groundwater windows’, and the lakes chemistry and sediment compositions.

A set of piezometers was placed in the vicinity of the lakes downslope from Mt Warrion in order to determine the chemistry and flow paths of the groundwater in the region, and link the latter to the water chemistry of the playas which are considered to be ‘windows into the groundwater’.

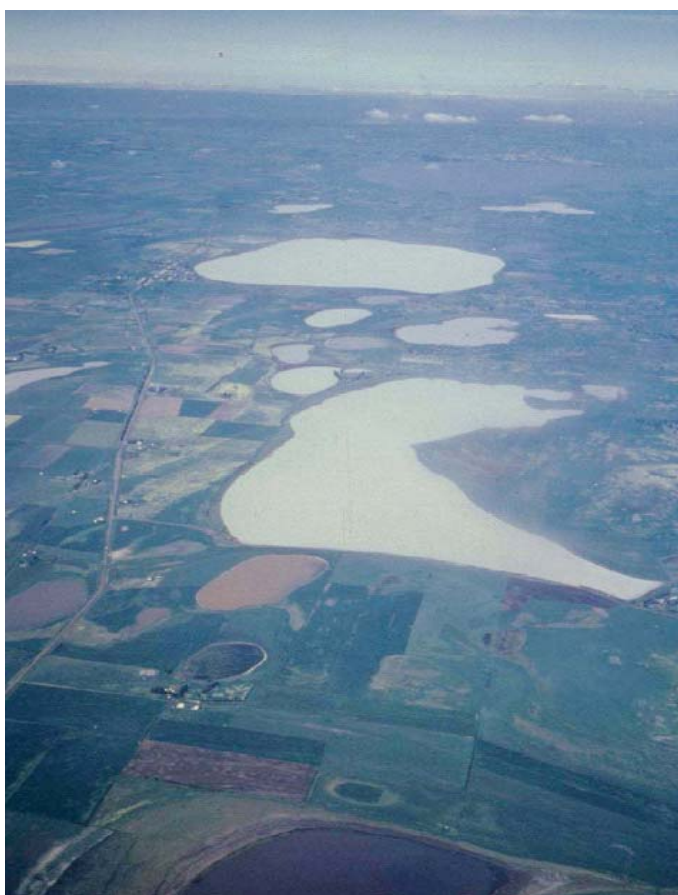


Figure 68. Oblique aerial photograph looking south showing the characteristic white colour of the dolomitic lakes with primary dolomite in suspension in the very turbid lake waters. Lake Cundare is in the forefront and the almost circular Lake Beeac. Note the colouration of the other lakes (pink for those yielding the hypersaline *Dunaliella* alga, black for other saline lakes) which do not contain dolomite or magnesite (reproduced from De Deckker 2003).

The work presented here clearly identifies that the volcanic rises in the region such as Warrion Hill (Figure 69) play a vital role in groundwater recharge and flow paths towards the where the playas are located. Water chemistry plays a major role in controlling the presence/absence of the biota inhabiting the lakes. For example, gastropods, such as the halobiont, euryhaline *Coxiella* sp., should normally be found in such playas and yet are absent. The ostracod *Platycypris baueri*, on the other hand, is found living in the lakes, but no valves are preserved in the sediments. Such information leads to determining the role lake water chemistry has on the biota, as well as interpreting biological records in lacustrine sediments.

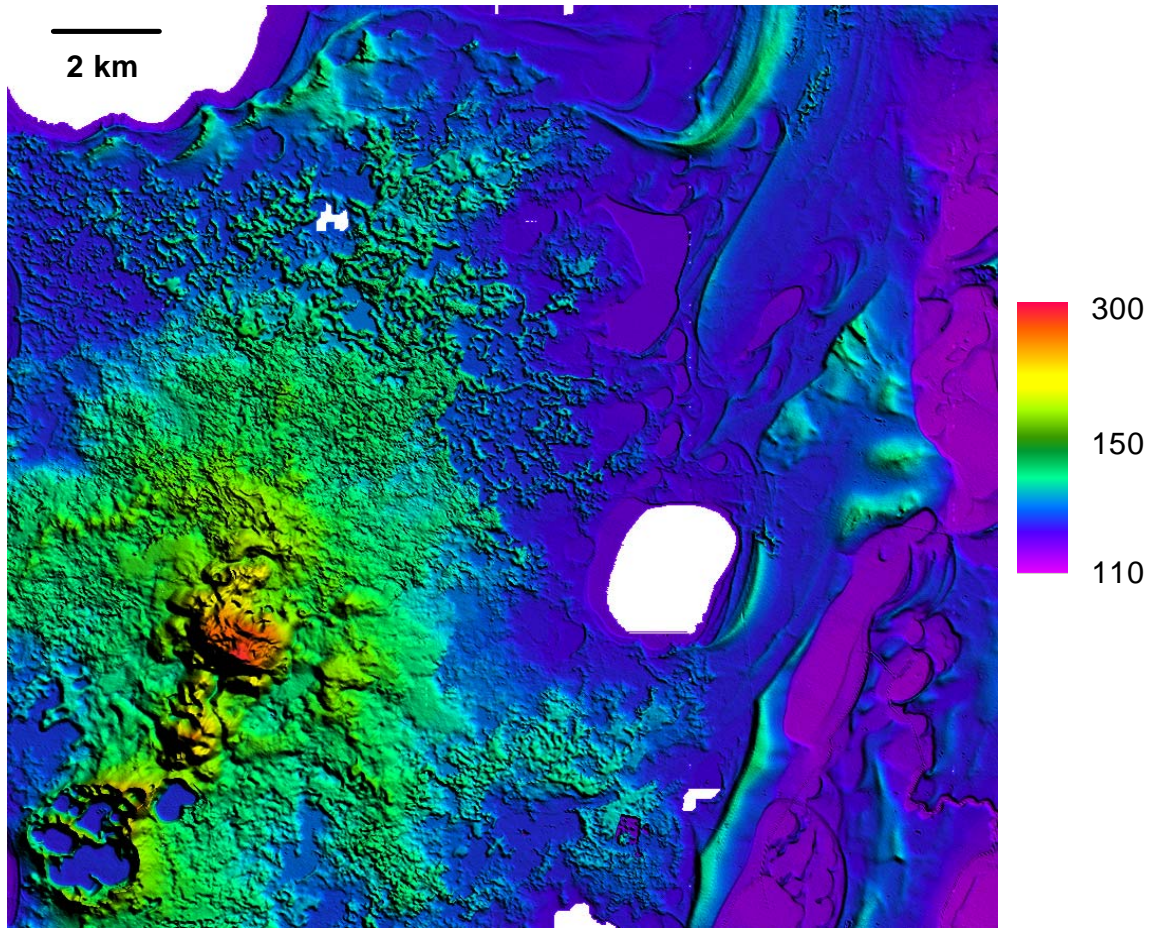


Figure 69. LiDar DEM of Lake Beac (white, centre right – no LiDar data due to presence of water) and surrounding areas showing flat dry lake floors at about 110-120 m and lunette/source-bordering dune complexes. Warrion Hill to the west of Lake Beac, Red Rock craters in the Southwest, and northeastern part of Lake Corangamite in the northwest. Note non-linear colour lookup table for elevation.

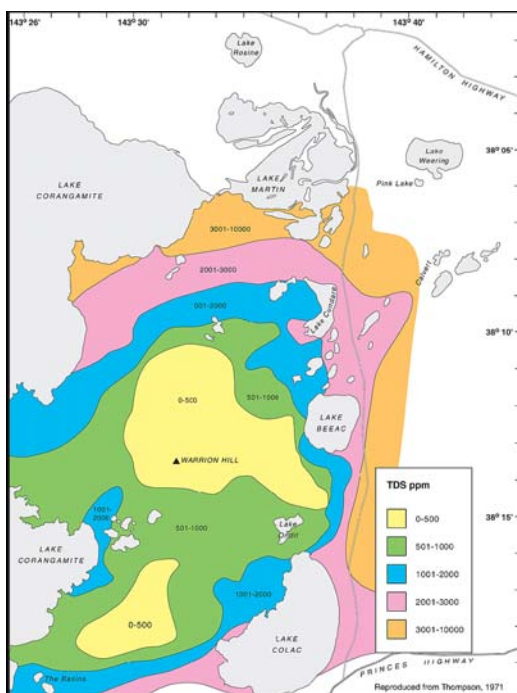


Figure 70. Groundwater map redrawn from Thompson's (1971) thesis showing the progressive salinity increase of the near surface groundwater away from Warrion Hill (reproduced from de Deckker 2003).

6.7 Day 5 Stop 6: Barabool Hills monocline

Dan Clark

(text of the first paragraph largely reproduced from Sandiford 2003a,b)

The southern uplands of Victoria include the Otway Ranges to the southwest of Melbourne and the Strezlecki Ranges to the southeast. Direct evidence for the impact of Quaternary faulting in shaping these ranges is best illustrated on the northwest side of the Otway Ranges, where Pliocene strandline systems equivalent to those of the Murray Basin onlap onto the ranges (Dickinson et al. 2001) (Figure 71). In this region, the geomorphic expression of these strandlines has been greatly accentuated by erosional landsculpting resulting in the development of a dramatic trellised drainage net. Since the strandlines provide a horizontal datum at the depositional time (Early–Middle Pliocene: Tickell et al. 1992) when sea level was less than 65 m above present-day sea level (Kotsonis 1996), they provide an extraordinary insight into the more recent tectonic activity. Profiles along individual strandlines rise from less than 120 m to ~250 m on the range flank, stepping over a series of small faults and monoclinical flexures with displacements of the ~10–50 m. Discrete structural highs, clearly visible in the landscape, forming the Simpson and Ferguson Hill ‘anticlines’ are bound by an east-northeast-trending array of en échelon faults and monoclines (Tickell et al. 1992) (Figure 71). The largest of these faults, the Colac Fault on the south side of the Ferguson Hill ‘anticline’, has a throw estimated at ~50 m. The maximum elevation of the preserved strandlines coincides with a prominent break in slope at ~250–300 m on the northwestern flanks of the Otway Ranges, beneath which the incised valleys follow the trend of the Pliocene strandlines further north. This break in slope almost certainly reflects the position of the Pliocene coastline implying that the ranges have experienced ~200–250 m of post-Middle–Late Pliocene uplift. Importantly, the uplift increases away from the axis of Late Pliocene–Quaternary volcanism centred on a low-lying (~100–150 m) region to the north of Figure 71. Consequently, the great proportion of the 200–250 m Late Pliocene–Quaternary uplift of the Otway Ranges can be attributed to fault-related neotectonic movements, rather than volcanic doming. To the southeast of the Otway Ranges, the correlative Pliocene is restricted to submarine sections to depths of ~140 m (Dickinson et al. 2001). This submarine Pliocene sequence exhibits a seismic character consistent with terrestrial deposition (Mallet & Holdgate 1985) implying the fault/faults on southeastern side of the Otway Ranges accommodate up to 350 m of movement, giving a cumulative, time-averaged displacement of at least ~100 m/10⁶ y.

A faulted monocline exposed in a railway cutting near Winchelsea on the north eastern boundary of the Otway Ranges is an expression of the deformation underlying this uplift (Figure 72). The monocline, which has an amplitude of several tens of metres, is mapped at 1:250,000 scale as the Mt Pollock Monocline (Abele, 1977). An examination of 20 m digital elevation data suggests that the monocline may be a continuation of the Barabool Hills Monocline (Figure 72, red dashed line). An easterly dipping reverse fault has broken through to the surface at the toe of the monocline (Figure 72, inset), displacing late Tertiary fluvial sediments (Moorabool Viaduct Member) and a lava flow estimated to be 2–3 Ma (B. Joyce, University of Melbourne, Written Communication, 2006) by more than a metre. The total displacement across the fault is not known. The intersection of the projection of the fault tip with the surface is not associated with a sharp topographic break, suggesting that the last faulting event occurred thousands to tens of thousands or more years ago. Local inversion of the drainage where it focused basalt flows in the southwest Otways is consistent with the Barabool Hills outcrop, constraining the age of incision and faulting to greater than *ca* 1 Ma and, most probably, less than *ca* 2 Ma in this region (Sandiford 2003b).

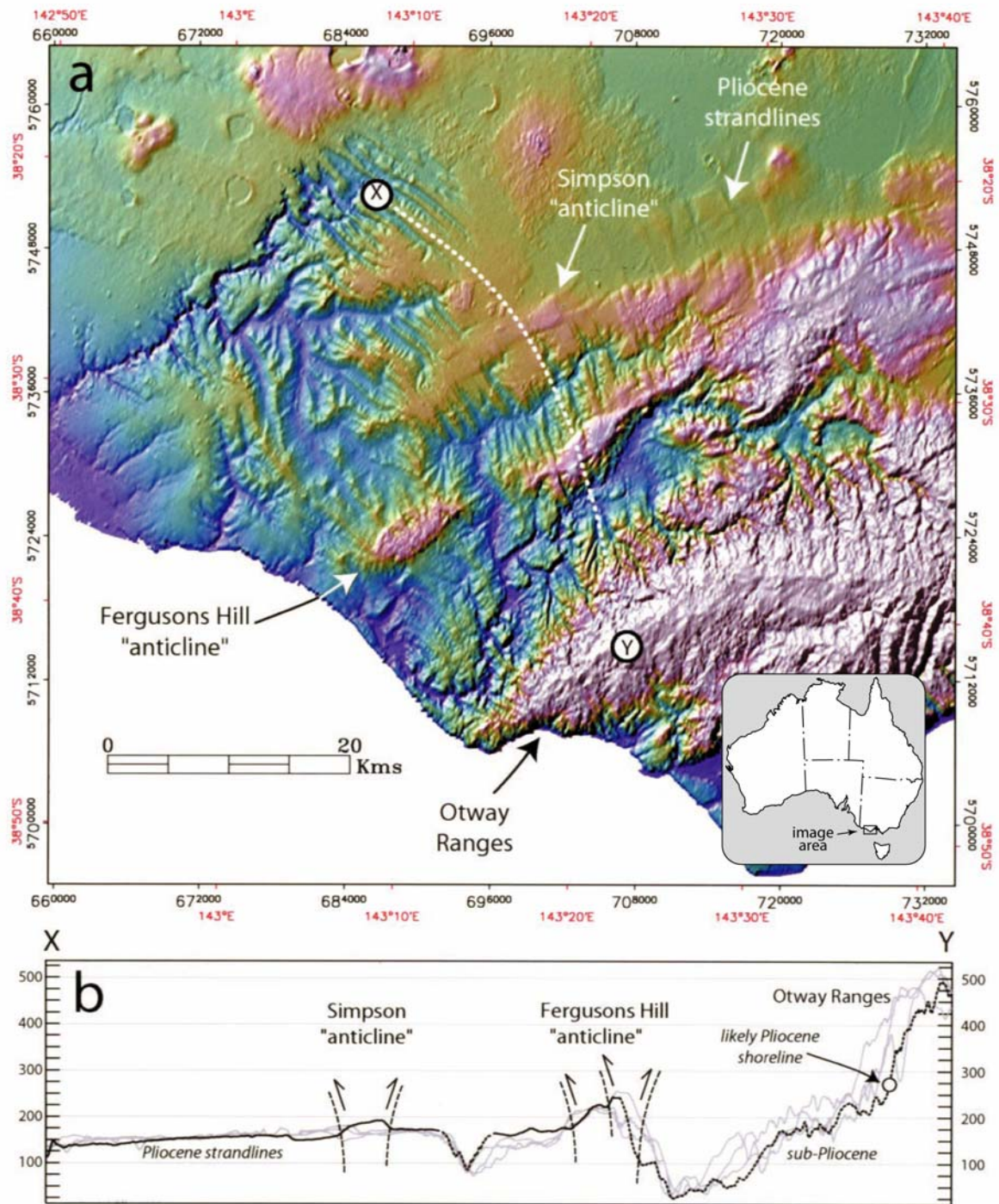


Figure 71. (a) Shaded digital elevation map of the northwest slopes of the Otway Ranges. (b) Topographic profile along Pliocene strandline across the Simpson and Fergusons Hill structural highs. These structural highs are defined by a ENE-trending en échelon array of faults cutting the Pliocene strandlines. Elevation of these horizontal Pliocene datum planes now rises from <120 m to the northwest of Cobden to ~260 m on the Ferguson Hill structure in the southeast, ~200 m higher than at deposition. Strandlines have been differentially etched to produce a trellised drainage. The former onlapping of the Pliocene strandlines onto the northwest flanks of the Otway Ranges is suggested by a prominent break in slope at ~250 m, beneath which the incised values follow the trends of the Pliocene strandlines. An important implication is that the Otway Ranges have witnessed ~200 m of post Middle–Late Pliocene uplift (reproduced from Sandiford 2003a. Copyright © Geological Society of Australia 2003).

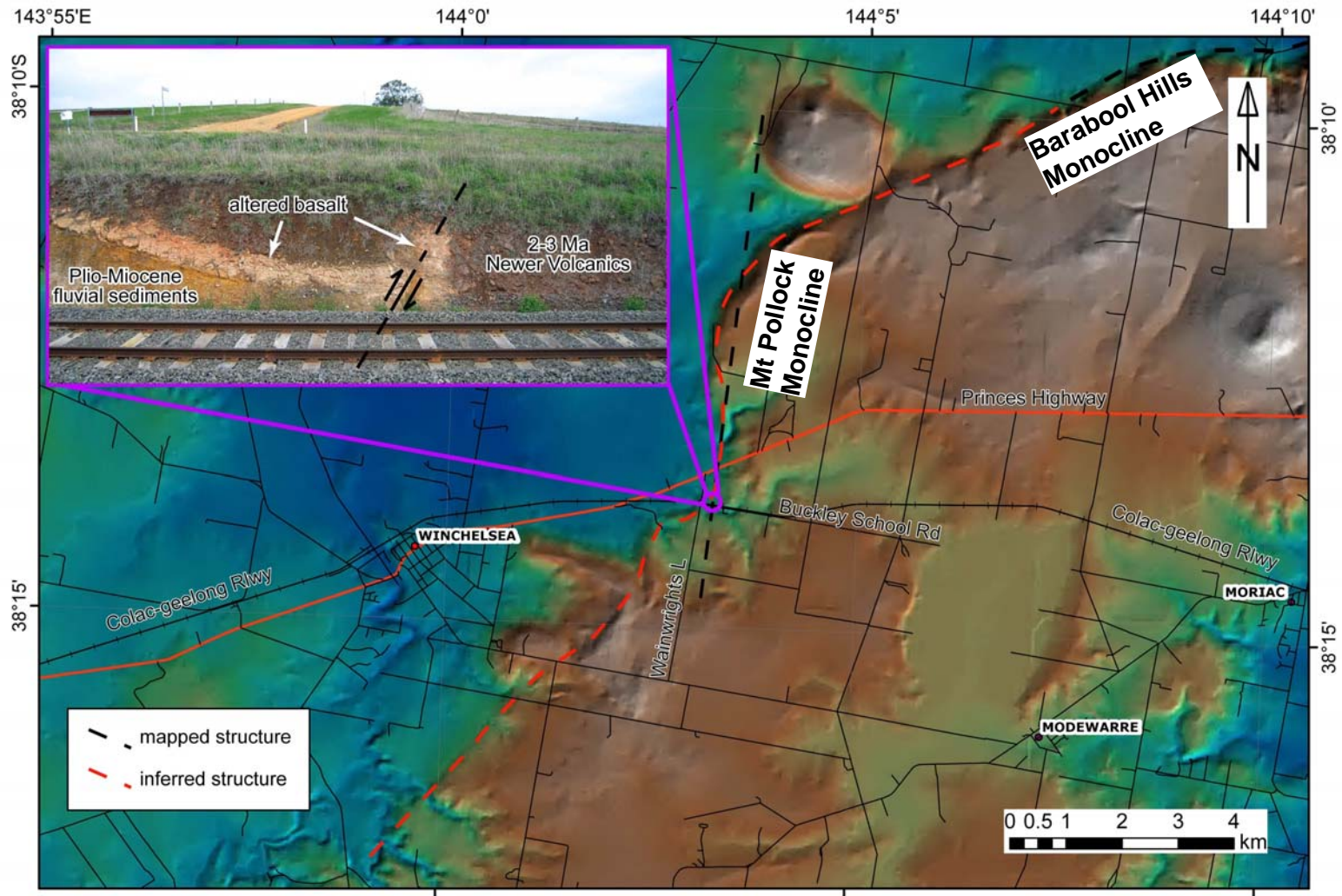


Figure 72. Shaded digital elevation map of the Barabool Hills monocline, northeast Otway Ranges. A continuous topographic break suggests that the Barabool Hills and Mt Pollock monoclines are contiguous. The inset shows reverse faulting at the toe of the monocline, which displaces late Tertiary fluvial sediments and a ca. 2-3 Ma lava flow. The lava flow is highly altered along its contact with the underlying sediments and along the fault plane. A lack of a sharp topographic break where the fault tip projects to the surface suggests many thousands of years have elapsed since the last faulting event.

7. ACKNOWLEDGEMENTS

The field excursion could not have been run without the efforts of the scientists who gave talks at the various stops: Steve Bourne, Dan Clark, Jon Clarke, Patrick de Deckker, David Gibson, Bernie Joyce, Mike Sandiford, Liz Reid and John Wilford. Thanks also to the staff of Terramin Australia Ltd who made the excursion stop at the Garwood Quarry at Strathalbyn possible, and supplied safety equipment. The trip was run under the auspices of the Environment, Engineering and Hydrogeological Specialist Group of the Geological Society of Australia, instigated by Ken Lawrie and ably organised by Tenai Luttrell and Heike Apps. Heike Apps and Kristen Cullen helped prepare the route maps.

Parts of these notes have been reproduced or based on published sources and web pages: these sources are acknowledged where used. In particular we thank the Geological Society of Australia who hold copyright for the articles Sandiford (2003a, 2003b), Hill et al (2005), and Wallace et al. (2005); illustrations and text extracts from these articles are included in this report. The Department of Primary Industries and Resources of South Australia (PIRSA) gave permission to reproduce several illustrations and text from Belperio (1995) and Anon (2001). The Royal Society of South Australia gave permission to reproduce Figures 31 and 33. Figures 35, 36 and 59 and the original scene from which Figure 34 was adapted are Copyright © Commonwealth of Australia, Geoscience Australia. All rights reserved. Reproduced by permission of the Chief Executive Officer, Geoscience Australia, Canberra, ACT. Apart from any use as permitted under the Copyright Act 1968 no part of these figures may be reproduced by any process without prior written permission from Geoscience Australia. Requests and enquiries concerning reproduction and rights of these figures should be addressed to the Manager Copyright, Geoscience Australia, GPO Box 378, Canberra ACT 2601, or by email to copyright@ga.gov.au.

8. REFERENCES

- Abele C 1977. Explanatory notes on the Queenscliff 1:250 000 geological map. Geological Survey of Victoria Report 1977/005: 82pp.
- Alderman AR & Skinner HCW 1957. Dolomite sedimentation in the southeast of South Australia. *American Journal of Science*, 255: 561-567.
- Alley NF 1977. Age and origin of laterite and silcrete duricrusts and their relationship to episodic tectonism in the Mid-North of South Australia. *Journal of the Geological Society of Australia*, 24: 107-116.
- Allison GB & Harvey PD 1983. Freshwater lakes. In Tyler MJ, Twidale CR, Ling JK & Holmes JW, *Natural History of the Southeast*. Royal Society of South Australia, Occasional Publication 3: 61-74.
- Anon 2001. Volcanoes of the Mount Gambier area. Minerals and Energy Division South Australia, Earth Resources Information Sheet M14.
- Belperio AP 1995 (compiler). Quaternary. In: Drexel JF & Preiss WV (eds), *The Geology of South Australia, Volume 2, The Phanerozoic*. Geological Survey of South Australia Bulletin 54: 219-281
- Bourman RP 1993. Modes of ferricrete genesis: evidence from south-eastern Australia. *Zeitschrift fur Geomorphologie*, 37: 77-101.
- Bourman RP 1995. A review of laterite studies in southern South Australia. *Transactions of the Royal Society of South Australia*, 119(1): 1-28.
- Bourman RP and Lindsay JM 1989. Timing, extent and character of late Cainozoic faulting of the eastern margin of the Mt Lofty Ranges, South Australia. *Transactions of the Royal Society of South Australia*, 113: 63-67.
- Bourman RP Belperio AP Murray-Wallace CV & Cann JH 1998. A last interglacial embayment fill at Normanville, South Australia, and its neotectonic implications. *Transactions of the Royal Society of South Australia*, 122: 63-67.
- Bourman RP Milnes AR & Oades JM 1987. Investigations of ferricretes and related surficial ferruginous materials in parts of Southern and Eastern Australia. *Zeitschrift fur Geomorphologie*: 64: 1-24.
- Bourman RP. & Lindsay JM 1989. Timing extent and character of late Cainozoic faulting on the eastern margin of the Mount Lofty Ranges, South Australia. *Transactions of the Royal Society of South Australia*, 113: 63-67.
- Brown RG 1965. Sedimentation in the Coorong lagoon, South Australia. University of Adelaide, PhD thesis (unpublished).
- Burne RV Bauld J & De Deckker P 1980. Saline lake charophytes and their geological significance. *Journal of Sedimentary Petrology*, 50: 281-293.
- Burne RV & Ferguson J 1983. Contrasting marginal sediments of a seasonally flooded saline lake – Lake Eliza, South Australia: significance for oil shale genesis. *BMR Journal of Australian Geology and geophysics*, 8: 99-108.

- Campana B 1958. The Mount Lofty Ranges and Kangaroo Island. In Glaessner MF and Parkin LW (eds), *Geology of South Australia*, Geological Society of Australia, Melbourne University Press, Melbourne: 3-27.
- Cann JH & De Deckker P 1981. Fossil Quaternary and living foraminifera from the Thalassic (non-marine) saline lakes, southern Australia. *Journal of Paleontology*, 55: 660-670.
- Cas R Simpson C & Sato H 1993. Newer Volcanics province – processes and products of phreomagmatic activity. IAVCEI Conference, Canberra 1993, Excursion Guide. Australian Geological Survey Organisation Record 1993/64.
- Currey DT 1964. The former extent of Lake Corangamite. *Proceedings of the Royal Society of Victoria* 77(2): 377-386.
- Daily B Milnes AR Twidale CR & Bourne JA 1979. Geology and Geomorphology. In Tyler MJ Twidale CR & Ling JK (eds), *Natural History of Kangaroo Island*. Royal Society of South Australia Occasional Publication, 2: 1-38.
- Daily B Twidale CR and Milnes AR 1974. The age of the lateritized summit surface on Kangaroo Island and adjacent regions of South Australia. *Journal of the Geological Society of Australia*, 21: 387-392.
- De Deckker P 2003. Saline playa-groundwater interactions in the western district of Victoria. In Roach IC (ed), *Advances in Regolith, Proceedings of the CRC LEME Regional Regolith Symposia 2003*: 91-94. CRC LEME Perth.
- De Deckker P & Geddes MC 1980. Seasonal fauna of ephemeral saline lakes near the Coorong Lagoon, South Australia. *Australian Journal of Marine and Freshwater Research*, 31(5): 677-699.
- De Deckker P & Last WM 1988. Modern dolomite deposition in continental, saline lakes, western Victoria, Australia. *Geology*, 16(1): 29-32.
- De Deckker P & Last WM 1989. Modern, non-marine dolomite in evaporitic playas of western Victoria, Australia. *Sedimentary Geology*, 64(4): 223-238.
- Denham D & Windsor CR 1991. The crustal stress pattern in the Australian continent. *Exploration Geophysics*, 22: 101-106.
- Denham D Alexander LG & Worotnicki G 1979. Stresses in the Australian crust; evidence from earthquake and in situ stress measurements. *BMR Journal of Australian Geology and Geophysics*, 4: 289-295.
- Dickinson JA Wallace MW Holdgate GR Daniels J Gallagher SJ & Thomas L 2001. Neogene tectonics in SE Australia: implications for petroleum systems. *The APPEA Journal*, 41: 37-52.
- Dickinson JA Wallace MW Holdgate GR Gallagher SJ & Thomas L 2002. Origin and timing of the Miocene–Pliocene unconformity in southeast Australia. *Journal of Sedimentary Research*, 72(2): 288-303.
- Ellis DJ 1971. The geology and petrology of the Mt Porndon volcanic complex. BSc Hons Thesis, University of Melbourne.
- Fenner C 1930. The major structural and physiographic features of South Australia. *Transactions of the Royal Society of South Australia*, 54: 1-36.

- Gibson DL 2004. An enhanced framework for natural resource studies in the Angas-Bremer Plains area, South Australia. CRC LEME Open File Report 172.
- Haq BU Hardenbol J & Vail R 1988. Mesozoic and Cainozoic chronostratigraphy and cycles of sea-level change. In Wilgus CK Posamentier H Ross CA & Kendall CGStC (eds) *Sea-level Changes: an Integrated Approach*. Society of Economic Paleontologists and Mineralogists Special Publication 42: 71-108
- Hill PJ & de Deckker P 2004. AUSCAN seafloor mapping and geological sampling survey on the Australian southern margin by RV Marion Dufresne in 2003: final project report. AGSO Record 2004/004.
- Hill PJ de Deckker P & Exon NF 2005. Geomorphology and evolution of the gigantic Murray canyons on the Australian southern margin. *Australian Journal of Earth Sciences*, 52: 117-136.
- Hillis RR & Reynolds SD 2000. The Australian stress map. *Journal of the Geological Society of London*, 157: 915-921.
- Hillis RR Enever JR & Reynolds SD 1999. In situ stress field of eastern Australia. *Australian Journal of Earth Sciences*, 43: 813-825.
- Holmes JW & Waterhouse JD 1983. Hydrology. In Tyler MJ, Twidale CR, Ling JK & Holmes JW, *Natural History of the Southeast*. Royal Society of South Australia, Occasional Publication 3: 49-59.
- Joyce EB 1988a. Cainozoic volcanism in Victoria. In Clark I Cook B & Cochrane GC (eds) *Victorian Geology Excursion Guide*: 71-80. Australian Academy of Science and Geological Society of Australia, Victorian Division.
- Joyce EB 1988b. Colac-Camperdown. In Clark I Cook B & Cochrane GC (eds) *Victorian Geology Excursion Guide*: 157-167. Australian Academy of Science and Geological Society of Australia, Victorian Division.
- Joyce EB 2003. Western volcanic plains, Victoria. In Anand RR & de Broekert P (editors) *Regolith Landscape Evolution across Australia*. CRC LEME Perth: 253-257.
- King LC 1976. Plantation remnants upon high lands. *Zeitschrift fuer Geomorphologie*, 20: 133-148.
- Kotsonis A 1996. Late Cainozoic climatic and eustatic record of the Loxton-Parilla Sands, Murray Basin, southeastern Australia. MSc Thesis, University of Melbourne (unpublished)
- Lamontagne S 2002. Groundwater delivery rate of nitrate and predicted change in nitrate concentration in Blue Lake, South Australia. *Marine and Freshwater Research*, 53(7): 1129-1142.
- Last WM & De Deckker P 1990. Modern and Holocene carbonate sedimentology of two saline volcanic maar lakes, southern Australia. *Sedimentology*, 37: 967-981.
- Last WM & De Deckker P 1992. Paleohydrology and paleochemistry of Lake Beeac, a saline playa in southern Australia. In: Robarts RD & Bothwell ML (eds), *Aquatic ecosystems in semi-arid regions: implications for resource management*. N.H.T.I. Symposium Series 7, Environment Canada, Saskatoon, Saskatchewan: 63-74.
- Leach JHJ 1977. Geology of the eastern Corangamite region and the fossil fauna of Bald Hill, near Foxhow. BSc(Hons) Thesis, School of Geology, The University of Melbourne.

- Leaney FWJ Allison GB Dighton JC & Trumbore S 1995. The age and hydrological history of Blue Lake, South Australia. *Palaeogeography, Palaeoclimatology, Palaeoecology* 118: 111-130.
- Lemon NM & McGowran B 1989. Structural development of the Willunga embayment, St. Vincent basin, South Australia. National Centre for Petroleum Geology and Geophysics, Adelaide, field guide (unpubl).
- Lindsay J 1986. New record and tectonic implications of a high-level *Lepidocyclina*-bearing limestone, Bremer Valley, eastern Mount Lofty Ranges. South Australia Department of Mines and Energy Report 86/66.
- Lukasik JJ & James NP 1998. Lithostratigraphic revision and correlation of the Oligo-Miocene Murray Supergroup, western Murray Basin, South Australia. *Australian Journal of Earth Sciences*, 45(6): 889-902.
- Lukasik JJ & James NP 2003. Deepening-upward subtidal cycles, Murray Basin, South Australia. *Journal of Sedimentary Research*, 73(5): 653-671.
- Lukasik JJ James NP McGowran B & Bone Y 2000. An epeiric ramp; low-energy, cool-water carbonate facies in a Tertiary inland sea, Murray Basin, South Australia. *Sedimentology*, 47(4): 851-881.
- Mallet CW & Holdgate GR 1985. Subsurface Neogene stratigraphy in the Nepean Peninsula, Victoria. Department of Mines and Energy South Australia Special Publication 5: 233-245.
- Maud RR 1972. Geology, geomorphology and soils of Central County Hindmarsh (Mount Compass-Milang), South Australia. CSIRO Soil Publication 29.
- May RM & Bourman BP 1984. Coastal landslumping in Pleistocene sediments at Sellicks Beach, South Australia. *Transactions of the Royal Society of South Australia*, 108: 85-94.
- McKee CO & Thomas L 1976. Geological interpretation of the gravity anomaly at Mt Porndon volcano, Victoria, Australia. In Johnson R.W. (ed), *Volcanism in Australasia*: 53-62. Elsevier.
- Mills K 1965. The structural petrology of the Milendella area of South Australia. PhD thesis, University of Adelaide, Adelaide (unpublished).
- Milnes AR Bourman RP & Northcote KH 1985. Field relationships of ferricretes and weathered zones in southern South Australia: a contribution to 'laterite' studies in Australia. *Australian Journal of Soil Research*, 23: 441-465.
- Nicholls IA Grieg AG Gray CM & Price RC 1993. Newer Volcanics Province – basalts, xenoliths and megacrysts. *Australian Geological Survey Organisation Record* 1993/58.
- Ollier CD 1969. *Volcanoes*. ANU Press.
- Paine M 2003. Nature and extent of Pliocene strandlines on the Dundas Tableland, southwestern Victoria. In Roach IC (editor), *Advances in Regolith, Proceedings of the CRC LEME Regional Regolith Symposia 2003*: 314-318. CRC LEME Perth.
- Paine MD Bennets DA Webb JA & Morand VJ 2004. Nature and extent of Pliocene strandlines in southwestern Victoria and their application to Late Neogene tectonics. *Australian Journal of Earth Sciences*, 51: 407-422.

- Rosen MR Miser DE Starcher MA & Warren JK 1989. Formation of dolomite in the Coorong region, South Australia. *Geochimica et Cosmochimica Acta*, 53: 661-669.
- Rosen MR Miser DE & Warren JK 1988. Sedimentology, mineralogy and isotopic analysis of Pellet Lake, Coorong region, South Australia. *Sedimentology*, 35(1): 105-122.
- Roy PS Whitehouse J Cowell PJ & Oakes G. 2000. Mineral sand occurrences in the Murray Basin, southeastern Australia. *Economic Geology* 95: 1107–1128.
- Sandiford M 2003a. Neotectonics of southeastern Australia: linking the Quaternary faulting record with seismicity and in situ stress. In Hillis RH & Müller D (eds), *Evolution and Dynamics of the Australian Plate*. Geological Society of Australia Special Publication 22 and Geological Society of America Special Paper 372: 101-113.
- Sandiford M 2003b. Geomorphic constraints on the late Neogene tectonics of the Otway Ranges. *Australian Journal of Earth Sciences*, 50: 69-80.
- Schwebel DA 1983. Quaternary dune systems. In Tyler MJ, Twidale CR, Ling JK & Holmes JW, *Natural History of the Southeast*. Royal Society of South Australia, Occasional Publication 3: 15-24.
- Sheard MJ 1978. Geological history of the Mount Gambier volcanic complex. *Transactions of the Royal Society of South Australia*, 102: 125-139.
- Skeats EW & James AVG 1937. Basaltic barriers and other surface features of the Newer Basalts of Western Victoria. *Proceedings of the Royal Society of Victoria*, 49: 245-278.
- Sprigg RC 1945. Some aspects of the geomorphology of portion of the Mount Lofty Ranges. *Transactions of the Royal Society of South Australia*, 70: 313-347.
- Sprigg RC 1947. Submarine canyons of the New Guinea and South Australian coasts. *Transactions of the Royal Society of South Australia*, 71: 296-310.
- Sprigg RC 1952. The geology of the south-east province, South Australia with special reference to Quaternary coastline migrations and modern beach developments. *Geological Survey of South Australia Bulletin* 29.
- Tamuly A 1969. The Blue Lake of Mount Gambier. Horace Lamb Centre for Oceanographical Research, Flinders University, Adelaide, Research Paper 28.
- Telfer AL 2000. Identification of processes regulating the colour and colour change in an oligotrophic, hardwater, groundwater fed lake, Blue Lake, Mount Gambier, South Australia. *Lakes and Reservoirs: Research and Management*, 5: 161-176.
- Telfer A 1994. Blue Lake, stormwater recharge and lake management. *Aqua Australis*, 1: 10-13.
- Thompson BR 1971. The geology and hydrogeology of the Corangamite region. MSc Thesis, University of Melbourne, unpublished.
- Thurgate ME 1996. The stromatolites of the cenote lakes of the Lower South East of South Australia. *Helictite* 34:17-25.
- Thurgate M & Spate A 2004. Limestone Coast 2004. Post Conference Ramsar Subterranean Wetlands Field Trip Notes, Closing workshop IGCP 448 – Global Karst Correlation, and The First

International Workshop on Ramsar Subterranean Wetlands, 10-17 October 2004 (unpublished).

Tickell SJ Edwards J & Abele C 1992. Port Campbell Embayment 1: 100 000 Map Geological Report. Geological Survey of Victoria Report 95.

Tokarev V Sandiford M & Gostin VA 1999. Landscape evolution in the Mt Lofty Ranges: implications for regolith development. In Taylor G and Pain C (eds), Regolith '98, New Approaches to an Old Continent, CRC LEME, 3rd Australian Regolith Conference, Kalgoorlie, WA, Proceedings:127-134.

Twidale CR & Bourne JA 1975. Geomorphological evolution of part of the eastern Mt Lofty Ranges, South Australia. Transactions of the Royal Society of South Australia, 99: 197-209.

Twidale CR 1976. Geomorphological evolution. In Twidale CR Tyler MJ & Webb BP (eds) Natural History of the Adelaide Region. Occasional Publication of the Royal Society of South Australia, 1: 43-59.

Twidale CR 1994. Gondwanan (Late Jurassic and Cretaceous) palaeosurface of the Australian craton. Palaeogeography, Palaeoclimatology, Palaeoecology, 112: 157-186.

Von der Borch CC 1965. The distribution and preliminary geochemistry of modern carbonate sediments from the Coorong area, South Australia. Geochimica et Cosmochimica Acta, 29: 781-799.

Von der Borch CC 1976. Stratigraphy and formation of Holocene dolomitic carbonate deposits of the Coorong area, South Australia. Journal of Sedimentary Petrology, 46: 952-966.

Von der Borch CC & Locke DE 1979. Geological significance of Coorong dolomites. Sedimentology, 26(6): 813-824.

Von der Borch CC Locke DE & Schwebel D 1975. Groundwater formation of dolomite in the Coorong region of South Australia. Geology 3(5): 283-285.

Wallace MW Dickinson JA Moore DH Sandiford M 2005. Late Neogene strandlines of southern Victoria; a unique record of eustasy and tectonics in southeast Australia. Australian Journal of Earth Sciences, 52(2): 279-297.

Warren JK 1988. Sedimentology of Coorong Dolomite in the Salt Creek region, South Australia. Carbonates and Evaporites, 3: 175-199.

Ward WT 1966. Geology, geomorphology and soils at the southwestern part of County Adelaide, South Australia. CSIRO Soil Publication 23.

Wilford JR 2004. Regolith-landforms and salt stores in the Angas-Bremer Hills. CRC LEME Open File Report 177. CRC LEME, Perth.

Williams WD & Buckney RT 1976. Stability of ionic proportions in five salt lakes in Victoria, Australia. Australian Journal of Marine and Freshwater Research, 27: 367-377.